Differential Susceptibility to Engineered Nanomaterial Induced Lung Inflammation and Toxicity

David K. Scoville

A dissertation submitted in partial fulfillment of the requirements for the degree of

Doctor of Philosophy

University of Washington
2017

Reading Committee:

Terrance J. Kavanagh, Chair
David L. Eaton
William A. Altemeier

Program Authorized to Offer Degree:
Environmental and Occupational Health Sciences
School of Public Health

University of Washington

Abstract

Differential Susceptibility to Engineered Nanomaterial Induced Lung Inflammation and Toxicity

David K. Scoville

Chair of Supervisory Committee:

Terrance J. Kavanagh

Department of Environmental and Occupational Health Sciences

Nanotechnology is a global industry producing a large variety of engineered nanomaterials (ENMs) for use in virtually every industry sector. Quantum dots (QDs) are ENMs with attractive semiconductor and fluorescent properties and commonly consist of a cadmium and selenium (CdSe) core surrounded by a zinc sulfide (Zn/S) shell. QDs have applications in biomedical research and potentially medicine as imaging tools and have multiple uses in electronics and energy industries. Silver nanoparticles (AgNPs) are composed of silver atoms and sometimes include other metals such as gold. AgNPs have been incorporated into numerous products as an antimicrobial agent. While these ENMs have beneficial uses, they have been shown to induce lung inflammation and toxicity in rodent models following pulmonary exposures. However, most QD and AgNP toxicity studies to date have only used one strain of mouse or rat and thus have not addressed the role of genetic variability as a potential modulator of susceptibility. My dissertation was primarily focused on investigating the role of genetic background as a determinant of susceptibility to QD- and AgNP-induced lung inflammation and toxicity utilizing multi-strain mouse models. We found substantial inter-strain variation in susceptibility to QD- and AgNP-induced pulmonary inflammatory responses across the Collaborative Cross (CC) founder mouse strains. Over the last decade,

the CC has created a panel of recombinant inbred (RI) mouse strains from eight genetically diverse founder strains to facilitate genetic mapping studies. Having established variability among the CC founder strains, we characterized the QD inflammatory response in a panel of CC RI inbred mouse strains in collaboration with researchers at the UNC. In collaboration with researchers at NYU we characterized the AgNP inflammatory response in 17 additional mouse strains (25 total strains). We used genome-wide association (GWA) mapping to identify genomic regions associated with QD- and AgNP-induced lung inflammation and toxicity containing candidate susceptibility genes that could modulate QD and AgNP responses and provide mechanistic insight. We also investigated the effects of QDs on lung mechanics and house dust mite (HDM) induced allergic airway disease in CC founder mouse strains we found initially to be more (A/J) and less (C57BL/6J) susceptible to QD-induced lung inflammation. Our results indicated that A/J mice were more susceptible to QD-induced changes lung mechanics. In addition, co-exposure to HDM+QDs enhanced cytokine production in A/J mice where HDM exposure alone did not result in significant increases and A/J mice had more lung type 2 innate lymphoid cells (ILC2s) than C57BL/6J mice. Significant inverse associations between glutathione and different endpoints across multiple studies highlighting the importance of redox balance in ENM induced lung inflammation and toxicity. The findings from these studies have important regulatory implications for ENMs in that genetic background of test animal strain is important to consider in risk models such that safety standards ensure adequate protection for sensitive populations.

Table of Contents

List of Figures.....iv

List of Tables.....vi

Acknowledgements.....vii

Chapter 1: Introduction.....1

Chapter 2: Susceptibility to Quantum Dot Induced Lung Inflammation Differs Widely Among the Collaborative Cross Founder Mouse Strains.....12

Chapter 3: Genome-Wide Association Mapping of Quantum Dot Induced Lung Inflammation and Toxicity in Collaborative Cross Recombinant Inbred Mouse Strains.....53

Chapter 4: Genetic Determinants of Susceptibility to Silver Nanoparticle-Induced Acute Lung Inflammation in Mice.....82

Chapter 5: Quantum Dot Induced Acute Changes in Lung Mechanics are Mouse Strain Dependent.....118

Chapter 6: Quantum Dots and Mouse Strain Influence House Dust Mite-Induced Allergic Airway Disease.....136

Chapter 7: Conclusions and future directions.....160

List of Figures

Figure 2.1 Total Cd in frozen lung tissue by strain at 8 hr post OPA and at earlier time points in AJ and B6 mice.
Figure 2.2 Flow cytometric detection of neutrophils and Gr1+ macrophages as percentages of total cells in bronchoalveolar lavage fluid (BALF).
Figure 2.3 Cytokines in BALF.
Figure 2.4 Levels of total protein in BALF and total glutathione levels in lung tissue.
Figure 2.5 Unsupervised Hierarchical Clustering Analysis of assay z-scores.
Figure 2.6 Regression analyses of MIP-1α, KC, BALF percent neutrophils compared to lung tissue Cadmium.
Figure 2.7 Regression analyses of MIP-1α, KC compared to BALF neutrophils.
Figure 2.S1 Ratio of the percent neutrophils in BALF in QD treated mice compared to strain matched saline controls.
Figure 2.S2 Regression analyses of levels of lung tissue glutathione and BALF neutrophils, cytokines, and lung Cd
Figure 2.S3 Detectable BALF cytokines with no significant individual strain differences between treatment groups.
Figure 2.S4 Study endpoints in Figures 2.1-2.4 in naïve and saline treated mice.

Figure 3.1 Percent neutrophils in BALF and KC levels in BALF for each QD and Saline treated mouse from 12 CC RI strains are shown overlaid on box plots.
Figure 3.2 Total protein in BALF and LDH levels in BALF for each QD and Saline treated mouse from 12 CC RI strains are shown overlaid on box plots.
Figure 3.3 Total lung glutathione and HMOX1 in BALF for each QD and Saline treated mouse from 12 CC RI strains are shown overlaid on box plots.
Figure 3.4 Scatter plots comparing % neutrophils in BALF to levels of BALF KC, levels of BALF KC to HMOX1.
Figure 3.5 CC founder strain and RI strain % neutrophils in BALF, total protein in BALF, and lung glutathione.
Figure 3.6 Manhattan plot with chromosomes and SNP location for SNP associations with levels of total BALF Protein.
Figure 3.S.1 SNPs on chromosomes 1, 4, 6 ,9, 12, and X (shown on plot as 20) from the BALF total protein GWA mapping. Red lines represent Bonferroni cutoff.
Figure 3.S.2 SNPs from GWA mapping for % neutrophils in BALF, and KC. Red lines represent Bonferroni cutoff.
Figure 3.S.3 Significant IPA pathways.
Figure 3.S.4 Diagram of the IPA visual cycle and nucleotide excision repair pathways.

Figure 4.1 Plot of % BALF neutrophils for each strain for AgNP (Ag) and citrate buffer (Ctrl) treated mice.
Figure 4.2 Manhattan plot showing the results from genome-wide analysis with EMMA.
Figure 4.3 Candidate QTL regions on chromosomes 18, 15, 4, and 1.
Figure 4.4 Plot of % BALF neutrophils for significant SNPs either in or near a candidate gene by allele and treatment group.
Figure 4.5 Correlations between % BALF neutrophils and mRNA levels from the Mouse Phenome Database for top candidate genes.
Figure 4.6 Expression of Nedd4l, Ano6 and Rnf220 mRNA and correlations between % BALF neutrophils and fold change of mRNA levels between individual AgNP mice over the mean of strain matched control mice from qRT-PCR for top candidate genes.
Figure 4.S.1 Hierarchical clustering of kinship matrix showing genetic relatedness of the 25 strains based on their alleles at the 65,594 SNPs used in this study.

Figure 4.S.2 SNPs that were among the top 10 in terms of –log(p) from different GWA studies performed using the initial and alternate analysis strategies.
Figure 4.S.3 Plot of % BALF neutrophils for the significant SNPs either in or near a candidate gene by strain, allele and treatment group illustrating allele distribution patterns.

Figure 5.1 Lung Mechanics for QD and saline treated A/J and C57BL/6 mice plotted as mean ± SEM on the y-axes with MTCH dose on the x-axis.
Figure 5.2 The % neutrophils and concentrations of total protein, IL-33, and KC in BALF and correlations between % neutrophils and KC levels in BALF.
Figure 5.3 Lung glutathione levels and correlations between G, R, and lung glutathione.

Figure 6.1 Levels of R, concentrations of total BALF protein and correlations of R and total BALF protein.
Figure 6.2 Concentrations of total CD45+ leukocytes and subpopulations.
Figure 6.3 Concentrations of BALF cytokines and correlations of R, IL-33, and KC.
Figure 6.4 Levels of lung ILC2s and correlations of MHC-II^{low} resident macrophages, and MHC-II^{high} resident macrophages and ILC2s.
Figure 6.5 Levels of total lung glutathione for each mouse are shown overlaid on a box plot. Correlations between ILC2s, and MHC-II^{low} resident macrophages, and lung glutathione.
Figure 6.S.1 Additional measures of lung mechanics in saline, HDM-sensitized, and HDM+QD co-exposed C57BL/6J and A/J mice.

List of Tables

Table 2.1 Broad sense heritability of qd response phenotypes for CC founder strains.
Table 2.S.1 Absolute Cell Numbers in BALF in BALF.
Table 2.S.2 Correlation between BALF Cytokines and % Neutrophils in BALF by Strain.

Table 3.1 Broad sense heritability of RI Mouse strain QD phenotypes.

Table 4.1 AgNP QTL Details.

Acknowledgements

First, I would like to thank my wife Caitlin for her continued patience, love, and support throughout this long and difficult journey. There is no way that I could have done this without her. Despite starting and finishing graduate school, and beginning a demanding career, she still found time to listen to my ideas and provide insightful feedback. She listened to countless practice presentations and helped motivate me to get away when needed to go hiking in the mountains, explore islands, etc.

I also want to thank my mentor Terry Kavanagh for his unending support, encouragement, and mentorship. Terry pushed me to be creative and after challenging me to thoroughly think ideas through, encouraged me to explore them. Terry provided me with an extraordinary number of opportunities to travel to meetings and to meet collaborators that were essential to my growth as a scientist. Terry's door is always open and despite managing an un-imaginable amount of work and responsibilities, never makes you feel like you are bothering him when you need help. I also would like to thank Bill Altemeier for initially allowing me to work in his lab with Dowon on a rotation project, for continuing throughout my time in graduate school to provide help and advice, and for ultimately serving on my Doctoral Advisory and Dissertation Reading Committees. I also need to thank Dave Eaton for serving on both my Master's, Doctoral Advisory, and Dissertation Reading Committees and providing sound advice. Dave also taught a pivotal course on gene x environment interactions and provided me an opportunity to write a book chapter on genomics in toxicology. I also want to thank Ed Kelly and Katie Kerr for being on my Doctoral Advisory Committee. Teal Hallstrand was also very generous with experimental advice and laboratory resources. I also have a number of collaborators outside the University of Washington that I would like to acknowledge including Ivan Rusyn, Terry Gordon, Samir Kelada, and Steve Kleeberger.

Additional current and former members of the Kavanagh and Hallstrand Labs also deserve enormous thanks. Dianne, Collin, and Lisa introduced me to the Kavanagh lab and provided invaluable help, guidance, and historical Kav Lab knowledge. Stefanie, Claire, and Nikki all helped me complete many experiments faster than I could have done without them. Chris C and Ryan provided key guidance on many of my studies and labored alongside me for many, many hours in North Carolina on the CC RI project. Chris S and Megan as my fellow students in the Kav Lab both helped me with my projects and with navigating the many hurdles on the way to finishing the program. Tyler V was only part of the Kav Lab for a rotation but helped me keep perspective on things throughout. Jimmy and Luke from the Hallstrand Lab welcomed me into their group and carried out many hours of work helping me with my project investigating QD effects on asthma in mice.

The support and inspiration from my family in North Carolina cannot be overstated. My parents selflessly supported me and my brother, provided us with countless opportunities, and lead by example to teach us to work hard and enjoy life. My mother- and father-in-law have also been extremely supportive of my aspirations and I owe them many thanks as well.

Finally, I would like to acknowledge the supportive efforts of many additional DEOHS faculty, staff, and students as well as the following funding sources for my research and financial support: NIH Grants - U19ES019544, U19ES019545, P30ES007033, T32ES007032, T32ES015459 (BEBTEH), R01ES016189, and the DEOHS Russell L Castner Research Award and Sheldon Murphy Fund.

Chapter 1

Introduction

David K. Scoville

Nanotechnology

Nanotechnology is being researched, manufactured, and/or commercialized in all 50 US states and many countries worldwide (The Project on Emerging Nanotechnologies 2017a). The engineered nanomaterials (ENMs) produced have physico-chemical properties that make them useful in products ranging from fuel additives to computing components to light emitting diodes (LEDs). However, data from toxicity studies in animals have generated concerns over potential health hazards associated with environmental and occupational exposures.

ENM Epidemiology

There are a small number of epidemiological studies published thus far focused on evaluating the potential health risks to associated with occupational ENM exposure in workers (Liou et al. 2015). Although most of these studies were cross sectional in design and/or were not sufficiently powered to definitively say whether ENM exposure is linked to disease in humans, some reported associations between exposure and biomarkers for pulmonary effects (induced sputum IL-8 and IL-1β, and fraction exhaled nitric oxide) (Cui 2013; Wu et al. 2014; Liou et al. 2015). Another cross-sectional study reported increased sneezing and allergic dermatitis (Liao et al. 2014). In a study with longitudinal follow-up, there was evidence for an ENM exposure-associated increase in cardiovascular inflammation (VCAM) and decrease in lung function at 6-months follow up (Liao et al. 2014). However, a subsequent published abstract describing an extended follow-up period over 4 years reported no significant associations between ENM exposure and health biomarkers.

Exposure assessments are challenging and have been noted as weaknesses in many ENM epidemiological studies (Liou et al. 2015). While Cui et al. performed a comprehensive exposure assessment measuring measured particle concentrations by mass and by particle number, other studies used control banding as a surrogate (Cui 2013; Liao et al. 2014; Liao et al. 2014; Wu et al. 2014). Control banding is a method for categorizing workers into risk groups for exposure comparison based on probability of exposure and how hazardous the potential exposure might be (Paik et al. 2008; Brouwer 2012). Larger studies with improved exposure assessment and longitudinal study designs will be needed to better determine ENM human health risks.

Quantum Dots

Quantum dots (QDs) are ENMs commonly comprised of a cadmium and selenium (CdSe) core with a zinc sulfide (ZnS) shell. QDs have outstanding fluorescent and semiconductor properties that make them ideal imaging tools in biomedical research and useful in electronics industries (Wu et al. 2003; Medintz et al. 2005; Jung et al. 2012). In rodent models, QDs induce lung inflammation and toxicity, characterized by increased neutrophilia, release of LDH, inflammatory cytokine production, and increased levels of DNA damage (Jacobsen et al. 2009; Ma-Hock et al. 2012; Ho et al. 2013; Ma-Hock et al. 2013; McConnachie et al. 2013; Roberts et al. 2013). Changes in lung function 17 days after exposure, and granuloma formation 90 days after exposure, have also been observed in mice (Ho et al. 2013). Particle coating modulates QD-induced lung inflammation and toxicity. In rats and mice, carboxylated QDs are more toxic than aminated and polyethylene glycol coated QDs (Ho et al. 2013; Roberts et al. 2013). QDs can induce oxidative stress and glutathione synthesis capacity modulates QD-induced lung inflammation and toxicity (Lovrić et al. 2005; Neibert and Maysinger 2011; McConnachie et al. 2013).

Silver Nanoparticles

Silver nanoparticles (AgNPs) consist mainly of silver atoms but can contain other metals, including gold (Holland et al. 2016). AgNPs are one of the ENMs selected by the NIEHS Centers for Nanotechnology Health Implications Research (NCNHIR) for rigorous *in vitro* and *in vivo* inter-laboratory evaluation. AgNPs have been incorporated into many consumer products because of their antimicrobial properties (The Project on Emerging Nanotechnologies 2017b). AgNPs have been shown to induce lung inflammation characterized by increased levels of BALF neutrophils, eosinophils, cytokines, in a particle size, coating, and test animal strain-dependent manner (Wang et al. 2014; Seiffert et al. 2015; Silva et al. 2015; Silva et al. 2016). AgNPs have also been shown to impact lung mechanics in mice and rats (Seiffert et al. 2015; Botelho et al. 2016). Retention of AgNPs in the mouse lung is also impacted by particle size and coating (Anderson et al. 2015; Anderson et al. 2015).

ENMs and Allergic Airway Disease

Approximately 8% of people in the US suffer from asthma, which is often characterized by airway hyperresponsiveness and chronic Th2 type lung inflammation (Kim and Mazza 2011; CDC 2017). Animal models of allergic airway disease using the experimental allergen ovalbumin have shown that ENMS can both act in place of traditional adjuvants to boost allergic sensitization to OVA in mice and exacerbate secondary immune responses during OVA challenges in mice sensitized to OVA with a traditional adjuvant (Brandenberger et al. 2013; Jonasson et al. 2013). Interestingly, in one study investigating AgNP effects on mice initially sensitized to OVA plus an adjuvant, pre-administration of AgNPs before OVA challenges reduced OVA-induced allergic inflammation (Park et al. 2010). A smaller number of studies have focused on ENMs and allergic airway disease caused by house dust mite antigen (HDM), which is both a mouse and human allergen (Ronzani et al. 2014; Shipkowski et al. 2015). These studies showed that co-exposure to multi-walled carbon nanotubes

(MWCNTs) and HDM increased allergic sensitization compared to mice exposed to HDM or MWCNTs alone (Ronzani et al. 2014). Exposure to MWCNTs in mice already sensitized to HDM initially increased level of total bronchoalveolar lavage fluid (BALF) inflammatory cells. At 21 days after MWCNT exposure in HDM-sensitized mice increased signs of lung fibrosis were observed compared to HDM sensitized mice and mice only exposed to MWCNTs.

Genetic Susceptibility and Toxicant Exposure

In addition to factors such as age, nutrition, and gender, genetic background can influence susceptibility to toxicant exposures. For example, genetic polymorphisms in the phase II metabolism gene NAT2 is known to modulate susceptibility to bladder cancer in smokers (García-Closas et al. 2005). Multi-strain mouse models have been used in toxicology to assess the influence of genetic background overall on trichloroethylene toxicity (Bradford et al. 2011). Genome-wide association (GWA) mapping methods using multi-strain mouse panels have been used to discover individual genes that modulate susceptibility to a variety of toxicants including acetaminophen, anthracyclines, isoniazid, and zinc oxide (Wesselkamper et al. 2005; Harrill et al. 2009; Church et al. 2014; Frick et al. 2015). In addition to providing valuable information about susceptibility that could improve the understanding of differences in response of human populations to toxic exposures, mechanistic information is also gained. Given the multitude of existing ENM formulations, testing all potential mechanisms of toxicity would be challenging. However, gene and pathway information from GWA mapping and other systems level methods could help prioritize certain mechanisms. Over the last decade, the Collaborative Cross (CC) has produced a large panel of recombinant inbred (RI) strains derived from eight CC founder strains that cover 90% of *M. Musculus* genetic variation (Churchill et al. 2004; Threadgill and Churchill 2012). The CC RI strains contain a large amount of evenly dispersed inter-strain genetic variation making them an excellent resource for GWA mapping (Aylor et al. 2011).

Dissertation Outline

The overall focus of my dissertation was to investigate the role of genetic background as a determinant of susceptibility to ENM-induced lung inflammation and toxicity. I chose to focus my genetic susceptibility work on on AgNPs because they are incorporated into numerous consumer products and are an NCNHIR particle that our laboratory was tasked with evaluating for *in vivo* pulmonary toxicity. I also chose to focus on QDs as they have applications in many industries and our laboratory has previously shown that susceptibility to QD-induced lung inflammation is modulated by *Gclm,* which is the modifier subunit in glutamate cysteine ligase (*Gcl*) which is the rate limiting enzyme in glutathione production. Differential responses across *Gclm* genotypes provided initial evidence for a genetic component in QD susceptibility (McConnachie et al. 2013). My first specific goal was to investigate the role of genetic background in acute QD- and AgNP induced lung inflammation and toxicity. There are concerns over potential occupational ENM impact on worker lung function. Furthermore, the effects of QDs on mouse lung mechanics have not been explored in the acute setting. While some research has been done on AgNP impact on allergic sensitization, to our knowledge this has not been addressed for QDs. Thus, my second goal was to investigate the role of genetic background modulating susceptibility to QD-induced changes in lung mechanics and HDM allergic sensitization.

Chapter 2. QDs have been shown to induce lung inflammation in mice and rats in multiple studies. However, QD studies to date have been performed in just one strain of mouse or rat rendering them unable to assess the role of genetic background in modulating susceptibility. In Chapter 2, I will discuss our work investigating the range of sensitivity to QD-induced lung inflammation and toxicity among the genetically diverse CC founder strains.

Chapter 3. The CC RI mouse strains have more genetic variation that traditional 2-parental strain RI panels. In Chapter 3, I will discuss our additional assessment of QD-induced lung inflammation and toxicity in CC RI mouse strains and our studies using GWA mapping to identify candidate susceptibility genes and pathways that may help explain differences in susceptibility to QD-induced changes in total BALF protein.

Chapter 4. AgNPs of different sizes and coatings have been shown to induced lung inflammation and toxicity in mice and rats. While there has been one study in rats where more than one strain was assessed, the role of genetic background in modulating susceptibility to AgNP-induced lung inflammation and toxicity has not been thoroughly investigated. In Chapter 4, I will discuss our research characterizing variation in sensitivity to AgNP-induced lung inflammation and toxicity across the CC founder strains and work we did in additional inbred mouse strains as part of a collaboration with researchers at NYU. I will also discuss our experiments using GWA mapping to discover candidate susceptibility genes that may partially underlie previously observed variation in susceptibility to AgNP-induced lung inflammation and toxicity.

Chapter 5. Lung function is one of many health parameters where concerns exist regarding potential detrimental effects of ENM occupational exposure. ENMs have been shown to impact mouse lung mechanics when assessed at least 2 weeks after high dose single exposures. In Chapter 5, I will discuss our work assessing the acute effects of QDs on mouse lung mechanics and the role of genetic background in modulating susceptibility in a more limited context using 2 mouse strains.

Chapter 6. Many ENMs have been shown to enhance allergic sensitization in models using OVA. However, there are few studies investigating the ENM effects on allergic sensitization using HDM, a mouse and human allergen, and no studies have investigated QDs in this

context. In Chapter 6, I will discuss our research evaluating the effects of co-exposure to QDs during sensitization to HDM and the role of genetic background in a more limited context using 2 mouse strains.

Chapter 7. Conclusions and future directions

Hypothesis and Specific Aims

My overall hypothesis was that genetic background is an important determinant of susceptibility to ENM induced lung inflammation and toxicity. To test this hypothesis, I developed 2 specific aims.

Specific Aim 1

Determine if genetic background modulates susceptibility to ENM-induced acute lung inflammation and toxicity.

Chapter 2

> **Specific Aim 1.1:** Characterize how genetic background modulates ENM-induced pulmonary inflammation and toxicity and establish a range of sensitivity across the CC founder strains.

Chapter 3

> **Specific Aim 1.2:** Further characterize inter-strain variability in QD-induced lung inflammation in CC RI strains, compare how phenotypes vary between parental founder and RI strains, and identify candidate susceptibility genes.

Chapter 4

Specific Aim 1.3: Further characterize the effect of genetic background on AgNP-induced lung inflammation using an expanded inbred mouse strain panel and identify candidate susceptibility genes.

Specific Aim 2: Investigate ENM effects on lung mechanics and allergic sensitization in mice that are susceptible and resistant to ENM-induced acute lung inflammation.

Chapter 5

Specific Aim 2.1: Investigate QD effects on lung mechanics in mice that are susceptible and resistant to QD-induced acute lung inflammation.

Chapter 6

Specific Aim 2.2: Investigate QD effects on allergic sensitization in mice that are susceptible and resistant to QD-induced acute lung inflammation.

Chapter 7 Conclusions and future directions

Chapter 1 References

Anderson, D. S., E. S. Patchin, R. M. Silva, D. L. Uyeminami, A. Sharmah, T. Guo, . . . L. S. Van Winkle (2015). "Influence of Particle Size on Persistence and Clearance of Aerosolized Silver Nanoparticles in the Rat Lung." Toxicological Sciences **144**(2): 366-381.

Anderson, D. S., R. M. Silva, D. Lee, P. C. Edwards, A. Sharmah, T. Guo, . . . L. S. Van Winkle (2015). "Persistence of silver nanoparticles in the rat lung: Influence of dose, size, and chemical composition." Nanotoxicology **9**(5): 591-602.

Aylor, D. L., W. Valdar, W. Foulds-Mathes, R. J. Buus, R. A. Verdugo, R. S. Baric, . . . G. A. Churchill (2011). "Genetic analysis of complex traits in the emerging Collaborative Cross." Genome Research **21**(8): 1213-1222.

Botelho, D. J., B. F. Leo, C. B. Massa, S. Sarkar, T. D. Tetley, K. F. Chung, . . . A. J. Gow (2016). "Low-dose AgNPs reduce lung mechanical function and innate immune defense in the absence of cellular toxicity." Nanotoxicology **10**(1): 118-127.

Bradford, B. U., E. F. Lock, O. Kosyk, S. Kim, T. Uehara, D. Harbourt, . . . I. Rusyn (2011). "Interstrain differences in the liver effects of trichloroethylene in a multistrain panel of inbred mice." Toxicological Sciences **120**(1): 206-217.

Brandenberger, C., N. L. Rowley, D. N. Jackson-Humbles, Q. Zhang, L. A. Bramble, R. P. Lewandowski, . . . J. R. Harkema (2013). "Engineered silica nanoparticles act as adjuvants to enhance allergic airway disease in mice." Particle and Fibre Toxicology **10**(1): 26.

Brouwer, D. H. (2012). "Control Banding Approaches for Nanomaterials." The Annals of Occupational Hygiene **56**(5): 506-514.

CDC. (2017). "CDC - Asthma - Data and Surveillance - Asthma Surveillance Data ", from http://www.cdc.gov/asthma/asthmadata.htm

Church, R. J., H. Wu, M. Mosedale, S. J. Sumner, W. Pathmasiri, C. L. Kurtz, . . . A. H. Harrill (2014). "A Systems Biology Approach Utilizing a Mouse Diversity Panel Identifies Genetic Differences Influencing Isoniazid-Induced Microvesicular Steatosis." Toxicological Sciences **140**(2): 481-492.

Churchill, G. A., D. C. Airey, H. Allayee, J. M. Angel, A. D. Attie, J. Beatty, . . . F. Zou (2004). "The Collaborative Cross, a community resource for the genetic analysis of complex traits." Nature Genetics **36**: 1133-1137.

Cui, L. (2013). Exposure assessment and inflammatory response among workers producing calcium carbonate nanomaterials Dissertation, University of Washington.

Frick, A., O. T. Suzuki, C. Benton, B. Parks, Y. Fedoriw, K. Richards, . . . T. Wiltshire (2015). "Identifying genes that mediate anthracyline toxicity in immune cells." Frontiers in Pharmacology **6**.

García-Closas, M., N. Malats, D. Silverman, M. Dosemeci, M. Kogevinas, D. W. Hein, . . . N. Rothman (2005). "NAT2 slow acetylation, GSTM1 null genotype, and risk of bladder cancer: results from the Spanish Bladder Cancer Study and meta-analyses." The Lancet **366**(9486): 649-659.

Harrill, A. H., P. B. Watkins, S. Su, P. K. Ross, D. E. Harbourt, I. M. Stylianou, . . . D. W. Threadgill (2009). "Mouse population-guided resequencing reveals that variants in CD44 contribute to acetaminophen-induced liver injury in humans." Genome Research **19**(9): 1507-1515.

Ho, C. C., H. Chang, H. T. Tsai, M. H. Tsai, C. S. Yang, Y. C. Ling and P. Lin (2013). "Quantum dot 705, a cadmium-based nanoparticle, induces persistent inflammation and granuloma formation in the mouse lung." Nanotoxicology **7**(1): 105-115.

Holland, N. A., L. C. Thompson, A. K. Vidanapathirana, R. N. Urankar, R. M. Lust, T. R. Fennell and C. J. Wingard (2016). "Impact of pulmonary exposure to gold core silver nanoparticles of different size and capping agents on cardiovascular injury." Particle and Fibre Toxicology **13**(1): 48.

Jacobsen, N. R., P. Moller, K. A. Jensen, U. Vogel, O. Ladefoged, S. Loft and H. Wallin (2009). "Lung inflammation and genotoxicity following pulmonary exposure to nanoparticles in ApoE-/- mice." Particle and Fibre Toxicology **6**(2).

Jonasson, S., B. Gustafsson A Fau - Koch, A. Koch B Fau - Bucht and A. Bucht (2013). "Inhalation exposure of nano-scaled titanium dioxide (TiO2) particles alters the inflammatory responses in asthmatic mice." Inhalation Toxicology **25**(4): 1091-7691.

Jung, H., W. Chung, C. H. Lee and S. H. Kim (2012). "Fabrication of white light-emitting diodes based on UV light-emitting diodes with conjugated polymers-(CdSe/ZnS) quantum dots as hybrid phosphors." Journal of Nanoscience and Nanotechnology **12**(7): 5407-5411.

Kim, H. and J. Mazza (2011). "Asthma." Allergy, Asthma & Clinical Immunology **7**(1): S2.

Liao, H.-Y., Y.-T. Chung, C.-H. Lai, S.-L. Wang, H.-C. Chiang, L.-A. Li, . . . S.-H. Liou (2014). "Six-month follow-up study of health markers of nanomaterials among workers handling engineered nanomaterials." Nanotoxicology **8**(sup1): 100-110.

Liao, H. Y., Y. T. Chung, C. H. Lai, M. H. Lin and S. H. Liou (2014). "Sneezing and allergic dermatitis were increased in engineered nanomaterial handling workers." Industrial Health **52**(3): 199-215.

Liou, S.-H., C. S. J. Tsai, D. Pelclova, M. K. Schubauer-Berigan and P. A. Schulte (2015). "Assessing the first wave of epidemiological studies of nanomaterial workers." Journal of Nanoparticle Research **17**: 413.

Lovrić, J., S. J. Cho, F. M. Winnik and D. Maysinger (2005). "Unmodified Cadmium Telluride Quantum Dots Induce Reactive Oxygen Species Formation Leading to Multiple Organelle Damage and Cell Death." Chemistry & Biology **12**: 1227-1234.

Ma-Hock, L., S. Brill, W. Wohlleben, P. M. A. Farias, C. R. Chaves, D. P. L. A. Tenório, . . . B. van Ravenzwaay (2012). "Short term inhalation toxicity of a liquid aerosol of CdS/Cd(OH)2 core shell quantum dots in male Wistar rats." Toxicology Letters **208**(2): 115-124.

Ma-Hock, L., P. M. Farias, T. Hofmann, A. C. Andrade, J. N. Silva, T. M. Arnaud, . . . B. van Ravenzwaay (2013). "Short term inhalation toxicity of a liquid aerosol of glutaraldehyde-coated CdS/Cd(OH) core shell quantum dots in rats." Toxicology Letters **225**(1): 20-26.

McConnachie, L. A., D. Botta, C. C. White, C. S. Weldy, H. W. Wilkerson, J. Yu, . . . T. J. Kavanagh (2013). "The Glutathione Synthesis Gene Gclm Modulates Amphiphilic Polymer-Coated CdSe/ZnS Quantum Dot-Induced Lung Inflammation in Mice." PLOS ONE **8**(5): e64165.

Medintz, I. L., H. T. Uyeda, E. R. Goldman and H. Mattoussi (2005). "Quantum dot bioconjugates for imaging, labelling and sensing." Nature Materials **4**: 435-446.

Neibert, K. D. and D. Maysinger (2011). "Mechanisms of cellular adaptation to quantum dots – the role of glutathione and transcription factor EB." Nanotoxicology **6**(3): 249-262.

Paik, S. Y., D. M. Zalk and P. Swuste (2008). "Application of a Pilot Control Banding Tool for Risk Level Assessment and Control of Nanoparticle Exposures." The Annals of Occupational Hygiene **52**(6): 419-428.

Park, H. S., K. H. Kim, S. Jang, J. W. Park, H. R. Cha, J. E. Lee, . . . S. S. Jung (2010). "Attenuation of allergic airway inflammation and hyperresponsiveness in a murine model of asthma by silver nanoparticles." International Journal of Nanomedicine **5**: 505-515.

Roberts, J. R., J. M. Antonini, D. W. Porter, R. S. Chapman, J. F. Scabilloni, S. H. Young, . . . R. R. Mercer (2013). "Lung toxicity and biodistribution of Cd/Se-ZnS quantum dots with different surface functional groups after pulmonary exposure in rats." Particle and Fibre Toxicology **10**: 5.

Ronzani, C., A. Casset and F. Pons (2014). "Exposure to multi-walled carbon nanotubes results in aggravation of airway inflammation and remodeling and in increased production of epithelium-derived innate cytokines in a mouse model of asthma." Archives of Toxicology **88**(2): 489-499.

Seiffert, J., F. Hussain, C. Wiegman, F. Li, L. Bey, W. Baker, . . . K. F. Chung (2015). "Pulmonary Toxicity of Instilled Silver Nanoparticles: Influence of Size, Coating and Rat Strain." PLOS ONE **10**(3): e0119726.

Shipkowski, K. A., A. J. Taylor, E. A. Thompson, E. E. Glista-Baker, B. C. Sayers, Z. J. Messenger, . . . J. C. Bonner (2015). "An Allergic Lung Microenvironment Suppresses Carbon Nanotube-Induced Inflammasome Activation via STAT6-Dependent Inhibition of Caspase-1." PLOS ONE **10**(6): e0128888.

Silva, R. M., D. S. Anderson, L. M. Franzi, J. L. Peake, P. C. Edwards, L. S. Van Winkle and K. E. Pinkerton (2015). "Pulmonary Effects of Silver Nanoparticle Size, Coating, and Dose over Time upon Intratracheal Instillation." Toxicological Sciences **144**(1): 151-162.

Silva, R. M., D. S. Anderson, J. Peake, P. C. Edwards, E. S. Patchin, T. Guo, . . . K. E. Pinkerton (2016). "Aerosolized Silver Nanoparticles in the Rat Lung and Pulmonary Responses over Time." Toxicological Pathology **44**(5): 673-686.

The Project on Emerging Nanotechnologies. (2017a). "US NanoMetro Map." from http://www.nanotechproject.org/inventories/map/.

The Project on Emerging Nanotechnologies. (2017b). "Consumer Products Inventory." 2017, from http://www.nanotechproject.org/cpi/.

Threadgill, D. W. and G. A. Churchill (2012). "Ten Years of the Collaborative Cross." Genetics **190**(2): 291-294.

Wang, X., Z. Ji, C. H. Chang, H. Zhang, M. Wang, Y.-P. Liao, . . . A. E. Nel (2014). "Use of Coated Silver Nanoparticles to Understand the Relationship of Particle Dissolution and Bioavailability to Cell and Lung Toxicological Potential." Small **10**(2): 385-398.

Wesselkamper, S. C., L. C. Chen and T. Gordon (2005). "Quantitative trait analysis of the development of pulmonary tolerance to inhaled zinc oxide in mice." Respiratory Research **6**(1): 1-12.

Wu, W. T., H. Y. Liao, Y. T. Chung, W. F. Li, T. C. Tsou, L. A. Li, . . . S. H. Liou (2014). "Effect of nanoparticles exposure on fractional exhaled nitric oxide (FENO) in workers exposed to nanomaterials." International Journal of Molecular Sciences **15**(1): 878-894.

Wu, X., H. Liu, J. Liu, K. N. Haley, J. A. Treadway, J. P. Larson, . . . M. P. Bruchez (2003). "Immunofluorescent labeling of cancer marker Her2 and other cellular targets with semiconductor quantum dots." Nature Biotechnology **21**(1): 41-46.

Chapter 2

Susceptibility to Quantum Dot Induced Lung Inflammation Differs Widely Among the Collaborative Cross Founder Mouse Strains

David K. Scoville[1], Collin C. White[1], Dianne Botta[1], Lisa A. McConnachie[1], Megan E. Zadworny[1], Stefanie C. Schmuck[1], Xiaoge Hu[2], Xiaohu Gao[2], Jianbo Yu[1], Russell L. Dills[1], Lianne Sheppard[1,3], Martha A. Delaney[4,5], William C. Griffith[1], Richard P. Beyer[1], Richard C. Zangar[6], Joel G. Pounds[6], Elaine M. Faustman[1] and Terrance J. Kavanagh[1]

Departments of [1]Environmental and Occupational Health Sciences, [2]Bioengineering, [3]Biostatistics, [4]Comparative Medicine and [5]Pathology, University of Washington, Seattle, WA 98195
[6]Systems Toxicology Group - Division of Biological Sciences, Pacific Northwest National Laboratory, Richland, WA 99352

Toxicology and Applied Pharmacology. 2015 Dec 1;289(2):240-50. (Epub 2015 Oct 21.)

Corresponding Author:
Terrance J. Kavanagh, PhD
Department of Environmental and Occupational Health Sciences
Box 354695
University of Washington
Seattle, WA 98195, USA.
Tel: (206) 685-8479
Fax: (206) 685-4696
E-mail: tjkav@uw.edu
Running Title: Mouse Strain Affects QD-induced Lung Inflammation

Abstract

Quantum Dots (QDs) are engineered semiconductor nanoparticles with unique physicochemical properties that make them potentially useful in clinical, research and industrial settings. However, a growing body of evidence indicates that like other engineered nanomaterials, QDs have the potential to be respiratory hazards, especially in the context of the manufacture of QDs and products containing them, as well as exposures to consumers using these products. The overall goal of this study was to investigate the role of mouse strain in determining susceptibility to QD-induced pulmonary inflammation and toxicity. Male mice from 8 genetically diverse inbred strains (the Collaborative Cross founder strains) were exposed to CdSe-ZnS core-shell QDs stabilized with an amphiphilic polymer. QD treatment resulted in significant increases in the percentage of neutrophils and levels of cytokines present in bronchoalveolar lavage fluid (BALF) obtained from NOD/ShiLtJ and NZO/HlLtJ mice relative to their saline (Sal) treated controls. Cadmium measurements in lung tissue indicated strain-dependent differences in disposition of QDs in the lung. Total glutathione levels in lung tissue were significantly correlated with percent neutrophils in BALF as well as with lung tissue Cd levels. Our findings indicate that QD-induced acute lung inflammation is mouse strain dependent, that it is heritable, and that the choice of mouse strain is an important consideration in planning QD toxicity studies. These data also suggest that formal genetic analyses using additional strains or recombinant inbred strains from these mice could be useful for discovering potential QD-induced inflammation susceptibility loci.

Introduction

The market for nanotechnology-enabled products continues to accelerate as the number of novel applications for engineered nanomaterials (ENMs) increases. This has raised concerns regarding environmental and occupational exposures to ENMs. Recent epidemiological studies of workers in ENM manufacturing facilities suggest that occupational ENM exposure may be associated with increased risk of respiratory and cardiovascular toxicity (Cui 2013; Liao et al. 2014; Lee et al. 2015). Thus, better understanding of ENM toxicity is important for human health and the continued success of the nanotechnology industry.

Quantum dots (QDs) are a class of ENM commonly composed of a cadmium/selenium (CdSe), cadmium/tellurium (CdTe), or cadmium/selenium/tellurium (CdSeTe) semiconductor crystalline core surrounded by a multilayer shell of higher band gap material such as zinc/sulfide (ZnS) (Dabbousi et al. 1997; Kim et al. 2004; Medintz et al. 2005; Azzazy et al. 2007; Ho et al. 2013). The superior optical properties such as brightness and photostability of QDs compared to traditional organic dyes make them useful imaging tools. Bioconjugated QDs have been used as excellent direct and indirect immunofluorescent probes for intra- and extracellular targets (Alivisatos 2004; Michalet et al. 2005; Zrazhevskiy et al. 2010; Probst et al. 2013); to label and deliver drugs to tumors (Savla et al. 2011); and to map sentinel lymph nodes *in vivo* (Gao et al. 2004; Kim et al. 2004). QDs have also been utilized as biosensors and in the electronics and energy industries (Hu et al. 2010; Jung et al. 2012; Bae et al. 2013).

The diverse uses of QDs highlight the need to fully understand their toxicity. QDs are known to be cytotoxic in a cell-type, dose, particle size, and surface coating-dependent manner, and release of Cd^{2+} ions plays a role in their cytotoxicity (Kirchner et al. 2005; Lovric et al. 2005; Clift et al. 2008; Hoshino et al. 2011; McConnachie et al. 2012; Smith et al. 2012). Previous studies have confirmed that Cd^{2+} ions can generate reactive oxygen species (ROS), that QDs can release Cd^{2+} ions, and that QDs have been observed to elicit

ROS production and to impact glutathione (GSH) levels (Derfus et al. 2004; Wang et al. 2004; Kirchner et al. 2005; Lovrić et al. 2005; Clift et al. 2010). Thus, QD-induced cytotoxicity is at least partially due to antioxidant depletion and oxidative stress. This is supported by studies in which GSH precursors and inducers have reduced QD cytotoxicity (Lovrić et al. 2005; Neibert and Maysinger 2011).

To our knowledge, no published epidemiological studies exist regarding environmental or occupational exposures to QDs. However, several *in vivo* animal studies have found little toxicity following intravenous administration QDs (Hauck et al. 2010; Su et al. 2011; Ye et al. 2012), which is important if QDs are to be used clinically. However, thrombi harboring QDs have been found in the lungs of mice injected with high doses of CdSe QDs, although thrombi formation was preventable with heparin pretreatment (Geys et al. 2008). In terms of dermal exposures, QDs can be taken up by human keratinocyte cells and showed little toxicity up to 20 nM in concentration (Zhang et al. 2011). QDs have also been shown to penetrate into the outer layers of stratum corneum and epidermis, but not all the way through, porcine skin (Zhang et al. 2008). In contrast, pulmonary exposure to QDs (a potential route of exposure in occupational settings) has been shown to result in neutrophilic and granulomatous inflammation, compromised alveolar-capillary barrier function, DNA damage, and cytotoxicity (Oberdorster et al. 2005; Jacobsen et al. 2009; Ma-Hock et al. 2012; Ho et al. 2013; Ma-Hock et al. 2013; Roberts et al. 2013). Furthermore, as observed for *in vitro* studies, surface coatings (i.e. -COOH vs. $-NH_2$ vs. polyethylene glycol) are known to influence the toxicity and disposition of QDs in mouse and rat lungs (Ho et al. 2013; Roberts et al. 2013). We chose to use trioctylphosphine oxide / poly (maleic anhydride-alt-1-tetradecene) (TOPO-PMAT) coated QDs in this study because of the reproducibility, stability, and solubility that is achieved through incorporating the hydrophobic surface ligand TOPO during synthesis and subsequently adding the amphiphilic polymer PMAT. TOPO-PMAT coating of CdSe/ZnS QDs also results in the retention of excellent optical properties (McConnachie et al. 2012).

Mice are often used as models for mammalian *in vivo* toxicity testing. Inbred strains of mice have been extensively used to investigate the role of genetic background in determining susceptibility to a number of agents. Moreover, through formal genetic analyses, differential responses of inbred mouse strains can increase our understanding of the mechanisms underlying toxicity by revealing genes that influence the response to toxic exposures (Festing et al. 2001; Harrill et al. 2009; Bradford et al. 2011).

The overarching goal of this study was to establish the range of sensitivity to QD-induced lung inflammation and toxicity among the 8 founder strains of the Collaborative Cross (CC), which is an international project to develop new recombinant inbred (RI) mouse strains having high inter-strain genetic variability (Churchill et al. 2004). The CC founder strains have the following designations: 129S1/SvImJ, A/J, C57BL/6J, NOD/LtJ and NZO/HlLtJ (which are traditional laboratory strains), and CAST/EiJ, PWK/PhJ and WSB/EiJ (which are strains recently derived from wild mice). Including 8 strains of mice in our experimental design allows for a robust examination of inter-strain variability, which is important since most *in vivo* QD toxicity studies have been limited to a single mouse strain and conclusions reached in one strain may not hold true for others. Indeed, we found that mouse strain has a major effect on QD-induced lung inflammation, suggesting that in future studies formal genetic analyses using additional strains or recombinant inbred strains from these mice could be useful for discovering loci that are associated with susceptibility to QD-induced inflammation.

Materials and Methods

Ethics Statement

The University of Washington Institutional Animal Care and Use Committee (IACUC) approved all animal procedures carried out in this study (UW Protocol Number 2384-08), and no adverse behavioral effects or apparent suffering were observed.

Animals

Specific pathogen free (SPF) male mice from the following strains were purchased from Jackson Laboratories (Bar Harbor, ME): 129S1/SvImJ (n=28; 12 QD treated, 12 saline, 4 naïve), C57BL/6J (n=49; 28 QD treated, 17 saline, 4 naïve), A/J (n=37; 22 QD treated, 11 saline, 4 naïve), CAST/EiJ, NOD/LtJ, NZO/HlLtJ, PWK/PhJ and WSB/EiJ (n=16; 6 QD, 6 saline, 4 naïve). Hereafter, mouse strain names are abbreviated as indicated in the parentheses following each strain: 129S1/SvImJ (129), C57BL/6J (B6), A/J (AJ), CAST/EiJ (CAST), NOD/LtJ (NOD), NZO/HlLtJ (NZO), PWK/PhJ (PWK) WSB/EiJ (WSB). Mice were received at approximately 6 weeks of age and all experiments were done within 4 weeks of arrival at the University of Washington. Baseline measures were made in naïve mice. Animals were housed under modified SPF conditions in an Association for Assessment and Accreditation of Laboratory Animal Care (AAALAC)-approved facility at the University of Washington.

Quantum dots

The amphiphilic polymer coated QDs used in this study were synthesized and characterized in the laboratory of Dr. Xiaohu Gao in the Department of Bioengineering at the University of Washington as previously described (Pellegrino et al. 2004; Bagalkot and Gao 2011; McConnachie et al. 2012; McConnachie et al. 2013). They consisted of a CdSe core, a ZnS shell, and an outer coating of tri-n-octylphosphine oxide, poly(maleic anhydride-alt-1-tetradecene (TOPO-PMAT).

Oropharyngeal aspiration of QDs

Animals were anesthetized prior to treatment using 4% Isoflurane. Mice received a dose of 6 µg Cd equivalents/kg body weight (BW) of 10 nM TOPO-PMAT CdSe/ZnS QDs in 0.9% sterile saline, which is comparable to a hypothetical 40 hr work week cumulative

exposure of 4.6 mg/kg calculated using the current Occupational Safety and Health Administration (OSHA) permissible exposure limit (PEL) of 5 μg/m^3 and average human breathing rates from the EPA Exposure Factors Handbook for ages 16-71 (1.62 m^3/hr), and 70 kg as a worker body weight. Oropharyngeal aspiration (OPA) was used to deliver either QDs or 1.53 μl/g BW 0.9% sterile saline as a vehicle control. As noted above, 4 naïve control animals from each strain received no treatment. Mice were euthanized using CO_2 narcosis and cervical dislocation eight hours after dosing. This time point was selected in order to detect both cytokines and neutrophils in the same BAL sample. Prior *in vitro* studies with alveolar macrophages had shown that although 4 hr after exposure to QDs was optimal for detection of cytokines, there was still a detectable level of cytokines at 8 hr [43]. Moreover, sufficient neutrophil influx was detected in mice 8 hr after QD exposure via nasal instillation(McConnachie et al. 2013). Tissues were removed and flash frozen in liquid nitrogen and bronchoalveolar lavage was performed as described below. Additional AJ and B6 mice were euthanized immediately, 30 min, 1 hr and 3 hr following OPA of the same dose of QDs (n=4 per time point) or Saline (n=2 at 3 hr, and 1 at the other time points) for the purpose of analyzing cadmium levels in lung tissue.

Bronchoalveolar lavage

Bronchoalveolar lavage (BAL) was performed 3 times with 3 lung inflations using 1 mL phosphate buffered saline (PBS) per lavage, as previously described (Weldy et al. 2011). CAST/EiJ, WSB/EiJ and PWK/PhJ mice received 700 μL PBS per lavage due to the reduced lung volume in these smaller strains.

Flow cytometry

BAL samples were centrifuged at ~500g to pellet cells. The supernatant from the 1st lavage was stored at -80 °C for later analyses and is referred to hereafter as bronchoalveolar lavage fluid (BALF). Supernatants from the 2nd and 3rd lavages were

discarded. The cells from all 3 lavages were then pooled and processed for immunophenotyping and flow cytometry to identify the relative number of macrophages and neutrophils present in BALF using a slightly modified method of that performed previously (Weldy et al. 2011). Cells were stained for CD11b, Ly-6G/Ly-6C (Gr1) and F4/80 with a phycoerythrin conjugated monoclonal antibody against Cd11b (AbCam, Cambridge, MA), biotinylated anti-mouse Gr1 conjugated to streptavidin/AlexaFluor350 (BioLegend, San Diego, CA) and anti-F4/80 conjugated to Alexafluor 488 (eBioscience, San Diego, CA). Gating of flow cytometric bivariate plots was used to determine the percentage of neutrophils and macrophages in BALF. Neutrophils were classified as cells high in Cd11b and low in F4/80 fluorescence. Macrophages were identified as being high in F4/80 fluorescence and either high or low in Gr1 fluorescence. $F4/80^{+}/Gr1^{hi}$ cells have been described in a previous study as inflammatory monocytes (Mosa et al. 2009).

BALF cytokine/inflammatory protein measurements using ELISA microarray

Slides were printed using a piezoelectric GeSiM NanoPlotter 2 and processed as described previously (Servoss et al. 2009). All ELISA reagents for the 18 cytokine assays (amphiregulin (AMR), eotaxin, granulocyte-colony stimulating factor (GCSF), interleukins 1α, 6, and 12 (IL-1α, 6, and 12), GRO1 oncogene (KC; CXCL1), matrix metalloproteinase 2 (MMP2), small inducible cytokine A5 (RANTES; CCL5), thymus and activation-regulated chemokine (TARC; CCL17), tumor necrosis factor (TNFα), vascular endothelial growth factor A (VEGF), monocyte chemotactic protein 1 (MCP1), macrophage-derived cytokine (MDC), macrophage inflammatory proteins 1α (MIP-1α, CCL3), 1β (MIP-1β, CCL4), 1γ (MIP-1γ, CCL9) and 2 (MIP-2, CXCL2)) were purchased from R&D Systems. In brief, for every chip, each of the 18 capture antibodies for the individual ELISAs were printed onto 4 spots. Samples were thawed on ice, centrifuged to remove any particulates, and diluted with 0.1 volume of 10X assay buffer (final assay concentration: 0.1 mg casein/ml and 1000 pg green fluorescent protein/ml) in PBS. Samples were then processed in triplicate on the ELISA chips

as described (Servoss et al. 2009). After overnight incubation with the samples, chips were washed and incubated with a mixture of biotinylated detection antibodies. The biotinylation signal was amplified using the biotinyltyramide amplification system and the fluorescent signal added using tagged streptavidin (Woodbury et al. 2002). The fluorescent intensity of the spots was imaged using a Tecan Reloaded laser scanner and quantitated using ScanArray Express software. Standard data were generated using serial dilutions of expressed antigens. The fluorescent data were normalized based on results from an internal calibrant assay (Zangar et al. 2009). Standard curves were then fit with the Protein Microarray Analysis Tool (ProMAT) using the four-parameter logistic curve-fitting option (White et al. 2006) and used by ProMAT to generate antigen concentration values for the samples based on the adjusted spot fluorescent intensities.

BALF total protein

Total protein in BALF samples was measured using the Bio-Rad Protein Assay (BioRad, Hercules, CA) according to the manufacturer's instructions and absorbance was read at 590 nm using a SpectraMax 190 spectrophotometric plate reader (Molecular Devices, Sunnyvale, CA). All samples and standards were analyzed in triplicate.

Cadmium analysis

Samples of frozen right lung tissue (~20 - 40 mg) from mice sacrificed 8 hr after OPA from each strain were randomly selected for analysis (6 QD treated and 3 saline treated). In addition, samples were also taken from an additional 4 QD treated AJ and B6 mice immediately, 30 min, 1 hr and 3 hr after OPA. For saline treated controls in both strains, samples were taken from 1 mouse immediately, 30 min and 1 hr after OPA, and from 2 mice 3 hr after OPA. Following nitric acid/microwave digestion, Cd levels were measured using inductively-coupled plasma mass spectrometry (ICP-MS) following a modified EPA Method 6020A with an Agilent 7500ce ICP-MS (US-EPA 2007). The cadmium

content in QD dosing solution was confirmed by the same method. The limit of quantification (LOQ) was 0.1 ng Cd per sample. The amount of Cd per tissue was normalized by tissue weight. Samples that had Cd levels below the LOQ were assigned the value of the LOQ / square root of 2 before being divided by lung tissue weight. The kinetics of Cd clearance from the lungs was assessed using an exponential decay model.

Lung total glutathione

Total glutathione levels in lung homogenates were measured after reducing all disulfide forms using previously described procedures (Weldy et al. 2011).

Statistical Analyses

All data were processed and analyzed using Microsoft Excel (Microsoft Corporation. Redmond, WA), GraphPad Prism (GraphPad Software, La Jolla, CA), and R (R Core Team 2014). Data from all endpoints were log transformed to improve normality prior to analysis. Two-way analysis of variance (ANOVA) was performed to examine QD treatment and mouse strain effects. If a significant treatment effect was detected, post-hoc t-tests were performed between treatment groups and resulting p-values were adjusted using the False Discovery Rate (FDR) method in the p.adjust function in R. Post hoc t-tests were performed separately between QD and saline groups and between saline and naïve groups. In a secondary analysis, we performed t-tests on absolute BALF cell numbers between QD and saline treated mice in each strain. The strain order in all data plots, which were created using the ggplot2 package in R, is determined by the ratio of the percent neutrophils in BALF in QD treated mice compared to strain matched saline controls in ascending order (Figure S1) (Wickham 2009). Colors used for mouse strains in the plots are those designated by the CC organizers for the founder strains. In order to reveal potential relationships among outcome measures across strains, a hierarchal clustering analysis was performed. Prior to clustering, non log-transformed data were converted into z-scores within

each assay, essentially normalizing each assay to a mean of 0 and a standard deviation of 1. Individual animal z-scores in each assay were averaged for each strain and treatment group. Clustering was performed using the heatmap.2 function in the gplots package in R, with defaults of Euclidean distance and complete linkage as methods for dendrogram formation (Warnes et al. 2013). This is a modified method from those used in previous nanomaterial studies where multiple groups and assays are compared (Shaw et al. 2008; McConnachie et al. 2012). Simple linear regression was used to further examine potential relationships seen in the cluster analysis and to analyze relationships between lung glutathione and BALF neutrophils, cytokines, and lung Cd. Broad-sense heritability was calculated using one-way ANOVA for select phenotypes to estimate the genetic contribution to the overall phenotypic variability. Inter-class correlation, $r_{1,}$ was calculated as (MSB - MSW)/(MSB + (n - 1)MSW), where MSB is the mean square between strains and MSW is mean square within strains obtained from ANOVA analysis, and n is the number of mice. The coefficient of genetic determination, g^2 was calculated as (MSB - MSW)/(MSB + (2n - 1)MSW) (Billat et al. 2005; Rutledge et al. 2014). The sensitivity analysis performed on percent neutrophils in BALF entailed removing potential outliers using Tukey's interquartile range (IQR) method which defines outliers as either less than Q1 minus 1.5 times, or Q3 plus 1.5 times the IQR within each strain and treatment group, and then repeating the two-way ANOVA and t-tests (Tukey 1977).

Results

Cd content in lung tissue

Cd was measured as a marker of QD presence in the lung 8 hours after exposure. Cd content was highly variable across the strains and a significant interaction between mouse strain and QD treatment was observed (Figure 1A) indicating strain dependent differences in disposition. B6, PWK, and WSB mice all had average levels of <0.1 ng Cd / mg tissue, with

B6 being the lowest (Figure 1A). AJ mice had an average of 0.16 ng Cd / mg tissue. The 129, CAST, NOD, and NZO mice had average Cd levels between 2.5 and 3 ng Cd / mg tissue (Figure 1A). In order to further investigate the notable variability present at 8 hr post OPA, we also measured Cd levels in AJ and B6 mice immediately, 30 min, 1 hr and 3 hr after OPA (Figure 1B). Interestingly, QDs appeared to have a longer half-life in AJ mice (4.5 hours, 95% CI: 2.8 to10.9 hr) compared to B6 mice (1.2 hours, 95% CI: 1.0 to 1.6 hr). In keeping with their slower clearance, QD treated AJ mice had significantly higher lung Cd levels at 8 hr than B6 mice. While there is a suggestion that AJ mice might have higher levels than B6 even immediately following QD exposure, this potential difference was not statistically significant.

Neutrophils in BALF

We found high variability across strains for BALF neutrophils and observed a significant interaction between mouse strain and QD treatment. In particular, NOD and NZO mice showed a significant increase in the percentage and absolute numbers of neutrophils in BALF following QD treatment compared to strain-matched saline-treated controls (Figure 2A and Table S1). Notably, with the exception of one mouse, all treatment groups of B6 had very few neutrophils. The presence of neutrophils in BALF from the remaining strains (129, AJ, CAST, PWK and WSB) was too variable to detect any statistically significant treatment related differences.

Macrophages in BALF

We found significant elevations in percent $Gr1^+$ macrophages in QD treated animals compared to saline controls in NZO and B6 mice (Figure 2B). Interestingly, 129, AJ, NOD, and PWK mice showed comparable levels of $Gr1^+$ macrophages in QD and saline treated mice, yet in these strains saline treated mice were different from their respective naïve controls (Figures 2B and S4). No differences were observed in absolute numbers of $Gr1^+$,

total macrophages, or total BALF cells between QD and saline treated mice in any strain (Table S1).

Cytokines in BALF

Of the 18 cytokines and inflammation-associated proteins assayed with the ELISA microarray, the concentration of 6 (IL-10, IL-1α, IL-12, IL-6, MIP-1β and MIP-2) were below the limit of detection. Of the remaining 12 cytokines analyzed all were affected by strain; Eotaxin, MDC, and RANTES were also affected by QD treatment, and KC, MIP-1α, MIP-1γ, G-CSF, were affected both by strain and QD treatment and had significant elevations in QD vs. saline treated mice in at least one strain (Figures 3 and S3). KC was elevated in QD treated AJ and WSB mice relative to their respective saline controls (Figure 3A). MIP-1α was elevated in BALF from QD treated NOD mice relative to saline controls (Figure 3B). In B6 and NZO mice, the levels of MIP-1α were similar in QD and saline treated mice but saline treated mice were different from their respective naïve controls (Figures 3B and S4). Levels of MIP-1γ were significantly higher in QD-treated AJ and 129 mice compared to their respective saline controls (Figure 3C). In CAST, NOD, and NZO mice, levels of MIP-1γ were similar in QD and saline treated mice but saline treated mice were different from their respective naïve controls (Figures 3C and S4). BALF G-CSF levels were elevated in QD treated AJ mice compared to saline controls (Figure 3D).

Total protein in BALF

We measured the total protein present in BALF supernatants as a marker of compromised capillary/alveolar barrier function. While we found both strain and treatment were significant factors contributing to absolute levels of protein, we were unable to detect within strain differences in post-hoc analyses between QD-treated and saline-treated controls (Figure 4A). In addition, in 129 mice, the levels of total protein in BALF were similar

in QD and saline treated mice but saline treated mice were different from their respective naïve controls (Figures 4A and S4).

Total glutathione in lung tissue

To investigate whether total lung glutathione levels were affected by QD exposure, total glutathione (consisting of GSH+GSSG) was measured in lung homogenates (Figure 4B). While QD treatment and mouse strain significantly influenced glutathione levels we were unable to detect within strain differences in post-hoc analyses between QD-treated and saline-treated controls (Figure 4B). In addition, in CAST, NZO, PWK and WSB levels of total glutathione were similar in QD and saline treated mice but saline treated mice were different from their respective naïve controls (Figures 4B and S4). Modest but significant inverse associations were observed between the levels of lung tissue glutathione and BALF neutrophils, cytokines, and lung Cd (Figure S2).

Clustering analysis

In order to objectively examine potential relationships among outcomes measures across all assay results among the different mouse strains and treatment groups, a cluster analysis of z-scores for each assay was performed (Figure 5). Interestingly, at the highest level of clustering, the algorithm separated all strains according to treatment. In addition, there is a cluster of high z-scores for almost all endpoints in QD treated NZO and AJ mice. Within this cluster, a block of particularly high scores can be seen for percent neutrophils in BALF, MIP-1α, KC, G-CSF, MIP-1γ, MDC, and Gr1+ macrophages. QD treated WSB and NOD mice had similar z-scores for many of the same outcomes as AJ and NZO mice but were not adjacently clustered. Overall, the heat map echoed the results from each assay analyzed separately, such that mouse strains showing significant QD treatment in a specific endpoint tended to have the highest z-scores and be clustered with that assay in the heat map.

Correlation of neutrophils in BALF with Cd levels in lung tissue and BALF Cytokines

To examine the relationship between lung Cd levels and the percentage of neutrophils in BALF, linear regression analysis was performed on the log-transformed values for neutrophils in BALF, versus the log-transformed lung tissue Cd levels. Relationships between lung Cd levels, BALF neutrophils, MIP-1α, KC, and G-CSF were also investigated in the same manner since MIP-1α, KC, and G-CSF were the cytokines most closely clustered with BALF neutrophils and that were affected by QD treatment in at least one mouse strain. Significant positive associations were found between Cd levels and MIP-1α (Figure 6A), KC (Figure 6B), G-CSF (Figure 6C), and between Cd levels and BALF neutrophils (Figure 6D). BALF neutrophils were also positively associated with the levels of MIP-1α (Figure 7A), KC (Figure 7B), and G-CSF (Figure 7C).

Heritability Estimates

Overall heritability for selected phenotypes was calculated separately for naïve, saline treated, and QD treated mice to estimate how much of the total variation was genetically determined (Table 1). Among naïve mice, the most heritable phenotypes were the levels of neutrophils in BALF, the levels of lung tissue glutathione, and the levels of BALF MIP-1γ. In saline and QD treated mice, BALF MIP-1γ was the trait with the highest heritability. Negative heritability estimates seen in saline treated mice indicate more phenotypic variability within rather than between strains. As seen in Figure S4, some animals (potentially outliers) were highly reactive to saline compared to other mice in the same strain, which can increase intra-strain variability and decrease heritability estimates. The heritability of BALF neutrophil response and glutathione levels were lower for saline and QD treated mice relative to that observed for naïve mice. However, heritability of these phenotypes was greater for QD-treated mice than saline treated mice.

Discussion

QDs have the potential to benefit society through many industrial and biomedical applications. However, their small size and heavy metal composition raises concerns about their safety. In this study we aimed to establish the range of sensitivity to QD-induced lung inflammation and toxicity among the 8 founder strains of the Collaborative Cross. We observed that exposure to TOPO PMAT CdSe/ZnS QDs via oropharyngeal aspiration induced an acute pulmonary inflammatory response in some of the mouse strains as defined by neutrophil influx and pro-inflammatory cytokine levels in BALF. NOD and NZO mouse strains exhibited significant increases in BALF neutrophils after QD exposure compared to saline treated controls. In addition, NOD and AJ mice exhibited significant increases in multiple pro-inflammatory cytokines relative to saline treated mice. Across all strains, we observed significant positive correlations between lung tissue Cd and BALF neutrophils in QD treated animals. In a secondary analysis, we reported absolute numbers of neutrophils, $Gr1^+$ and total macrophages, and total BALF cells and found that QD-treated NOD and NZO mice had significantly higher levels of neutrophils compared to strain matched saline controls (Table S1).

To examine the robustness of the results for percent neutrophils in BALF, our primary indicator of inflammation, we performed a sensitivity analysis. We found two differences between the primary and sensitivity analyses in terms of statistical significance. First, the interaction between strain and treatment in the two-way ANOVA became marginally significant ($p=0.068$) in the sensitivity analysis. The second difference we observed was that in the sensitivity analysis, QD-treated AJ mice showed significant increases in BALF neutrophils compared to their strain-matched saline control mice.

In the clustering analysis, data for the different outcome measures were normalized using z-score conversions in order to examine potential relationships across strains and treatments. Overall, we found that AJ mice clustered with NZO mice and had z-scores similar to those of NOD mice for neutrophils and many of the inflammatory cytokines. These

observations complement the results from the sensitivity analysis suggesting that AJ mice are likely as susceptible to QDs as these other strains.

In addition, MIP-1α and KC were the two cytokines clustered nearest to neutrophils in AJ and NZO QD treated mice, indicating that these two strains had some of the highest standardized values for neutrophil influx as well as these neutrophil chemotactic proteins. MIP-1α (CCL3) is a C-C motif chemokine known to recruit neutrophils through receptors CCR1 and CCR5 (Reichel et al. 2012). Up-regulation of MIP-1α has been observed after bleomycin or single wall carbon nanotube exposures in mice (Chou et al. 2008; Saito et al. 2008). In the case of bleomycin, which induces oxidative stress and fibrosis, IL-6 was shown to mediate levels of MIP-1α (Saito et al. 2008). KC is a C-X-C motif chemokine that binds CXCR2 and is the mouse functional equivalent to human IL-8. Increases in lung KC levels have been observed in previous nanomaterial studies in rodents (Rossi et al. 2010; Ma-Hock et al. 2012; Ho et al. 2013). In a recent study of work place exposure to calcium carbonate nanoparticles, increases in the level of IL-8 were associated with increased exposure to these particles, indicating that ENM exposed workers may have increased lung neutrophil influx and inflammation (Cui 2013). Other ENM human exposure studies in the workplace have shown decreased pulmonary function, and increased signs of oxidative stress in the lung including increased malondialdehyde and 4-hydroxyhexenal in exhaled breath (Lee et al. 2015). Increased levels of vascular cell adhesion molecule 1 (VCAM), a proposed biomarker for cardiovascular disease, were also observed in one of the studies (Vasan 2006; Liao et al. 2014).

In our studies, NOD mice had KC and MIP-1α z-score values similar to those in AJ and NZO mice were not clustered together with these strains due to their responses in the other assays. Even though WSB mice did not exhibit statistically significant increases in BALF neutrophils, they had levels of KC similar to those of NOD mice, possibly indicating that they are also susceptible to QD-induced lung inflammation. Interestingly, across all strains, MIP1-α and KC levels were the 1st and 2nd most strongly correlated with BALF

neutrophils and lung Cd (Figure 6). However, the strength and significance of the relationship appears to be different among the individual strains. While the exact explanation for these differences in response to these cytokines is obviously complicated, it is likely related to their genetics. For example, when we examined the correlation between KC cytokine levels and percent neutrophils within the individual strains, 5 strains (129, B6, AJ, NOD and NZO) showed a significant correlation (Table S2). The same 5 strains also showed significant correlations between percent neutrophils and G-CSF which regulates the development and release of bone marrow derived neutrophils, and potentially influences chemotaxis (Table S2) (Noursadeghi et al. 2005; Hamilton and Achuthan 2013). Seven strains (all strains except PWK) showed a significant correlation between Mip1a and percent neutrophils in BALF (Table S2). Thus, it may be that certain strains respond more vigorously to one cytokine as the primary driver of neutrophilia (e.g. Mip1α but not KC for WSB mice), whereas other strains respond to all 3 factors (129, B6, AJ, NOD and NZO). Still others (PWK mice) seem not to respond to KC, MIP1a, or G-CSF. Furthermore, there are likely other cytokines, alarmins or other chemotactic factors that we have not measured that also drive the neutrophil response in a strain dependent manner. In addition, the significant increases in BALF of KC, MIP-1α, and G-CSF and their correlation with BALF neutrophils and lung Cd suggests the potential involvement of the nuclear factor kappa-light-chain-enhancer of activated B cells (NF-κB) signaling pathway in the observed QD-induced inflammation since the transcription of all three of these genes can be induced by NF-κB (Grove and Plumb 1993; Ohmori et al. 1995; Abraham 2003). In addition, AJ, 129 and NZO mice had the highest z-scores for MIP-1γ which has been associated with dendritic cell recruitment (Zhao et al. 2003; Rose et al. 2010).

Overall, the results of our study are in agreement with other studies investigating QD-induced pulmonary toxicity and injury in that all studies including our own have shown neutrophilic inflammation and pro-inflammatory cytokine induction (Jacobsen et al. 2009; Ma-Hock et al. 2012; Ho et al. 2013; Ma-Hock et al. 2013; Roberts et al. 2013). Increased

total protein levels in BALF is a valuable measure of alveolar/capillary barrier integrity (Matute-Bello et al. 2011). In contrast to other studies that found increased total BALF protein, with QD treatment, we did not observe increased total BALF protein in QD treated mice compared to genetically matched controls (Jacobsen et al. 2009; Roberts et al. 2013). We interpreted these findings as evidence that the alveolar/capillary barrier was not severely compromised after QD exposure. Moreover, preliminary examinations of representative lung tissue sections prepared from all eight strains found no consistent treatment-related histopathological changes (not shown). To our knowledge, our study is the first to evaluate QD-induced inflammatory responses in the lungs of different mouse strains.

We evaluated the levels of glutathione, which is an important thiol antioxidant and is known to form complexes with Cd and other metals, as a marker of oxidative stress and to determine its potential role in the observed inflammatory response (Ballatori 1994). Depletion of GSH has been used previously as a marker of oxidative stress associated with QD exposure in an *in vitro* study where no GSSG was detected (Clift et al. 2010). In our study, we observed that total glutathione levels were affected significantly by both strain and treatment and to varying degrees were correlated with levels of Cd, BALF neutrophils and cytokines (Figure S2). However, we were unable to detect within strain differences in glutathione between QD and saline treated mice. Also, while not statistically significant, B6 mice, the strain most resistant to neutrophil influx, appear to have increased total glutathione in QD treated animals relative to saline controls, which may indicate that they are synthesizing more glutathione *de novo* after QD treatment. In an *in vitro* study investigating the role of glutathione in cellular response to QD exposure, uncapped CdTe QDs increased the levels of total and oxidized (GSSG) glutathione in rat pheochromocytoma (PC12) cells when measured 24 hr after exposure (Neibert and Maysinger 2011). In our previous work, we exposed both cells and mice to the same relatively stable TOPO PMAT QDs used in this current study. We found them to be not very cytotoxic. However, they can

increase transcription of the glutathione synthesis gene *Gclm* both *in vitro* and *in vivo* (McConnachie et al. 2012; McConnachie et al. 2013). We interpret our findings and those of other studies investigating QD exposure, glutathione, oxidative stress, and inflammation as evidence that pulmonary exposure to the QDs used in this study may result in mild oxidative stress and that GSH may potentially influence the inflammatory response. However, this may depend on the mouse strain being used, as well as the dose, coating and stability of the QDs (Derfus et al. 2004; Wang et al. 2004; Kirchner et al. 2005; Lovrić et al. 2005; Clift et al. 2010; Su et al. 2010).

Measuring tissue levels of Cd as a marker for QD exposure is a common method in *in vivo* QD toxicity studies. When we assessed Cd levels 8 hr after OPA, we uncovered a surprising amount of variability across the different strains. Some strains had remarkably higher levels of Cd (129, AJ, CAST, NOD, NZO) than others (B6, PWK, and WSB). To further investigate the observed variability, we also measured lung tissue Cd levels in AJ and B6 mice immediately following OPA, and at 30 min, 1 hr, and 3 hr after dosing. Interestingly, the half life of QDs in the lung appeared to be longer in AJ than B6 mice and at 8 hr after QD exposure, AJ mice had significantly higher lung Cd levels than B6 mice. While not statistically significant, there is a suggestion that QD treated AJ mice might have higher levels of Cd than B6 mice immediately following OPA. This suggested immediate difference could be due to inherent strain differences in alveolar size and airway branching architecture (Soutiere et al. 2004; Metzger et al. 2008). Differences in lung physiology could also potentially explain part of the difference in QD clearance between B6 and AJ mice. A previous study using intratracheal administration of QDs in rats found that almost 100% of administered Cd remaining in the lung at 1 and 3 days compared with the lung-associated lymph nodes (LALN), and kidneys (Roberts et al. 2013). However, starting at 7 days and continuing through the last measurement at 28 days, lung levels decreased and LALN and kidney levels increased. It should be noted that the kidney had ~3 times as much Cd as the LALN at all detectable points (Roberts et al. 2013). A similar pattern was observed when

QDs were constantly inhaled such that over time Cd levels decreased in the lung, but increased in the liver and kidney between days 5 and 26 of exposure (Ma-Hock et al. 2012). Again, the lung held the majority of the Cd compared to other measured tissues (Ma-Hock et al. 2012). Even though half life in the lung was not calculated in these studies, it would have certainly been longer than those calculated in our study, which could possibly be explained by differences in species, dosing methods (OPA vs intra-tracheal instillation and inhalation), and in QD coatings (-COOH and -NH2 coated vs TOPO-PMAT). In addition, we previously measured lung Cd in mice following intra-nasal administration of QDs and showed that the kinetics of QD clearance up to 24 hr after nasal-instillation from the lungs were dependent on glutathione synthesis capacity (McConnachie et al. 2013). In this study, lung Cd was mildly but significantly associated with lung total glutathione levels. Results from our study and others suggest that Cd distribution following pulmonary exposure is likely species and strain dependent and that lung glutathione is a modulating factor in mice.

Interestingly, we also observed that in some outcome measures, saline and QD treated mice responded similarly but were different than naïve mice of the same strain, suggesting that strains exhibiting this pattern across multiple outcome measures may be highly reactive regardless of the type of treatment, and thus may not be particularly useful for isolating QD specific effects. Nonetheless, our positive estimates of heritability for a number of outcome measures (MIP-1α, MIP-1γ, KC, neutrophils and GSH) infer a genetic component for the QD induced inflammatory response.

In conclusion, TOPO-PMAT coated QDs induce mouse strain-dependent acute lung inflammation when delivered via oropharyngeal aspiration. Specifically, NOD and NZO mice showed significant increases in BALF neutrophils. NOD mice also showed significant increases in some pro-inflammatory cytokines in QD-treated mice over saline controls. Both NOD and NZO mice should be considered sensitive strains. AJ mice could also possibly be considered a sensitive strain given significant increases relative to saline controls in all pro-inflammatory cytokines where strain differences were detectable and the fact that when a

potential outlier was removed, they showed highly significant increases in BALF neutrophils between these groups as well. In contrast, QD treatment did not elicit inflammation in B6 mice and we consider this strain to be the most resistant of the CC founder strains. Other strains showed high variability in BALF neutrophils and it is difficult to draw conclusions regarding their susceptibility. In addition, our data provide evidence that MIP1α and to a lesser degree KC and G-CSF appear to be important components of the QD-induced neutrophil response in the lung. The significant associations observed in our data between Cd, glutathione, and BALF neutrophils suggest that TOPO-PMAT QDs induce mild oxidative stress. Collectively, the data from this study confirm that the ability of QDs to cause pulmonary inflammation depends on which mouse strain is examined and suggests that formal genetic analyses using additional strains or recombinant inbred strains derived from these mice could be useful for discovering potential QD-induced inflammation susceptibility loci.

Acknowledgements

The authors wish to thank Drs. Christopher M. Carosino, Samir N. Kelada, Ivan Rusyn and Terry Gordon for their helpful comments and suggestions. This work was supported by NIH Grants U19ES019545, U19ES019544, R01ES016189, P30ES007033 and T32ES015459.

Chapter 2 References

Abraham, E. (2003). "Nuclear factor-kappaB and its role in sepsis-associated organ failure." The Journal of Infectious Diseases **187 Suppl 2**: S364-369.

Alivisatos, P. (2004). "The use of nanocrystals in biological detection." Nature Biotechnology **22**(1): 47-52.

Azzazy, H. M. E., M. M. H. Mansour and S. C. Kazmierczak (2007). "From diagnostics to therapy: Prospects of quantum dots." Clinical Biochemistry **40**(13–14): 917-927.

Bae, W. K., Y.-S. Park, J. Lim, D. Lee, L. A. Padilha, H. McDaniel, . . . V. I. Klimov (2013). "Controlling the influence of Auger recombination on the performance of quantum-dot light-emitting diodes." Nature Communications **4**.

Bagalkot, V. and X. Gao (2011). "siRNA-Aptamer Chimeras on Nanoparticles: Preserving Targeting Functionality for Effective Gene Silencing." ACS Nano **5**(10): 8131-8139.

Ballatori, N. (1994). "Glutathione mercaptides as transport forms of metals." Advances in Pharmacology **27**: 271-298.

Billat, V. L., E. Mouisel, N. Roblot and J. Melki (2005). "Inter- and intrastrain variation in mouse critical running speed." Journal of Applied Physiology **98**(4): 1258-1263.

Bradford, B. U., E. F. Lock, O. Kosyk, S. Kim, T. Uehara, D. Harbourt, . . . I. Rusyn (2011). "Interstrain differences in the liver effects of trichloroethylene in a multistrain panel of inbred mice." Toxicological Sciences **120**(1): 206-217.

Chou, C.-C., H.-Y. Hsiao, Q.-S. Hong, C.-H. Chen, Y.-W. Peng, H.-W. Chen and P.-C. Yang (2008). "Single-Walled Carbon Nanotubes Can Induce Pulmonary Injury in Mouse Model." Nano Letters **8**(2): 437-445.

Churchill, G. A., D. C. Airey, H. Allayee, J. M. Angel, A. D. Attie, J. Beatty, . . . F. Zou (2004). "The Collaborative Cross, a community resource for the genetic analysis of complex traits." Nature Genetics **36**: 1133-1137.

Clift, M. J., M. S. Boyles, D. M. Brown and V. Stone (2010). "An investigation into the potential for different surface-coated quantum dots to cause oxidative stress and affect macrophage cell signalling in vitro." Nanotoxicology **4**(2): 139-149.

Clift, M. J. D., B. Rothen-Rutishauser, D. M. Brown, R. Duffin, K. Donaldson, L. Proudfoot, . . . V. Stone (2008). "The impact of different nanoparticle surface chemistry and size on uptake and toxicity in a murine macrophage cell line." Toxicology and Applied Pharmacology **232**(3): 418-427.

Cui, L. (2013). Exposure assessment and inflammatory response among workers producing calcium carbonate nanomaterials Dissertation, University of Washington.

Dabbousi, B. O., J. Rodriguez-Viejo, F. V. Mikulec, J. R. Heine, H. Mattoussi, R. Ober, . . . M. G. Bawendi (1997). "(CdSe)ZnS Core−Shell Quantum Dots: Synthesis and Characterization of a Size Series of Highly Luminescent Nanocrystallites." The Journal of Physical Chemistry B **101**(46): 9463-9475.

Derfus, A. M., W. C. W. Chan and S. N. Bhatia (2004). "Probing the Cytotoxicity of Semiconductor Quantum Dots." Nano Letters **4**(1): 11-18.

Festing, M. F. W., P. Diamanti and J. A. Turton (2001). "Strain differences in haematological response to chloroamphenicol succinate in mice: implications for toxicological research." Food and Chemical Toxicology **39**(4): 375-383.

Gao, X., Y. Cui, R. M. Levenson, L. W. K. Chung and S. Nie (2004). "In vivo cancer targeting and imaging with semiconductor quantum dots." Nature Biotechnology **22**(8): 969-976.

Geys, J., A. Nemmar, E. Verbeken, E. Smolders, M. Ratoi, M. F. Hoylaerts, . . . P. H. M. Hoet (2008). "Acute Toxicity and Prothrombotic Effects of Quantum Dots: Impact of Surface Charge." Environ Health Perspect **116**(12): 1607-1613.

Grove, M. and M. Plumb (1993). "C/EBP, NF-kappa B, and c-Ets family members and transcriptional regulation of the cell-specific and inducible macrophage inflammatory

protein 1 alpha immediate-early gene." Molecular and Cellular Biology **3**(9): 5276-5289.
Hamilton, J. A. and A. Achuthan (2013). "Colony stimulating factors and myeloid cell biology in health and disease." Trends in Immunology **34**(2): 81-89.
Harrill, A. H., P. B. Watkins, S. Su, P. K. Ross, D. E. Harbourt, I. M. Stylianou, . . . D. W. Threadgill (2009). "Mouse population-guided resequencing reveals that variants in CD44 contribute to acetaminophen-induced liver injury in humans." Genome Research **19**(9): 1507-1515.
Hauck, T. S., R. E. Anderson, H. C. Fischer, S. Newbigging and W. C. Chan (2010). "In vivo quantum-dot toxicity assessment." Small **6**(1): 138-144.
Ho, C. C., H. Chang, H. T. Tsai, M. H. Tsai, C. S. Yang, Y. C. Ling and P. Lin (2013). "Quantum dot 705, a cadmium-based nanoparticle, induces persistent inflammation and granuloma formation in the mouse lung." Nanotoxicology **7**(1): 105-115.
Hoshino, A., S. Hanada and K. Yamamoto (2011). "Toxicity of nanocrystal quantum dots: the relevance of surface modifications." Archives of Toxicology **85**: 707-720.
Hu, X., H. Han, L. Hua and Z. Sheng (2010). "Electrogenerated chemiluminescence of blue emitting ZnSe quantum dots and its biosensing for hydrogen peroxide." Biosensors and Bioelectronics **25**(7): 1843-1846.
Jacobsen, N. R., P. Moller, K. A. Jensen, U. Vogel, O. Ladefoged, S. Loft and H. Wallin (2009). "Lung inflammation and genotoxicity following pulmonary exposure to nanoparticles in ApoE-/- mice." Particle and Fibre Toxicology **6**(2).
Jung, H., W. Chung, C. H. Lee and S. H. Kim (2012). "Fabrication of white light-emitting diodes based on UV light-emitting diodes with conjugated polymers-(CdSe/ZnS) quantum dots as hybrid phosphors." Journal of Nanoscience and Nanotechnology **12**(7): 5407-5411.
Kim, S., Y. T. Lim, E. G. Soltesz, A. M. De Grand, J. Lee, A. Nakayama, . . . J. V. Frangioni (2004). "Near-infrared fluorescent type II quantum dots for sentinel lymph node mapping." Nature Biotechnology **22**(1): 93-97.
Kirchner, C., T. Liedl, S. Kudera, T. Pellegrino, A. Muñoz Javier, H. E. Gaub, . . . W. J. Parak (2005). "Cytotoxicity of colloidal CdSe and CdSe/ZnS nanoparticles." Nano letters **5**: 331-338.
Lee, J. S., Y. C. Choi, J. H. Shin, J. H. Lee, Y. Lee, S. Y. Park, . . . I. J. Yu (2015). "Health surveillance study of workers who manufacture multi-walled carbon nanotubes." Nanotoxicology **9**: 802-811.
Liao, H.-Y., Y.-T. Chung, C.-H. Lai, S.-L. Wang, H.-C. Chiang, L.-A. Li, . . . S.-H. Liou (2014). "Six-month follow-up study of health markers of nanomaterials among workers handling engineered nanomaterials." Nanotoxicology **8**(sup1): 100-110.
Lovric, J., H. S. Bazzi, Y. Cuie, G. R. Fortin, F. M. Winnik and D. Maysinger (2005). "Differences in subcellular distribution and toxicity of green and red emitting CdTe quantum dots." Journal of Molecular Medicine (Berl) **83**(5): 377-385.
Lovrić, J., S. J. Cho, F. M. Winnik and D. Maysinger (2005). "Unmodified Cadmium Telluride Quantum Dots Induce Reactive Oxygen Species Formation Leading to Multiple Organelle Damage and Cell Death." Chemistry & Biology **12**: 1227-1234.
Ma-Hock, L., S. Brill, W. Wohlleben, P. M. A. Farias, C. R. Chaves, D. P. L. A. Tenório, . . . B. van Ravenzwaay (2012). "Short term inhalation toxicity of a liquid aerosol of CdS/Cd(OH)2 core shell quantum dots in male Wistar rats." Toxicology Letters **208**(2): 115-124.
Ma-Hock, L., P. M. Farias, T. Hofmann, A. C. Andrade, J. N. Silva, T. M. Arnaud, . . . B. van Ravenzwaay (2013). "Short term inhalation toxicity of a liquid aerosol of glutaraldehyde-coated CdS/Cd(OH) core shell quantum dots in rats." Toxicology Letters **225**(1): 20-26.
Matute-Bello, G., G. Downey, B. B. Moore, S. D. Groshong, M. A. Matthay, A. S. Slutsky and W. M. Kuebler (2011). "An Official American Thoracic Society Workshop Report:

Features and Measurements of Experimental Acute Lung Injury in Animals." American Journal of Respiratory Cell and Molecular Biology **44**(5): 725-738.
McConnachie, L. A., D. Botta, C. C. White, C. S. Weldy, H. W. Wilkerson, J. Yu, . . . T. J. Kavanagh (2013). "The Glutathione Synthesis Gene Gclm Modulates Amphiphilic Polymer-Coated CdSe/ZnS Quantum Dot-Induced Lung Inflammation in Mice." PLOS ONE **8**(5): e64165.
McConnachie, L. A., C. C. White, D. Botta, M. E. Zadworny, D. P. Cox, R. P. Beyer, . . . T. J. Kavanagh (2012). "Heme oxygenase expression as a biomarker of exposure to amphiphilic polymer-coated CdSe/ZnS quantum dots." Nanotoxicology **7**(2): 181-191.
Medintz, I. L., H. T. Uyeda, E. R. Goldman and H. Mattoussi (2005). "Quantum dot bioconjugates for imaging, labelling and sensing." Nature Materials **4**: 435-446.
Metzger, R. J., O. D. Klein, G. R. Martin and M. A. Krasnow (2008). "The branching programme of mouse lung development." Nature **453**(7196): 745-750.
Michalet, X., F. F. Pinaud, L. A. Bentolila, J. M. Tsay, S. Doose, J. J. Li, . . . S. Weiss (2005). "Quantum dots for live cells, in vivo imaging, and diagnostics." Science **307**(5709): 538-544.
Mosa, A., C. Trumstedt, E. Eriksson, O. Soehnlein, F. Heuts, K. Janik, . . . M. E. Rottenberg (2009). "Nonhematopoietic cells control the outcome of infection with Listeria monocytogenes in a nucleotide oligomerization domain 1-dependent manner." Infection and Immunity **77**(7): 2908-2918.
Neibert, K. D. and D. Maysinger (2011). "Mechanisms of cellular adaptation to quantum dots – the role of glutathione and transcription factor EB." Nanotoxicology **6**(3): 249-262.
Noursadeghi, M., M. B. Pepys, R. Gallimore and J. Cohen (2005). "Relationship of granulocyte colony stimulating factor with other acute phase reactants in man." Clinical and Experimental Immunology **140**(1): 97-100.
Oberdorster, G., E. Oberdorster and J. Oberdorster (2005). "Nanotoxicology: an emerging discipline evolving from studies of ultrafine particles." Environmental Health Perspectives **113**(7): 823-839.
Ohmori, Y., S. Fukumoto and T. A. Hamilton (1995). "Two structurally distinct kappa B sequence motifs cooperatively control LPS-induced KC gene transcription in mouse macrophages." Journal of Immunology **155**(7): 3593-3600.
Pellegrino, T., L. Manna, S. Kudera, T. Liedl, D. Koktysh, A. L. Rogach, . . . W. J. Parak (2004). "Hydrophobic Nanocrystals Coated with an Amphiphilic Polymer Shell: A General Route to Water Soluble Nanocrystals." Nano Letters **4**(4): 703-707.
Probst, C. E., P. Zrazhevskiy, V. Bagalkot and X. Gao (2013). "Quantum dots as a platform for nanoparticle drug delivery vehicle design." Advanced Drug Delivery Reviews **65**(5): 703-718.
R Core Team. (2014). "R: A language and environment for statistical computing, R Foundation for Statistical Computing, Vienna Austria." from http://www.r-project.org/.
Reichel, C. A., D. Puhr-Westerheide, G. Zuchtriegel, B. Uhl, N. Berberich, S. Zahler, . . . F. Krombach (2012). "C-C motif chemokine CCL3 and canonical neutrophil attractants promote neutrophil extravasation through common and distinct mechanisms." Blood **120**(4): 880-890.
Roberts, J. R., J. M. Antonini, D. W. Porter, R. S. Chapman, J. F. Scabilloni, S. H. Young, . . . R. R. Mercer (2013). "Lung toxicity and biodistribution of Cd/Se-ZnS quantum dots with different surface functional groups after pulmonary exposure in rats." Particle and Fibre Toxicology **10**: 5.
Rose, C. E., Jr., J. A. Lannigan, P. Kim, J. J. Lee, S. M. Fu and S. S. Sung (2010). "Murine lung eosinophil activation and chemokine production in allergic airway inflammation." Cellular & Molecular Immunology **7**(5): 361-374.

Rossi, E. M., L. Pylkkänen, A. J. Koivisto, M. Vippola, K. A. Jensen, M. Miettinen, . . . H. Alenius (2010). "Airway Exposure to Silica-Coated TiO2 Nanoparticles Induces Pulmonary Neutrophilia in Mice." Toxicological Sciences **113**(2): 422-433.
Rutledge, H., D. L. Aylor, D. E. Carpenter, B. C. Peck, P. Chines, L. E. Ostrowski, . . . S. N. P. Kelada (2014). "Genetic Regulation of Zfp30, CXCL1, and Neutrophilic Inflammation in Murine Lung." Genetics **198**(2): 735-745.
Saito, F., S. Tasaka, K.-i. Inoue, K. Miyamoto, Y. Nakano, Y. Ogawa, . . . A. Ishizaka (2008). "Role of Interleukin-6 in Bleomycin-Induced Lung Inflammatory Changes in Mice." American Journal of Respiratory Cell and Molecular Biology **38**(5): 566-571.
Savla, R., O. Taratula, O. Garbuzenko and T. Minko (2011). "Tumor targeted quantum dot-mucin 1 aptamer-doxorubicin conjugate for imaging and treatment of cancer." Journal of Controlled Release **153**: 16-22.
Servoss, S. L., R. Gonzalez, S. Varnum and R. C. Zangar (2009). High-Throughput Analysis of Serum Antigens Using Sandwich ELISAs on Microarrays. Methods in Molecular Biology, Tumor Biomarker Discovery. M. A. Tainsky. New York, Humana Press. **250**.
Shaw, S. Y., E. C. Westly, M. J. Pittet, A. Subramanian, S. L. Schreiber and R. Weissleder (2008). "Perturbational profiling of nanomaterial biologic activity." Proceedings of the National Academy of Sciences of the United States of America **105**(21): 7387-7392.
Smith, W. E., J. Brownell, C. C. White, Z. Afsharinejad, J. Tsai, X. Hu, . . . D. L. Eaton (2012). "In Vitro Toxicity Assessment of Amphiphillic Polymer-Coated CdSe/ZnS Quantum Dots in Two Human Liver Cell Models." ACS Nano **6**(11): 9475-9484.
Soutiere, S. E., C. G. Tankersley and W. Mitzner (2004). "Differences in alveolar size in inbred mouse strains." Respiratory Physiology and Neurobiology **140**(3): 283-291.
Su, Y., M. Hu, C. Fan, Y. He, Q. Li, W. Li, . . . Q. Huang (2010). "The cytotoxicity of CdTe quantum dots and the relative contributions from released cadmium ions and nanoparticle properties." Biomaterials **31**: 4829-4834.
Su, Y., F. Peng, Z. Jiang, Y. Zhong, Y. Lu, X. Jiang, . . . Y. He (2011). "In vivo distribution, pharmacokinetics, and toxicity of aqueous synthesized cadmium-containing quantum dots." Biomaterials **32**(25): 5855-5862.
Tukey, J. W. (1977). Exploratory Data Analysis. Reading, MA, Addison-Wesley.
US-EPA (2007). Method 6020A: Inductively Coupled Plasma-Mass Spectrometry.
Vasan, R. S. (2006). "Biomarkers of Cardiovascular Disease: Molecular Basis and Practical Considerations." Circulation **113**(19): 2335-2362.
Wang, Y., J. Fang, S. S. Leonard and K. M. Krishna Rao (2004). "Cadmium inhibits the electron transfer chain and induces Reactive Oxygen Species." Free Radical Biology and Medicine **36**(11): 1434-1443.
Warnes, G., B. Bolker, L. Bonebakker, R. Gentleman, W. Huber Andy Liaw, T. Lumley, . . . B. Venables. (2013). "gplots: Various R programming tools for plotting data. R package version 2.11.3.", from http://cran.r-project.org/package=gplots.
Weldy, C. S., C. C. White, H.-W. Wilkerson, T. V. Larson, J. A. Stewart, S. E. Gill, . . . T. J. Kavanagh (2011). "Heterozygosity in the glutathione synthesis gene Gclm increases sensitivity to diesel exhaust particulate induced lung inflammation in mice." Inhalation Toxicology **23**(12): 724-735.
White, A. M., D. S. Daly, S. M. Varnum, K. K. Anderson, N. Bollinger and R. C. Zangar (2006). "ProMAT: protein microarray analysis tool." Bioinformatics **22**(10): 1278-1279.
Wickham, H. (2009). ggplot2: Elegant Graphics for Data Analysis, Springer Publishing Company, Incorporated.
Woodbury, R. L., S. M. Varnum and R. C. Zangar (2002). "Elevated HGF Levels in Sera from Breast Cancer Patients Detected Using a Protein Microarray ELISA." Journal Proteome Research **1**(3): 233-237.

Ye, L., K.-T. Yong, L. Liu, I. Roy, R. Hu, J. Zhu, . . . P. N. Prasad (2012). "A pilot study in non-human primates shows no adverse response to intravenous injection of quantum dots." Nature Nanotechnology **7**(7): 453-458.

Zangar, R. C., D. S. Daly, A. M. White, S. L. Servoss, R. M. Tan and J. R. Collett (2009). "ProMAT Calibrator: A Tool for Reducing Experimental Bias in Antibody Microarrays." Journal of Proteome Research **8**(8): 3937-3943.

Zhang, L. W., W. Bäumer and N. A. Monteiro-Riviere (2011). "Cellular uptake mechanisms and toxicity of quantum dots in dendritic cells." Nanomedicine **6**(5): 777-791.

Zhang, L. W., W. W. Yu, V. L. Colvin and N. A. Monteiro-Riviere (2008). "Biological interactions of quantum dot nanoparticles in skin and in human epidermal keratinocytes." Toxicology and Applied Pharmacology **228**: 200-211.

Zhao, X., A. Sato, C. S. Dela Cruz, M. Linehan, A. Luegering, T. Kucharzik, . . . A. Iwasaki (2003). "CCL9 is secreted by the follicle-associated epithelium and recruits dome region Peyer's patch CD11b+ dendritic cells." The Journal of Immunology **171**(6): 2797-2803.

Zrazhevskiy, P., M. Sena and X. Gao (2010). "Designing multifunctional quantum dots for bioimaging, detection, and drug delivery." Chemical Society Reviews **39**(11): 4326-4354.

Table 1.
Broad sense heritability of qd response phenotypes for CC founder strains.

	Naïve		Saline		QD	
Phenotype	r^1	g^2	r^1	g^2	r^1	g^2
BALF Neutrophils	0.62	0.49	-0.02*	-0.01*	0.15	0.09
BALF Protein	0.44	0.31	0.28	0.18	0.33	0.22
Lung GSH	0.56	0.42	0.27	0.25	0.41	0.28
BALF G-CSF	0.30	0.20	-0.15*	-0.08*	0.39	0.27
BALF KC	0.38	0.26	0.24	0.15	0.64	0.50
BALF MIP-1α	0.29	0.19	0.29	0.19	0.60	0.46
BALF MIP-1γ	0.51	0.38	0.59	0.45	0.77	0.66
BALF $Gr1^+$ Macs	0.05	0.03	0.27	0.17	0.41	0.28

* Negative heritability estimate seen in saline treated mice indicate more phenotypic variability within rather than between strains. As seen in Figure S4, some animals (potentially outliers) were highly reactive to saline compared to other mice in the same strain, which can increase intra-strain variability and decrease heritability estimates.

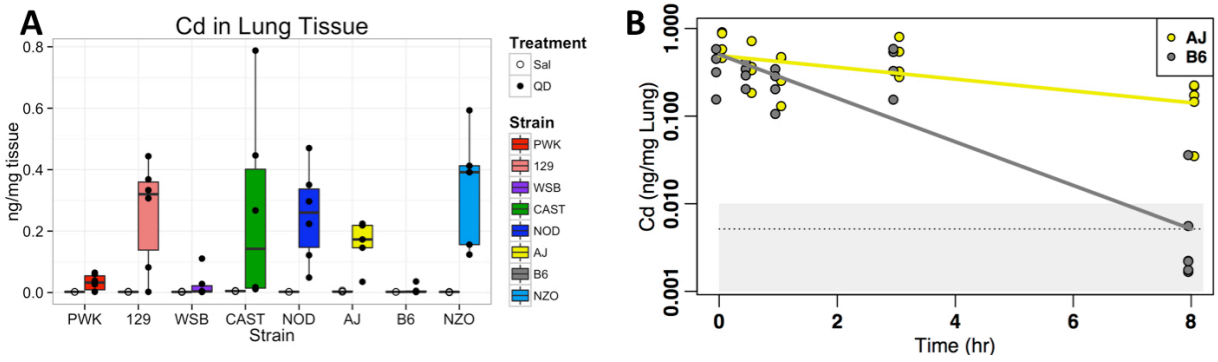

Figure 1. Total Cd in frozen lung tissue by strain at 8 hr post OPA (A) and at earlier time points in AJ and B6 mice (B). Cd levels at 8 hr are shown using box plots to indicate the median, 25th and 75th percentiles of the data, and potential outliers (A). Individual animal data for each treatment group and strain is plotted on top of the boxplots. At earlier time points, the mean Cd values and standard errors are shown for both treatment groups of B6 and AJ mice.

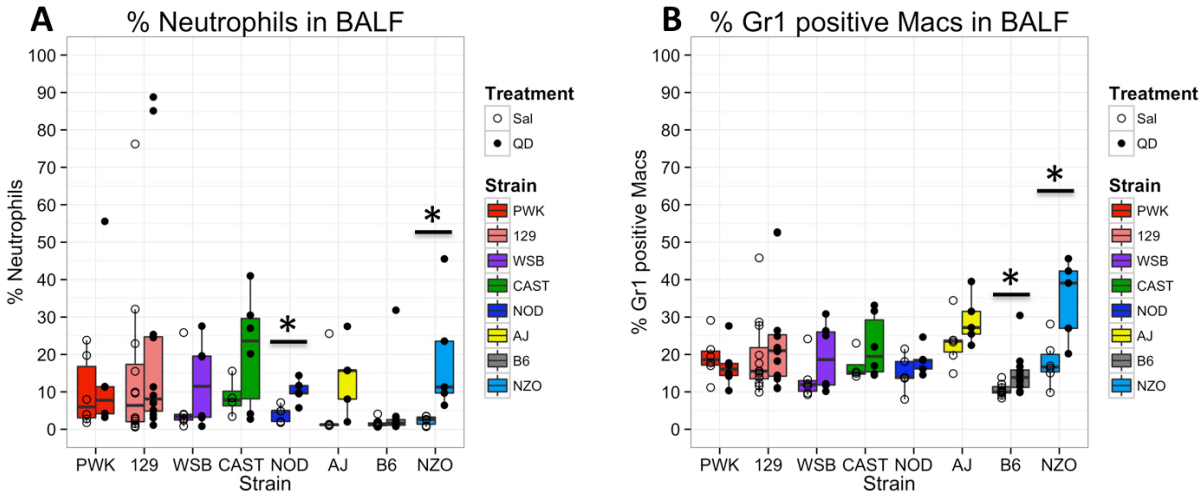

Figure 2. Flow cytometric detection of (A) neutrophils and (B) Gr1^{+} macrophages as percentages of total cells in BALF. Levels of neutrophils and Gr1^{+} macrophages are shown using box plots to indicate the median, 25th and 75th percentiles of the data, and potential outliers. Individual animal data for each treatment group and strain is plotted on top of the boxplots. *=Significant difference between treatment groups within a strain using an FDR of 10%.

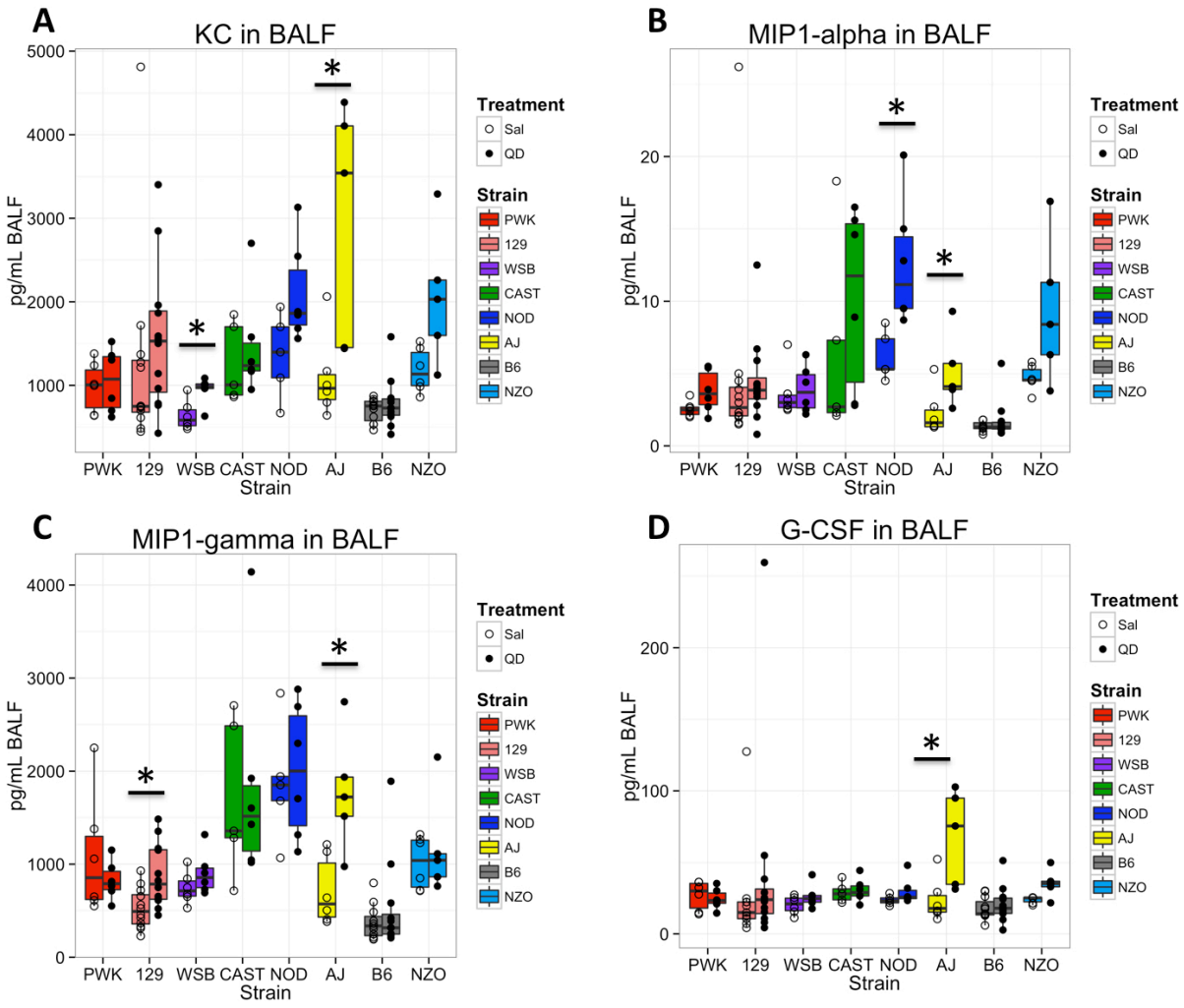

Figure 3. Cytokines in bronchoalveolar lavage fluid. Results are shown for those cytokines where at least one strain showed a significant elevation for QD treated vs. saline treated mice. Data are shown using box plots to indicate the median, 25th and 75th percentiles of the data, and potential outliers. Individual animal data for each treatment group and strain is plotted on top of the boxplots. *=Significant difference between treatment groups within a strain using an FDR of 10%.

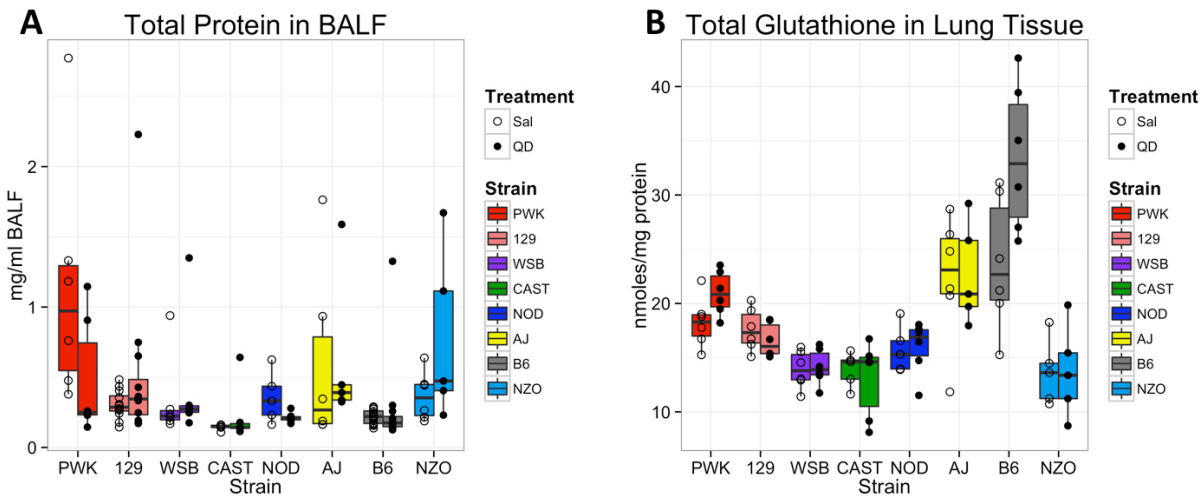

Figure 4. Levels of (A) total protein in BALF and (B) total glutathione levels in lung tissue. For both measures, data are shown using box plots to indicate the median, 25th and 75th percentiles of the data, and potential outliers. Individual animal data for each treatment group and strain is plotted on top of the boxplots. *=Significant difference between treatment groups within a strain using an FDR of 10%.

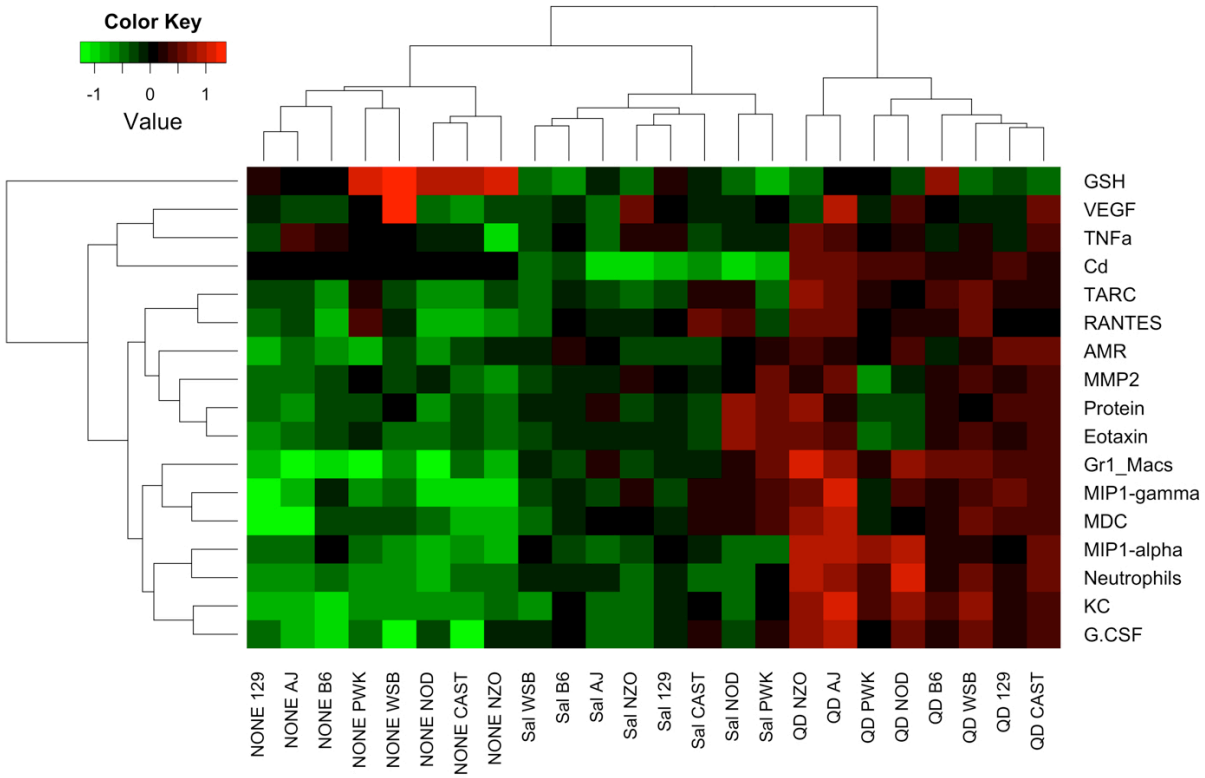

Figure 5. Unsupervised Hierarchical Clustering Analysis. Results from all treatment groups from all assays were converted to z-scores across each assay. Bright red indicates a high positive z-score and bright green indicates a high negative z-score. Inside the heat map, white indicates that data was not collected for that assay and treatment group.

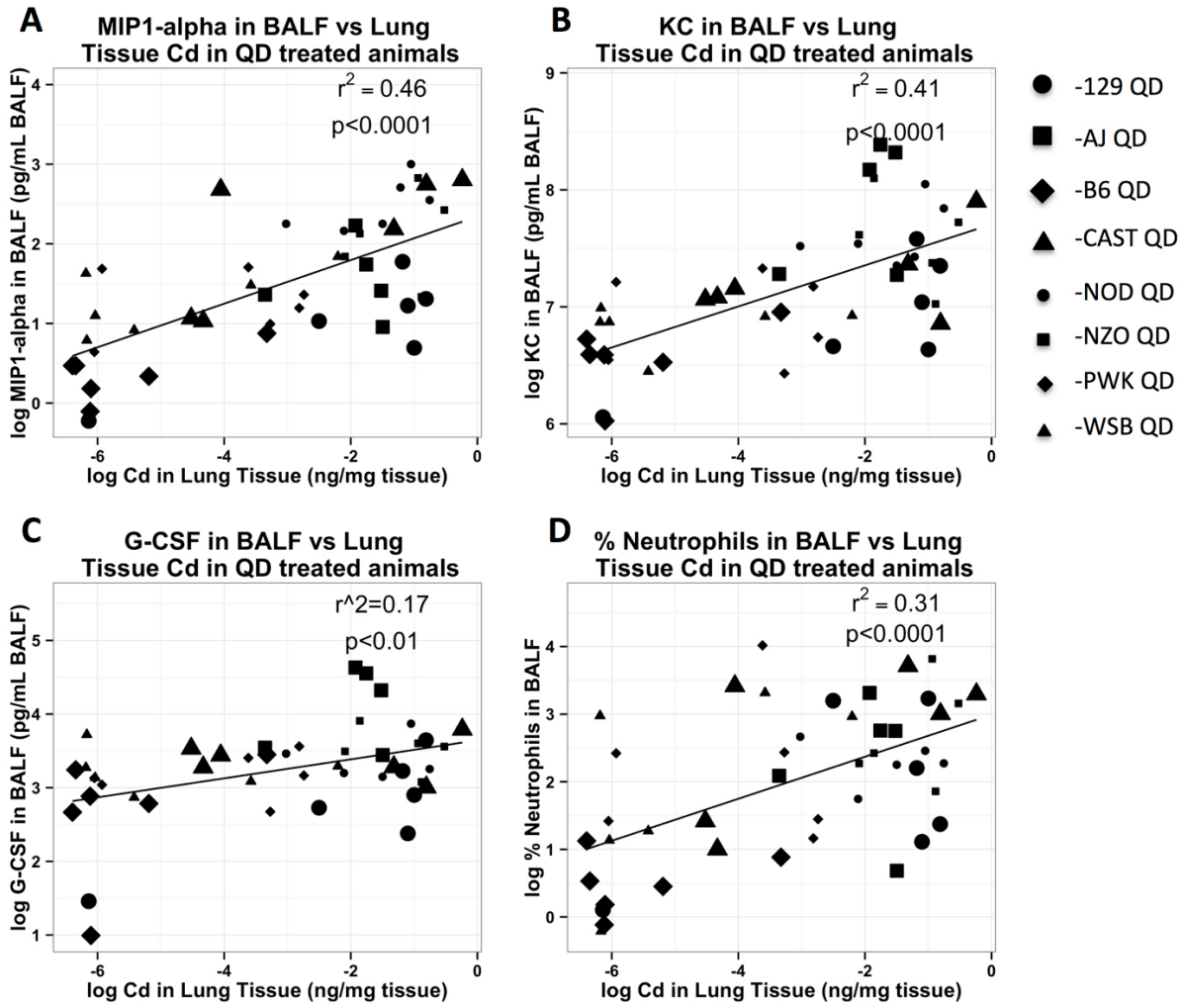

Figure 6. Regression analyses of MIP-1α, KC, BALF percent neutrophils compared to lung tissue Cd. All analyses only contain animals where measurements exist for both parameters so only the QD treated animals are included since saline treated animals have virtually no detectable Cd and are therefore not informative. Size and shape of the symbols are used to distinguish among the different mouse strains.

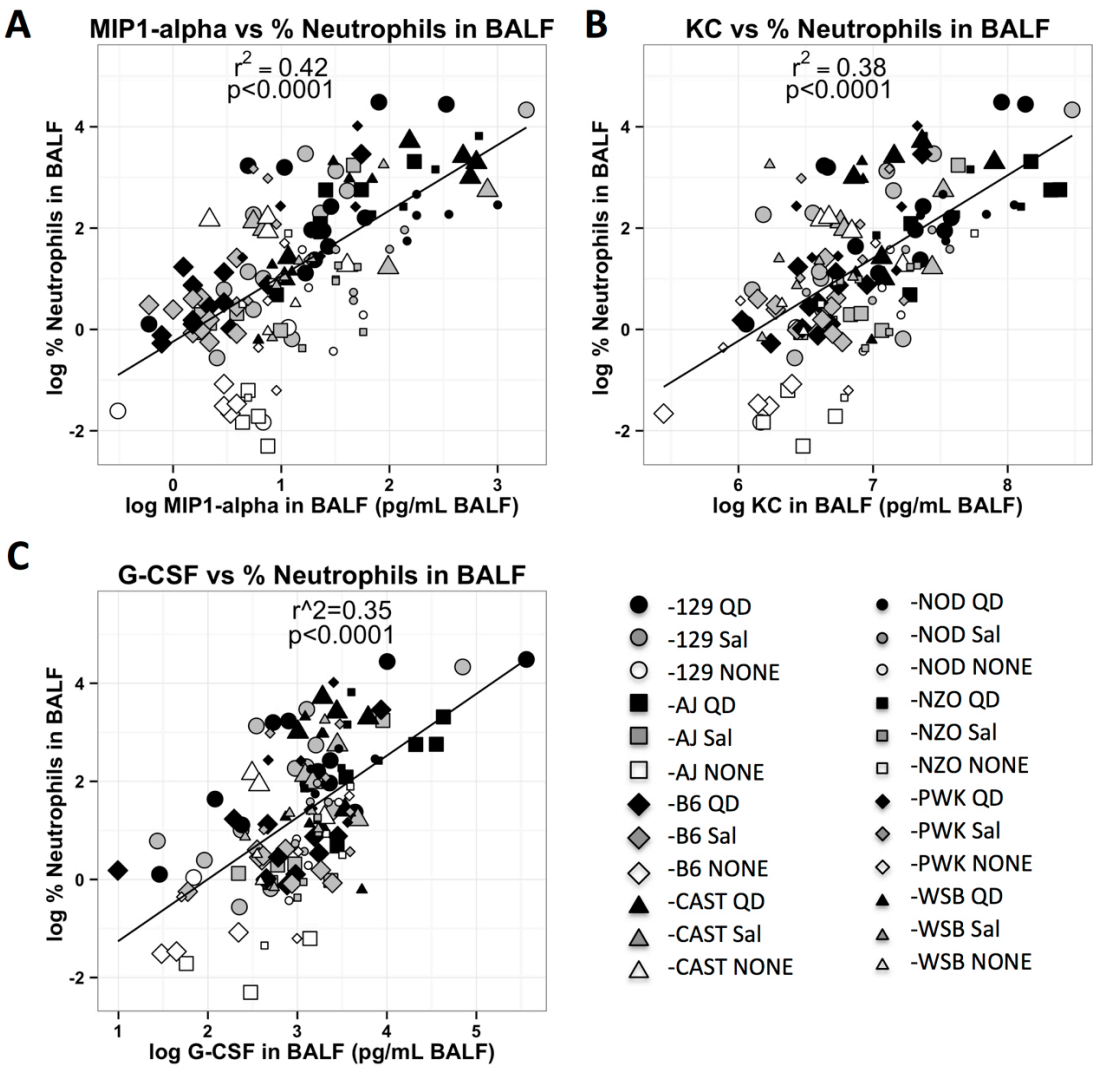

Figure 7. Regression analyses of MIP-1α, KC compared to BALF neutrophils. All analyses only contain animals where measurements exist for both parameters and in the cases where Cd is one of the parameters. Size, shape and fill are used to distinguish among the different mouse strains and treatment groups.

Supplemental Information

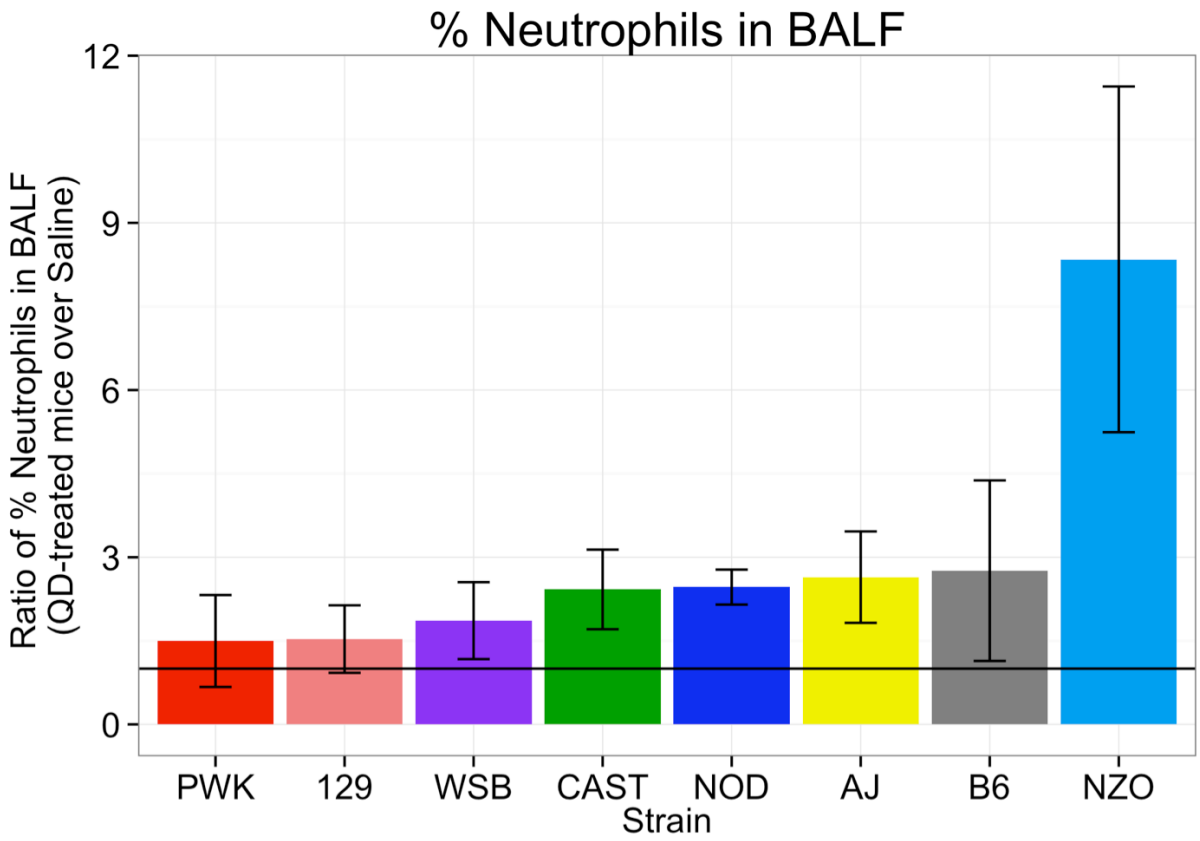

Figure S1.

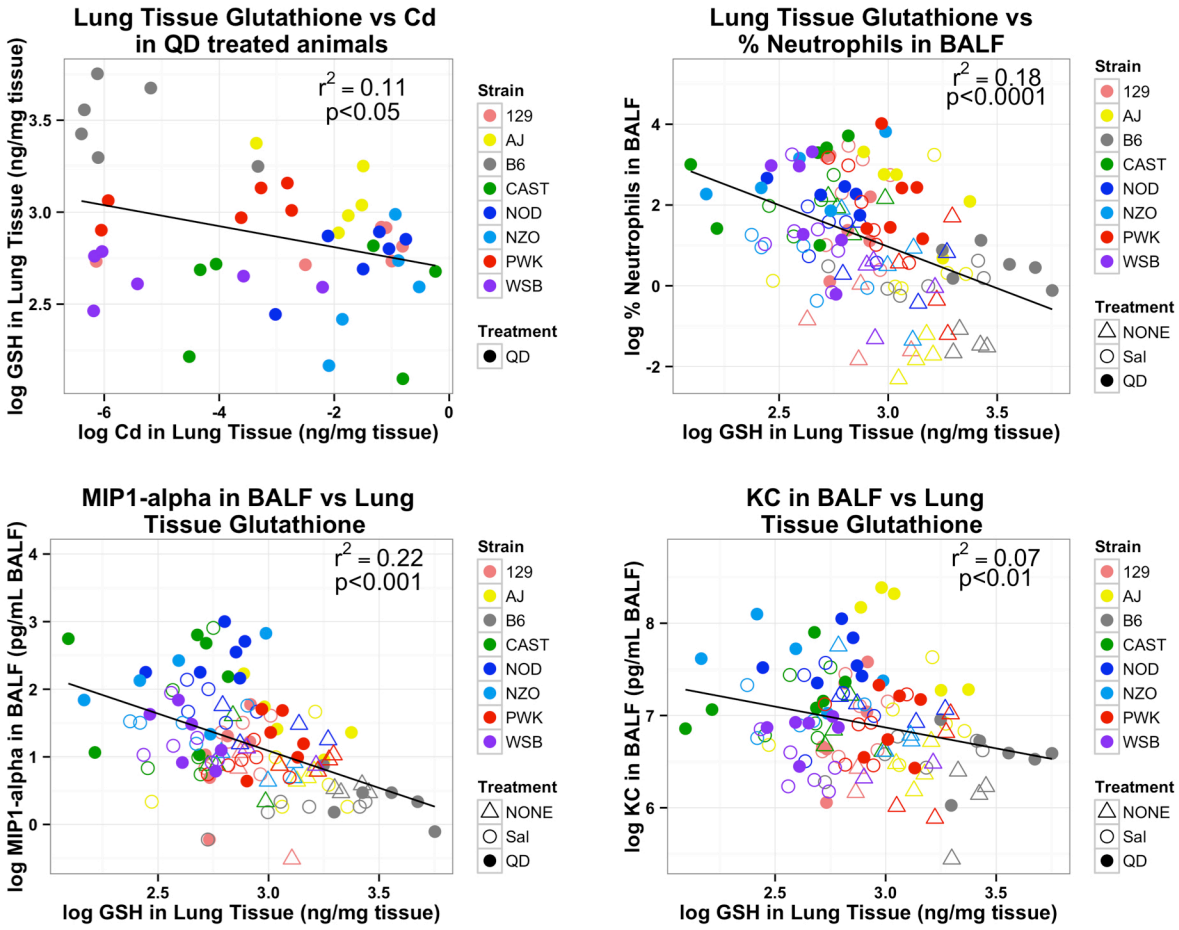
Lung Tissue Glutathione vs Cd in QD treated animals
r2 = 0.11
p<0.05
log GSH in Lung Tissue (ng/mg tissue)
log Cd in Lung Tissue (ng/mg tissue)
Lung Tissue Glutathione vs % Neutrophils in BALF
r2 = 0.18
p<0.0001
log % Neutrophils in BALF
log GSH in Lung Tissue (ng/mg tissue)
MIP1-alpha in BALF vs Lung Tissue Glutathione
r2 = 0.22
p<0.001
log MIP1-alpha in BALF (pg/mL BALF)
log GSH in Lung Tissue (ng/mg tissue)
KC in BALF vs Lung Tissue Glutathione
r2 = 0.07
p<0.01
log KC in BALF (pg/mL BALF)
log GSH in Lung Tissue (ng/mg tissue)
Strain
129
AJ
B6
CAST
NOD
NZO
PWK
WSB
Treatment
QD
NONE
Sal

Figure S2.

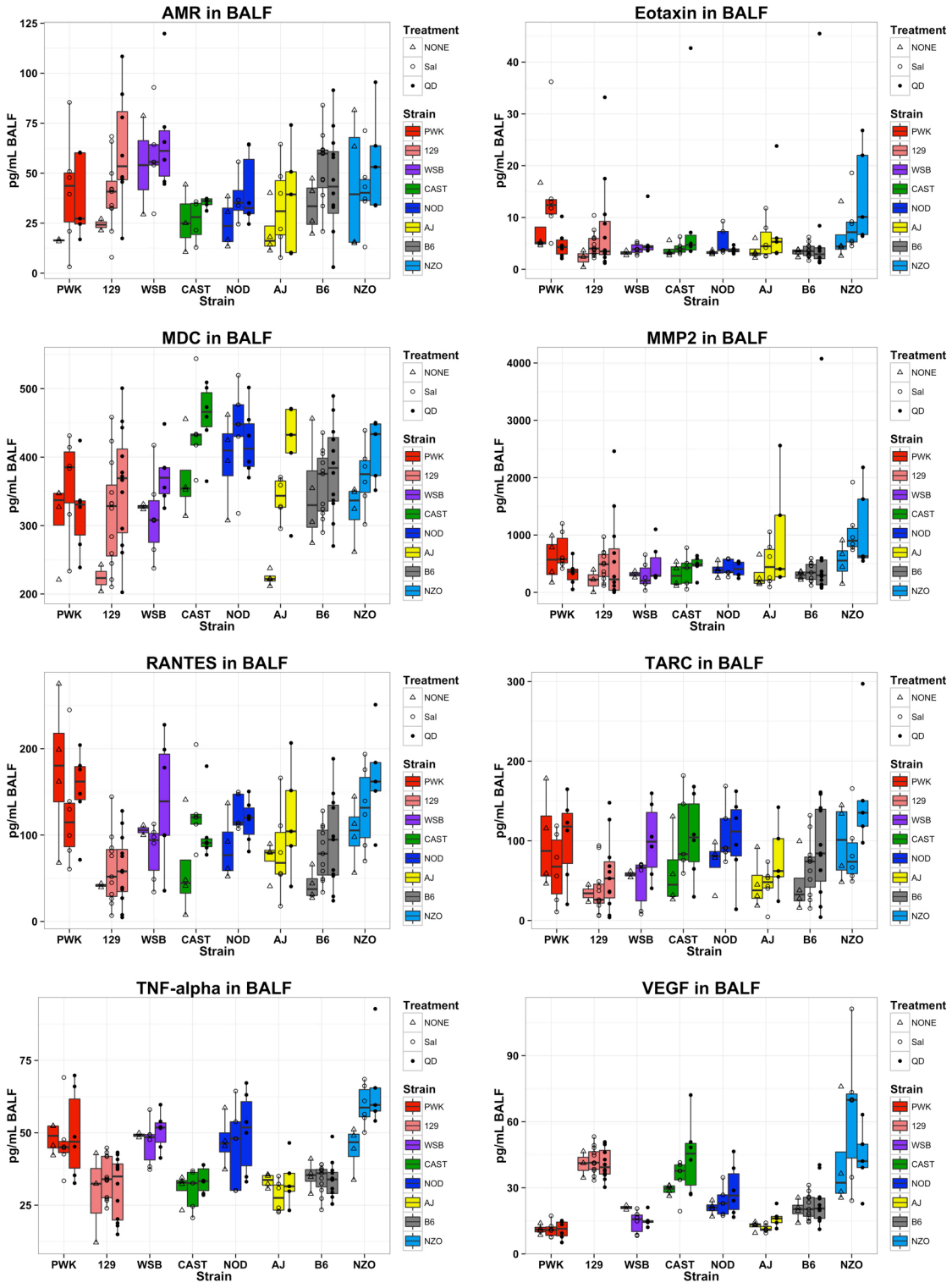
AMR in BALF
Eotaxin in BALF
MDC in BALF
MMP2 in BALF
RANTES in BALF
TARC in BALF
TNF-alpha in BALF
VEGF in BALF
pg/mL BALF
Strain
PWK
129
WSB
CAST
NOD
AJ
B6
NZO
Treatment
NONE
Sal
QD

Figure S3.

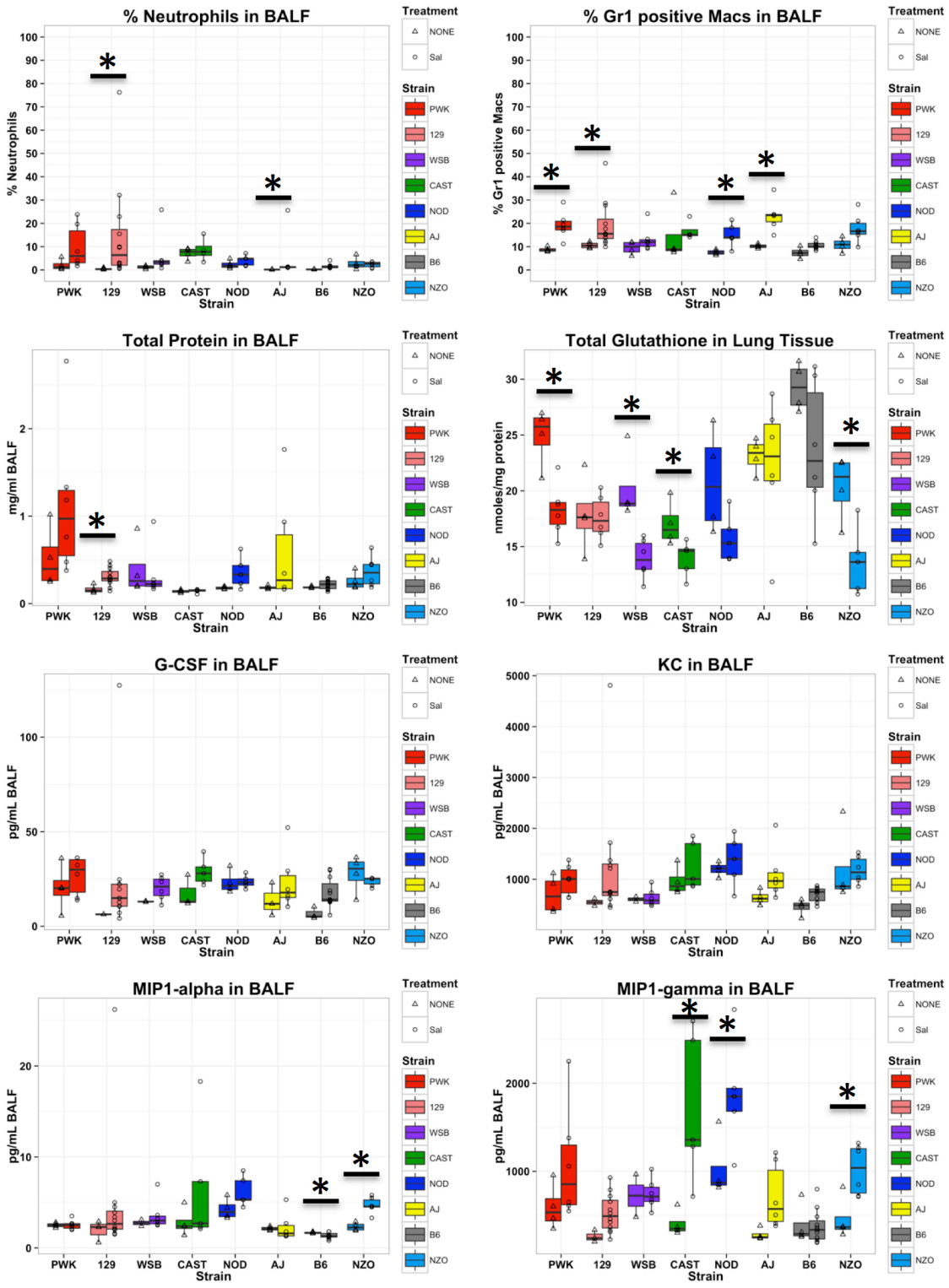
% Neutrophils in BALF
% Neutrophils
% Gr1 positive Macs in BALF
% Gr1 positive Macs
Total Protein in BALF
mg/ml BALF
Total Glutathione in Lung Tissue
nmoles/mg protein
G-CSF in BALF
pg/mL BALF
KC in BALF
pg/mL BALF
MIP1-alpha in BALF
pg/mL BALF
MIP1-gamma in BALF
pg/mL BALF
Strain
PWK
129
WSB
CAST
NOD
AJ
B6
NZO
Treatment
NONE
Sal

Figure S4.

Table S1. Absolute Cell Numbers in BALF in BALF ($x10^3$) (mean ± SE)

		Naïve	Saline	QD
Neutrophils	129	0.12 ± 0.05	2.82 ± 1.17	17.71 ± 10.69
	AJ	0.04 ± 0.00	1.14 ± 0.92	3.96 ± 1.40
	B6	0.07 ± 0.01	0.33 ± 0.05	1.08 ± 0.75
	CAST	1.32 ± 0.18	2.29 ± 0.62	6.54 ± 1.93
	NOD	0.96 ± 0.58	1.56 ± 0.31	3.93 ± 0.50*
	NZO	0.50 ± 0.23	1.09 ± 0.15	13.09 ± 8.94*
	PWK	0.23 ± 0.10	2.24 ± 0.87	6.27 ± 4.36
	WSB	0.20 ± 0.08	2.33 ± 1.44	3.67 ± 1.33
Macrophages	129	24.74 ± 12.56	17.14 ± 12.04	16.84 ± 9.01
	AJ	26.02 ± 5.95	17.32 ± 6.90	19.71 ± 12.54
	B6	27.09 ± 4.49	21.28 ± 10.50	17.43 ± 8.77
	CAST	16.03 ± 2.436	20.86 ± 2.673	19.86 ± 3.72
	NOD	31.66 ± 14.18	31.98 ± 19.83	32.24 ± 8.67
	NZO	18.39 ± 8.04	54.57 ± 34.49	35.10 ± 20.05
	PWK	13.80 ± 5.281	19.97 ± 6.50	22.44 ± 6.37
	WSB	13.18 ± 4.61	27.69 ± 7.33	22.54 ± 3.25
$Gr1^+$ Macrophages	129	5.16 ± 0.96	5.96 ± 0.92	7.71 ± 0.87
	AJ	26.02 ± 5.95	11.2 ± 1.85	13.25 ± 3.92
	B6	27.09 ± 4.49	17.76 ± 2.58	13.68 ± 1.96
	CAST	16.03 ± 2.436	6.45 ± 1.01	6.89 ± 1.1
	NOD	31.66 ± 14.18	28.25 ± 4.35	24.81 ± 3.18
	NZO	18.39 ± 8.04	38.39 ± 12.37	20.95 ± 7.03
	PWK	13.80 ± 5.281	15.47 ± 2.39	18.34 ± 2.6
	WSB	13.18 ± 4.61	24.02 ± 2.59	19.16 ± 1.18
Total Cells	129	27.20 ± 6.89	21.87 ± 3.88	37.31 ± 10.72
	AJ	28.81 ± 3.36	20.03 ± 2.76	25.23 ± 6.85
	B6	30.01 ± 2.53	22.81 ± 3.14	19.63 ± 2.77
	CAST	19.33 ± 1.20	25.96 ± 1.57	29.46 ± 2.30
	NOD	36.23 ± 7.82	41.46 ± 5.46	39.47 ± 3.77
	NZO	20.77 ± 4.44	59.26 ± 14.33	52.03 ± 15.92
	PWK	15.75 ± 2.63	24.05 ± 2.60	30.77 ± 4.78
	WSB	16.10 ± 2.66	33.65 ± 3.60	29.24 ± 1.28

*=$p<0.05$ for t-test between QD and Saline treated mice.

Table S2. Correlation between BALF Cytokines and % Neutrophils in BALF by Strain

	Strain	Correlation Coefficient*	p-value
KC	129	0.67	<0.001
	AJ	0.89	<0.001
	B6	0.69	<0.001
	CAST	0.027	0.34
	NOD	0.72	<0.01
	NZO	0.64	<0.01
	PWK	0.34	0.11
	WSB	0.092	0.36
MIP-1α	129	0.72	<0.001
	AJ	0.72	<0.01
	B6	0.35	<0.05
	CAST	0.57	<0.05
	NOD	0.66	<0.01
	NZO	0.75	<0.001
	PWK	0.32	0.12
	WSB	0.9	<0.001
G-CSF	129	0.75	<0.001
	AJ	0.86	<0.001
	B6	0.6	<0.001
	CAST	0.29	0.81
	NOD	0.68	<0.01
	NZO	0.77	<0.001
	PWK	0.18	0.24
	WSB	0.23	0.22

* - Pearson's Correlation Coefficient

Chapter 3

Genome-Wide Association Mapping of Quantum Dot Induced Lung Inflammation and Toxicity in Collaborative Cross Recombinant Inbred Mouse Strains.

David K Scoville[1], Christopher M Carosino[1], Ryan S McMahan[1,2], Collin C White[1], Stefanie C Schmuck[1], Megan M Cartwright[1], Zahra Afsharinejad[1], Theo K. Bammler[1], Xiaohu Gao[3], Samir N Kelada[4], Oksana Kosyk[5], Ivan Rusyn[5,6], Terrance J Kavanagh[1]

Departments of [1]Environmental and Occupational Health Sciences, [2]Medicine and[3]Bioengineering, University of Washington, Seattle, WA 98195; [4]Genetics and [5]Environmental Sciences and Engineering, University of North Carolina, Chapel Hill, NC 27599; [6]Veterinary Integrative Biosciences, Texas A&M University, College Station, TX, 77843

Corresponding Author:
Terrance J. Kavanagh, PhD
Department of Environmental and Occupational Health Sciences
Box 354695
University of Washington
Seattle, WA 98195, USA.
Tel: (206) 685-8479
Fax: (206) 685-4696
E-mail: tjkav@uw.edu
Running Title: Mouse GWAS for QD-Induced Lung Inflammation

Abstract

Quantum dots (QDs) are engineered nanoparticles commonly composed of a CdSe/ZnS core/shell and application-specific outer coatings. QDs have uses in electronics, biomedical research and medicine. However, their small size, heavy metal composition and multitude of potential uses have generated concerns regarding potential toxicity. Since nanoparticle toxicity is often composition and coating dependent, and is also dependent on the genetics of mouse strains used to assess such toxicity, the mechanisms by which nanoparticles generate toxicity can be complicated. Accordingly, systems genetics methods, including genome wide association mapping, might provide insights for further mechanistic studies. The Collaborative Cross (CC) consortium has generated a large and genetically diverse panel of recombinant inbred (RI) mouse strains from a founding panel of 8 genetically diverse inbred mouse strains. In previous studies, we found that the eight inbred founder strains varied widely in susceptibility to QD-induced lung inflammation and toxicity. In this study, we further assessed QD-induced lung inflammation and toxicity in 12 CC RI mouse strains. Since the RI strains are unique combinations of the founder genomes, and since lung inflammation is a polygenic trait, we hypothesized that the RI strains would also vary in their susceptibility to QD-induced lung inflammation. We also hypothesized that we would observe phenotypes outside the range of those observed in the founder strains; and that we would be able to map quantitative trait loci (QTLs) associated with QD-induced lung inflammation and toxicity. We found that levels of bronchoalveolar lavage fluid (BALF) neutrophils, the chemokine KC, and protein were significantly different across the 12 CC RI strains and treatment groups; that BALF protein levels of some RI strains were outside the range of the CC founder strains; and that broad QTLs could be identified for QD-induced changes in BALF protein levels using only 12 CC RI strains.

Introduction

Nanotechnology research has produced many different engineered nanomaterial (ENM) enabled products in many sectors with obvious benefits to society. Quantum dots (QDs) are ENMs with physico-chemical properties that make them valuable as imaging tools in biomedical research and potentially in clinical settings (Wu et al. 2003; Kim et al. 2004). QDs are also of use in the electronics industry (Jung et al. 2012; Bae et al. 2013). However, it has been demonstrated in rodent models that QDs can induce lung inflammation and toxicity following pulmonary exposures (Jacobsen et al. 2009; Ma-Hock et al. 2012; McConnachie et al. 2013; Scoville et al. 2015). As with other ENMs, QD-induced lung inflammation and toxicity in rodents have been shown to vary by coating and choice of test animal strain (Ho et al. 2013; Ma-Hock et al. 2013; Roberts et al. 2013; Scoville et al. 2015; Seiffert et al. 2015). The multitude of ENM formulations presents a challenge for mechanistic toxicity testing. However, if genes and pathways associated with ENM toxicity can be identified and validated, then certain mechanisms may present as a higher priority for follow on studies than others. In addition, novel targets could potentially be placed into high-throughput screening assays for other ENM materials and formulations.

Quantitative trait loci (QTL) mapping is an unbiased approach for identifying candidate genes and pathways involved in certain genetically based phenotypes. QTLs are regions of the genome statistically associated with phenotypic variation. In biological and biomedical science, traditional QTL study designs start with 2 parental inbred mouse strains that significantly differ from each other for a given phenotype, and then breeding either a back-crossed population or inter-crossed F2 populations for mapping (Liu 1998; Broman 2001; Zou 2009). Genome-wide association (GWA) mapping is a recent adaptation to QTL mapping using inbred or recombinant inbred (RI) mouse strains taking advantage of high density genome-wide single nucleotide polymorphism (SNP) genotyping technologies (Payseur and Place 2007). One advantage is that genotype data is readily available to the

public for most commercially available inbred and RI mouse strains, reducing the burden on the investigator. In addition to mechanistic insights, candidate genes that are polymorphic in humans may provide an opportunity to identify sensitive populations. Estimates of population variability may also be possible when multi-strain mouse panels are assayed (Chiu et al. 2014).

The Collaborative Cross (CC) consortium has generated a large genetically diverse panel of recombinant inbred (RI) mouse strains from a founding panel of 8 inbred mouse strains representing 90% of mouse genetic diversity in *M. musculus* as a resource for systems genetics studies (Threadgill and Churchill 2012). Studies on mice from CC RI lines still in the inbreeding process (pre-CC) showed more than the expected number of recombination sites, and that these are evenly distributed across the genome, which is advantageous for QTL mapping as genomic regions without variation cannot be interrogated (Aylor et al. 2011; Threadgill et al. 2011). Furthermore, pre-CC mice have shown immunological phenotypes outside the range of the founder strains showing the potential for large contrast across completed RI strains, which would be helpful for genetic mapping (Aylor et al. 2011; Phillippi et al. 2014). While many studies using panels of existing inbred mouse strains have had success using unbiased methods to identify genetic factors associated with response to toxic exposures (including ozone, vanadium pentoxide, acetaminophen, isoniazid, and hyperoxia), it is expected that CC RI mouse strains will be an even more powerful resource for discovering QTLs associated with toxic exposures (Harrill et al. 2009; Bauer and Kleeberger 2010; Church et al. 2014; Nichols et al. 2014; Walters et al. 2014).

We have previously investigated QD-induced lung inflammation and toxicity in the CC founder strains and found a wide range of responses among these strains (Scoville et al. 2015). In this study, we further investigated the QD-induced pulmonary inflammatory response in 12 CC RI strains. The CC RI strain genomes are unique combinations of the CC founder strain genomes, and phenotypes within pre-CC mice have been observed beyond

the range of the founder strains. Thus, we hypothesized that the CC RI strains would also vary in their susceptibility to QD-induced lung inflammation and toxicity; that we would observe phenotypes that were outside the range of the founder strains; and that we would be able to map QTLs associated with QD-induced lung inflammation and toxicity. As will be further explained, we found significant strain and treatment differences overall across the 12 CC RI strains for levels of neutrophils, levels of the cytokine KC, and total protein in bronchoalveolar lavage fluid (BALF), and that these phenotypes were heritable. We also found that some RI strains had levels of protein in BALF, interpreted as a measure of alveolar/capillary barrier integrity, that exceeded levels in the founder strains. Furthermore, we mapped QTLs on chromosomes 1, 4, 9, and 12 containing over 150 significant Bonferroni corrected SNPs. While QTLs were broad and contained hundreds of genes, this is the first genetic mapping of QD induced lung inflammation that we are aware of and it is encouraging that broad QTLs can be mapped with just 12 CC RI strains. These results warrant future studies with additional RI strains to narrow QTLs and candidate gene lists for additional follow up and validation.

Methods

Animals and Dosing

Male mice from 12 CC RI strains (CC002/Unc, CC003/Unc, CC004/TauUnc, CC005/TauUnc, CC006/TauUnc, CC010/GeniUnc, CC011/Unc, CC012/GeniUnc, CC015/Unc, CC025/GeniUnc, CC038/GeniUnc, CC043/GeniUnc) were ordered from the University of North Carolina (UNC) Systems Genetics Core Facility. The range of ages was 9-11 weeks old. Prior to relocation to UNC, strain names containing “Tau”, “Geni”, or “Unc” were previously bred at Tel Aviv University, Israel; Geniad, Australia; or Oak Ridge National Labs, USA, respectively. Mice acclimated in a specific pathogen free (SPF) vivarium at UNC prior to experiments. All experiments were approved by the UNC Institutional Animal Care and

Use Committee (IACUC). Mice were anesthetized using Isoflurane and given 1.53 µL/g bodyweight (BW) of either 10 nM QDs (6 µg/kg bodyweight Cd equivalents) (n=4 per strain) or an equivalent volume of 0.9% saline (n=3 per strain) using oropharyngeal aspiration (OPA). Mice were euthanized using CO_2 narcosis followed by cervical dislocation eight hours after dosing.

Quantum Dots

QDs used in this study were synthesized and characterized in the laboratory of Dr. Xiaohu Gao in the Department of Bioengineering at the University of Washington as previously described (Pellegrino et al. 2004; Bagalkot and Gao 2011; McConnachie et al. 2012; McConnachie et al. 2013). Briefly, the QDs are approximately 12 nm in diameter. They are composed of a Cadmium/Selenium (Cd/Se) core with a Zinc Sulfide (Zn/S) shell. They were further modified with an outer amphiphilic polymer coating of tri-n-octylphosphine oxide, poly(maleic anhydride-alt-1-tetradecene (TOPO-PMAT) allowing for biostability and retention of optimal fluorescent properties.

Bronchoalveolar lavage (BAL) and Lung Tissue Collection

Three lavages were performed with 1 mL phosphate buffered saline (PBS) with exception of CC043/GeniUnc and CC025/GeniUnc. Similar to our previous study in the CC founder strains during which we lowered the lavage volume for smaller strains due to reduced lung volume (Scoville et al. 2015), we used 800 µL PBS for these two strains. Following lavage, the right lung was flash frozen and stored at -80°C. The left lung was inflated with 10% neutral buffered formalin (NBF) and then fixed for 24 hr before storage in 70% ethanol.

BAL samples were centrifuged (500g, 10 min) and the supernatant from the 1st lavage (hereafter referred to as BALF) was stored at -80°C. Cells from all lavages were combined and red blood cells were lysed using BD FACS Lysing Solution (BD Biosciences,

San Jose, CA). BALF cell samples were fixed in 0.2% paraformaldehyde and stored at 4°C before immunostaining for identification of inflammatory cells.

Acute Lung Inflammation: BALF Inflammatory Cells and KC

Cells were immunostained and prepared for flow cytometry using an approach previously described in (Weldy et al. 2011; Scoville et al. 2015). Briefly, samples were labeled with antibodies against mouse Cd11b (Cd11b-phycoerythrin (PE), AbCam, Cambridge, MA), F4/80 (F4/80-Alexafluor 488, eBioscience, San Diego, CA), and Gr1 (Gr1-biotin/streptavidin-AlexaFluor350, BioLegend, San Diego, CA). Neutrophils were classified as Cd11b-high and F4/80-low, and macrophages as Cd11b-low and F4/80-high. Newly recruited macrophages were classified as being F4/80-high and Gr1 positive. Levels of the neutrophil recruiting cytokine KC were measured by the Functional Genomics and Proteomics Core of the Interdisciplinary Center for Exposures, Disease, Genomics, and Environment at the University of Washington in duplicate using a Meso Scale Discovery V-plex assay (Meso Scale Discovery - Meso Scale Diagnostics, Rockville, MD).

Alveolar/Capillary Barrier Integrity and Lung Cytotoxicity

As an indicator of alveolar/capillary barrier integri*ty* between the airspace and circulation, we measured total protein in BALF using the Bio-Rad Protein Assay (BioRad, Hercules, CA). Levels of lactate dehydrogenase activity in BALF representing cytotoxicity was measured using CytoTox 96 Non-Radioactive Cytotoxicity Assay (Promega Corporation, Madison, WI).

Oxidative Stress and Glutathione

Levels of the antioxidant glutathione were measured in triplicate in lung tissue as previously described (Weldy et al. 2011). Briefly, lung tissue samples were homogenized and treated with sulfosalicylic acid and protein precipitates were pelleted by centrifugation.

Supernatants were reduced with TCEP (tris(2-carboxyethyl) phosphine) and total glutathione was derivatized with napthelene-2,3-dicarboxaldehyde. Glutathione standards were prepared in 5% 5-sulfosalicylic acid and were treated identically to samples. After interpolation of GSH quantities from the standard curve, values were normalized to total lung tissue protein levels in samples prepared by the same method as total protein in BALF. Heme oxygenase-1 (HMOX1), which is upregulated during oxidative stress, was measured using ELISA (Immunoset, Enzo Life Sciences, Farmingdale, NY).

Statistical Analyses

We tested for significant mouse strain and treatment group and mouse strain*treatment group interactions using a two-way ANOVA on log transformed data. Post-hoc analyses were done using two-sided t-tests with Welch's correction for differences in variance between the comparison groups where appropriate. Simple linear regression was used to examine relationships between % neutrophils in BALF, KC, and HMOX1. R packages nlme and ape were used to calculate between and within-strain variance components for heritability estimates (Paradis et al. 2004; Visscher et al. 2008; Almasy and Blangero 2010; Felix et al. 2012; Pinheiro et al. 2016). We compared individual CC RI strain phenotypes to average CC founder strain phenotypes measured with the same methods by one-way ANOVA followed by Dunnett's test using the combined founder strains as the reference group. Genetic mapping was performed using the EMMA (Efficient Mixed Model Association) R package (Kang et al. 2008). Genotype data (NCBI build 38/UCSC build mm10) for the 12 RI strains came from the GigaMuga genotyping array (Morgan et al. 2016). Individual animal data were run using the emma.REML.t algorithm with treatment group as a covariate. The UCSC genome browser was used to retrieve transcripts within expanded QTL regions (Kent et al. 2002). Pathway analysis was done using Ingenuity Pathway Analysis (IPA) software (Qiagen, Germantown MD). Data was managed in Microsoft Excel and R. All analyses were done using R and plots were generated using ggplot2 (Wickham 2009).

Results

Acute Lung Inflammation: BALF Inflammatory Cells and KC

We found that levels of neutrophils in BALF were significantly different across the 12 CC RI mouse strains and observed a significant interaction between mouse strain and QD treatment group (Figure 1A). However, we were not able to detect any significant individual strain differences between treatment groups, except for the CC004/TauUnc strain, where levels of neutrophils were significantly higher in saline compared to QD treated mice. Broad sense heritability estimates of % neutrophils in BALF were 0.58 and 0.67 for QD and saline treated RI mice (Table 1). We found that levels of KC were significantly different across mouse strains and between saline and QD treated mice overall (Figure 1B). Furthermore, we determined that levels of KC in BALF were significantly increased by QD treatment in CC011/Unc mice. Broad sense heritability estimates of KC in BALF were 0.30 and 0.42 for QD and saline treated RI mice (Table 1). We also observed a significant correlation between BALF KC and % BALF neutrophils (r^2=0.23, $p<0.0001$).

Alveolar/Capillary Barrier Integrity and Lung Cytotoxicity

Concentrations of BALF protein, a measure of alveolar/capillary barrier integrity, were significantly different across mouse strains and between QD and saline treated mice overall (Figure 2A). However, we were unable to uncover any significant differences between QD and saline treated mice from individual mouse strains. Broad sense heritability estimates of KC in BALF were 0.74 and 0.57 for QD and saline treated RI mice, respectively (Table 1). We found that levels of LDH in BALF, a measure of cytotoxicity, were significantly affected by mouse strain (Figure 2B). Broad sense heritability estimates of KC in BALF were 0.35 and 0.59 for QD and saline treated RI mice, respectively (Table 1).

Oxidative Stress and Glutathione

Levels of glutathione were not significantly different across mouse strains or between treatment groups overall (Figure 3A). Levels of HMOX1 in lung tissue were significantly different across mouse strains (Figure 3B). The broad sense heritability estimates of lung HMOX1 were 0.29 and 0.21 for QD and saline treated RI mice, respectively; and broad sense heritability estimates of lung GSH were 0.04 and <0.01 for QD and saline treated RI mice, respectively (Table 1).

Regression analysis of inflammation, cytotoxicity and oxidative stress markers.

Since we previously found significant associations across the CC Founder strains between levels of BALF Neutrophils and KC, we also sought to explore these relationships in the CC RI strains with the addition of HMOX1 since we found that HMOX1 varied significantly across the RI strains. We found significant positive associations between % neutrophils and KC in BALF (Figure 4A), and between lung HMOX1 and KC in BALF (Figure 4B).

Comparison of CC RI Mouse Strain Phenotypes to CC Founder Strains

As other studies have observed phenotypes in pre-CC strains outside the range of the founder strains, we compared the range of BALF neutrophils, total protein, and KC in the 12 CC RI strains to variability in the CC founder strains (Figure 5). We found that % neutrophils in 3 RI strains (CC010/GeniUnc, CC011/Unc, CC043/GeniUnc) in mice were significantly lower than the founder strain average (Figure 5A). Levels of total protein in BALF in 7 CC RI strains (CC002/Unc, CC006/TauUnc, CC010/GeniUnc, CC011/Unc, CC015/Unc, CC025/GeniUnc, CC038/GeniUnc) were greater than the CC founder strain average (Figure 5B). Levels of glutathione in 1 RI strain (CC025/GeniUnc) were significantly less than the founder strain average (Figure 5C).

Genome-wide Association (GWA) Mapping of CC RI mouse strain QD phenotypes

We observed significant differences across strains and treatment groups (BALF total protein and KC), significant strain*treatment group interaction (% BALF neutrophils) and heritable phenotypes in QD and saline treated CC RI mice. Based on high heritability and the fact that CC RI BALF protein levels were observed beyond the range of the founder strains, we chose BALF total protein as our primary phenotype for genome-wide association mapping. We performed QTL mapping using the EMMA R package incorporating individual animal data and treatment as a co-variate (Kang et al. 2008). SNPs identified using the GigaMuga genotyping array with no allelic differences across these 12 CC RI mouse strains were filtered out, and we tested 110,852 SNPs covering all autosomes, sex chromosomes, and mitochondria (Morgan et al. 2016). For total BALF protein, we detected 177 significant SNPs on chromosomes 1, 2, 3, 4, 6, 9, and 12, and X, using the Bonferroni correction (Figure 6). Single SNPs were found on chromosomes 6 and X, but no QTL peak could be discerned and these SNPs were not near genes (Figure S1). Broad QTL peaks were found on chromosomes 1, 2, 3, 4, 9, and 12 (Figure S1). There were, 3 significant SNPs in the peaks on chromosomes 1 and 2. The chromosome 3 peak contained 2 significant SNPs. We found 112 significant SNPs in the chromosome 4 QTL region. Two distinct QTL regions were evident on chromosome 9 containing 15 significant SNPs. The proximal region held 4 significant SNPs and the distal region contained 11. On chromosome 12, the QTL region held 40 significant SNPs.

Multiple SNPs were also significant after using Bonferroni correction for levels of neutrophils in BALF (Figure S2). However, since the SNPs were distributed across 13 chromosomes, we chose to prioritize the total BALF protein for further analysis. While no significant SNPs were found for levels of KC, there were suggestive regions on chromosomes 2, 6, 14, 15, 17 (Figure 2S).

Discussion

Building on previous findings of differential susceptibility in the CC founder strains (Scoville et al. 2015), we further assessed QD-induced lung inflammation and toxicity in 12 CC RI mouse strains using the same exposure method. We found that levels of BALF neutrophils differed significantly across the 12 CC RI mouse strains overall and a significant mouse strain*treatment group interaction was observed. This implies that the CC RI strains may differ in susceptibility but that we lack statistical power to determine which strains may be more susceptible than others. However, this study was designed with genetic mapping in mind, where even a relatively small number of replicate animals within each strain can substantially increase mapping power compared to only having one animal per strain (Kang et al. 2008). Broad sense heritability estimates, assessing the proportion of a given phenotype attributable to genetics, for % neutrophils in BALF were 0.58 and 0.67 for QD treated and saline treated RI mice indicating that this is a heritable trait in RI mice. CC Founder estimates of heritability were lower by comparison (0.15 QD, -0.02 Sal), but as noted by the authors, some founder strains had potential outliers which would lead to increased within-strain variation and lower heritability estimates. Furthermore, direct comparisons of % neutrophils in BALF between the CC RI strains and CC founder strains, revealed that all but one of the RI strains were similar to the founder strain average, suggesting that RI values in general do not exceed the range of the founders.

Levels of the KC also differed significantly across the 12 CC RI strains and between treatment groups. We further determined that QD treated CC011/Unc had significantly increased levels of KC than strain-matched saline controls. Heritability estimates (0.30-QD, 0.42-Sal) were comparable with estimates observed in the founder strains (0.64-QD, 0.24-Saline; (Scoville et al. 2015). The correlation between % neutrophils and KC in BALF among the CC RI strains (0.23, $p<0.0001$) was also comparable to that observed in the CC founder strains (0.38, $p<.0001$; (Scoville et al. 2015). Direct comparisons of levels of KC between the CC RI strains and CC founder strains were not made as different assays were used in

the different studies. We also observed a significant positive associated between lung HMOX1 and KC levels in BALF (0.13, $p<0.001$) suggesting a connection between low levels of oxidative stress (as indicated by lung HMOX1) and KC levels.

BALF protein levels differed significantly across both the CC RI strains and between QD and saline treatment groups, also suggesting potential differences in susceptibility. Heritability estimates in the RI strains (0.74-QD, 0.57-Sal) were higher than estimates in the CC founders (QD-0.28, Sal-0.33; (Scoville et al. 2015). In addition, several RI strains had significantly higher protein levels than the CC founder average confirming phenotypic values outside the range of the CC founders. We used the EMMA R package for genetic mapping with individual animal data, which increased statistical power, and designated treatment group as a co-variate (Kang et al. 2008). We found 177 significant SNPs (Bonferroni corrected) on chromosomes 1,2,3, 4, 6, 9, 12 and chromosome X. Using the UCSC genome browser, we found that the single SNPs on chromosomes 6 and X with no evident QTL peaks were not in close proximity to any genes. Broad QTL peaks were observed on chromosomes 1, 2, 3, 4, 9 (2 distinct regions), and 12. Given the large number of significant SNPs found, we chose to pursue pathway analysis, which has been used as an approach to give biological context to groups of GWA mapped SNPs (Eleftherohorinou et al. 2009; Zhong et al. 2010; Kao et al. 2017). To determine what genes were encompassed by the chromosomes 4, 9, and 12 QTL regions, lists were made by subtracting 1000 base pairs from the genetic position of the most proximal SNP and adding 1000 base pairs to the most distal SNP in each QTL region. Using the UCSC Genome Browser, we identified over 300 transcripts contained in the expanded QTL regions. Ingenuity Pathway Analysis Software (IPA) converted the list of transcripts to a list of 234 known genes. IPA identified 14 pathways that were significantly enriched ($p<0.05$) (Figure S3). The two most significant canonical pathways were the visual cycle and nucleotide excision repair (NER) (Figure S4). The genes from our list in the IPA visual cycle pathway are retinol dehydrogenase 11 and 12 (RDH11 and RDH 12), and retinoid isomerohydrolase (RPE65), which suggests that QDs

may interact with retinol/retinoic acid metabolism. Retinoic acid is involved with alveolar epithelial cell regeneration (Yang et al. 2015).

A previous mouse study indicated that QDs induced DNA damage to BAL cells using the single-cell gel electrophoresis (COMET) assay (Jacobsen et al. 2009). The genes from the present study that are in the IPA NER pathway were Mnat1, Rad23B, and *Xpa.* Rad23B is involved in recognizing DNA lesions and recruiting transcription factor II H (TFIIH). Mnat1 (MAT1) is a component of TFIIH which is involved with unwinding DNA for lesion repair. Xpa helps coordinate the removal of TFIIH once the double stranded DNA is opened (Compe and Egly 2012). NER proteins are thought to contribute the repair of a variety of damage including oxidative DNA damage, which would be consistent with the ability of QDs to induce oxidative stress (Lovrić et al. 2005; Neibert and Maysinger 2011; Pascucci et al. 2011; Marteijn et al. 2014).

Overall, results from this study suggest that susceptibility to QD-induced lung inflammation may differ across the 12 CC RI strains we investigated. While the 12 CC RI strains showed a similar phenotypic range as the CC founders for glutathione and % neutrophils, the range of BALF protein levels in the CC RI mice was greater. The strength of the relationship between KC and % neutrophils in BALF was comparable with that observed previously in the CC founders. Results from pathway analysis using a gene list derived from over 150 significant SNPs identified with GWA mapping indicate that CC RI may be differentially susceptible to QD interactions with retinol/retinoic acid metabolism and QD-induced DNA damage.

In conclusion, CC RI mice combined with computational methods that incorporate within-strain replicates and control for population structure are a powerful GWA mapping resource given that broad QTLs could be mapped with just 12 CC RI strains and less than 100 total mice. Future studies investigating QD-induced DNA damage, together with QD-induced lung inflammation and toxicity phenotyping studies in additional CC RI strains are

warranted. Such studies will assist in GWA mapping resolution, and help to narrow the list of candidate genes associated with QD-induced lung injury.

Chapter 3 References

Almasy, L. and J. Blangero (2010). "Variance Component Methods for Analysis of Complex Phenotypes." Cold Spring Harbor protocols **2010**(5).

Aylor, D. L., W. Valdar, W. Foulds-Mathes, R. J. Buus, R. A. Verdugo, R. S. Baric, . . . G. A. Churchill (2011). "Genetic analysis of complex traits in the emerging Collaborative Cross." Genome Research **21**(8): 1213-1222.

Bae, W. K., Y.-S. Park, J. Lim, D. Lee, L. A. Padilha, H. McDaniel, . . . V. I. Klimov (2013). "Controlling the influence of Auger recombination on the performance of quantum-dot light-emitting diodes." Nature Communications **4**.

Bagalkot, V. and X. Gao (2011). "siRNA-Aptamer Chimeras on Nanoparticles: Preserving Targeting Functionality for Effective Gene Silencing." ACS Nano **5**(10): 8131-8139.

Bauer, A. K. and S. R. Kleeberger (2010). "Genetic mechanisms of susceptibility to ozone-induced lung disease." Annals of the New York Academy of Sciences **1203**(1): 113-119.

Broman, K. W. (2001). "Review of statistical methods for QTL mapping in experimental crosses." Lab Animal **30**(7): 44-52.

Chiu, W. A., J. L. Campbell, Jr., H. J. Clewell, 3rd, Y. H. Zhou, F. A. Wright, K. Z. Guyton and I. Rusyn (2014). "Physiologically based pharmacokinetic (PBPK) modeling of interstrain variability in trichloroethylene metabolism in the mouse." Environmental Health Perspectives **122**(5): 456-463.

Church, R. J., H. Wu, M. Mosedale, S. J. Sumner, W. Pathmasiri, C. L. Kurtz, . . . A. H. Harrill (2014). "A Systems Biology Approach Utilizing a Mouse Diversity Panel Identifies Genetic Differences Influencing Isoniazid-Induced Microvesicular Steatosis." Toxicological Sciences **140**(2): 481-492.

Compe, E. and J.-M. Egly (2012). "TFIIH: when transcription met DNA repair." Nature Reviews Molecular Cell Biology **13**(6): 343-354.

Eleftherohorinou, H., V. Wright, C. Hoggart, A.-L. Hartikainen, M.-R. Jarvelin, D. Balding, . . . M. Levin (2009). "Pathway Analysis of GWAS Provides New Insights into Genetic Susceptibility to 3 Inflammatory Diseases." PLOS ONE **4**(11): e8068.

Felix, T. M., K. A. Hughes, E. A. Stone, J. M. Drnevich and J. Leips (2012). "Age-Specific Variation in Immune Response in Drosophila melanogaster Has a Genetic Basis." Genetics **191**(3): 989-1002.

Harrill, A. H., P. B. Watkins, S. Su, P. K. Ross, D. E. Harbourt, I. M. Stylianou, . . . D. W. Threadgill (2009). "Mouse population-guided resequencing reveals that variants in CD44 contribute to acetaminophen-induced liver injury in humans." Genome Research **19**(9): 1507-1515.

Ho, C. C., H. Chang, H. T. Tsai, M. H. Tsai, C. S. Yang, Y. C. Ling and P. Lin (2013). "Quantum dot 705, a cadmium-based nanoparticle, induces persistent inflammation and granuloma formation in the mouse lung." Nanotoxicology **7**(1): 105-115.

Jacobsen, N. R., P. Moller, K. A. Jensen, U. Vogel, O. Ladefoged, S. Loft and H. Wallin (2009). "Lung inflammation and genotoxicity following pulmonary exposure to nanoparticles in ApoE-/- mice." Particle and Fibre Toxicology **6**(2).

Jung, H., W. Chung, C. H. Lee and S. H. Kim (2012). "Fabrication of white light-emitting diodes based on UV light-emitting diodes with conjugated polymers-(CdSe/ZnS) quantum dots as hybrid phosphors." Journal of Nanoscience and Nanotechnology **12**(7): 5407-5411.

Kang, H. M., N. A. Zaitlen, C. M. Wade, A. Kirby, D. Heckerman, M. J. Daly and E. Eskin (2008). "Efficient Control of Population Structure in Model Organism Association Mapping." Genetics **178**(3): 1709-1723.

Kao, P. Y. P., K. H. Leung, L. W. C. Chan, S. P. Yip and M. K. H. Yap (2017). "Pathway analysis of complex diseases for GWAS, extending to consider rare variants, multi-

omics and interactions." Biochimica et Biophysica Acta (BBA) - General Subjects **1861**(2): 335-353.
Kent, W. J., C. W. Sugnet, T. S. Furey, K. M. Roskin, T. H. Pringle, A. M. Zahler, . . . David (2002). "The Human Genome Browser at UCSC." Genome Research **12**(6): 996-1006 -- http://genome.ucsc.edu/.
Kim, S., Y. T. Lim, E. G. Soltesz, A. M. De Grand, J. Lee, A. Nakayama, . . . J. V. Frangioni (2004). "Near-infrared fluorescent type II quantum dots for sentinel lymph node mapping." Nature Biotechnology **22**(1): 93-97.
Liu, B. (1998). Statistical Genomics - Linkage, Mapping, and QTL Analysis. Boca Raton, Florida, CRC Press.
Lovrić, J., S. J. Cho, F. M. Winnik and D. Maysinger (2005). "Unmodified Cadmium Telluride Quantum Dots Induce Reactive Oxygen Species Formation Leading to Multiple Organelle Damage and Cell Death." Chemistry & Biology **12**: 1227-1234.
Ma-Hock, L., S. Brill, W. Wohlleben, P. M. A. Farias, C. R. Chaves, D. P. L. A. Tenório, . . . B. van Ravenzwaay (2012). "Short term inhalation toxicity of a liquid aerosol of CdS/Cd(OH)2 core shell quantum dots in male Wistar rats." Toxicology Letters **208**(2): 115-124.
Ma-Hock, L., P. M. Farias, T. Hofmann, A. C. Andrade, J. N. Silva, T. M. Arnaud, . . . B. van Ravenzwaay (2013). "Short term inhalation toxicity of a liquid aerosol of glutaraldehyde-coated CdS/Cd(OH) core shell quantum dots in rats." Toxicology Letters **225**(1): 20-26.
Marteijn, J. A., H. Lans, W. Vermeulen and J. H. J. Hoeijmakers (2014). "Understanding nucleotide excision repair and its roles in cancer and ageing." Nature Reviews Molecular Cell Biology **15**(7): 465-481.
McConnachie, L. A., D. Botta, C. C. White, C. S. Weldy, H. W. Wilkerson, J. Yu, . . . T. J. Kavanagh (2013). "The Glutathione Synthesis Gene Gclm Modulates Amphiphilic Polymer-Coated CdSe/ZnS Quantum Dot-Induced Lung Inflammation in Mice." PLOS ONE **8**(5): e64165.
McConnachie, L. A., C. C. White, D. Botta, M. E. Zadworny, D. P. Cox, R. P. Beyer, . . . T. J. Kavanagh (2012). "Heme oxygenase expression as a biomarker of exposure to amphiphilic polymer-coated CdSe/ZnS quantum dots." Nanotoxicology **7**(2): 181-191.
Morgan, A. P., C.-P. Fu, C.-Y. Kao, C. E. Welsh, J. P. Didion, L. Yadgary, . . . F. Pardo-Manuel de Villena (2016). "The Mouse Universal Genotyping Array: From Substrains to Subspecies." G3: Genes|Genomes|Genetics **6**(2): 263.
Neibert, K. D. and D. Maysinger (2011). "Mechanisms of cellular adaptation to quantum dots – the role of glutathione and transcription factor EB." Nanotoxicology **6**(3): 249-262.
Nichols, J. L., W. Gladwell, K. C. Verhein, H.-Y. Cho, J. Wess, O. Suzuki, . . . S. R. Kleeberger (2014). "Genome-wide association mapping of acute lung injury in neonatal inbred mice." The FASEB Journal **28**(6): 2538-2550.
Paradis, E., J. Claude and K. Strimmer. (2004). "A{PE}: analyses of phylogenetics and evolution in R language." 20, from https://cran.r-project.org/package=ape.
Pascucci, B., M. D'Errico, E. Parlanti, S. Giovannini and E. Dogliotti (2011). "Role of nucleotide excision repair proteins in oxidative DNA damage repair: an updating." Biochemistry (Moscow) **76**(1): 4-15.
Payseur, B. A. and M. Place (2007). "Prospects for Association Mapping in Classical Inbred Mouse Strains." Genetics **175**(4): 1999-2008.
Pellegrino, T., L. Manna, S. Kudera, T. Liedl, D. Koktysh, A. L. Rogach, . . . W. J. Parak (2004). "Hydrophobic Nanocrystals Coated with an Amphiphilic Polymer Shell: A General Route to Water Soluble Nanocrystals." Nano Letters **4**(4): 703-707.

Phillippi, J., Y. Xie, D. R. Miller, T. A. Bell, Z. Zhang, A. B. Lenarcic, . . . J. A. Frelinger (2014). "Using the emerging Collaborative Cross to probe the immune system." Genes and Immunity **15**(1): 38-46.

Pinheiro, J., D. Bates, S. DebRoy, D. Sarkar and R. C. Team. (2016). "nlme: Linear and Nonlinear Mixed Effects Models." from http://cran.r-project.org/package=nlme.

Roberts, J. R., J. M. Antonini, D. W. Porter, R. S. Chapman, J. F. Scabilloni, S. H. Young, . . . R. R. Mercer (2013). "Lung toxicity and biodistribution of Cd/Se-ZnS quantum dots with different surface functional groups after pulmonary exposure in rats." Particle and Fibre Toxicology **10**: 5.

Scoville, D. K., C. C. White, D. Botta, L. A. McConnachie, M. E. Zadworny, S. C. Schmuck, . . . T. J. Kavanagh (2015). "Susceptibility to quantum dot induced lung inflammation differs widely among the Collaborative Cross founder mouse strains." Toxicology and Applied Pharmacology **289**(2): 240-250.

Seiffert, J., F. Hussain, C. Wiegman, F. Li, L. Bey, W. Baker, . . . K. F. Chung (2015). "Pulmonary Toxicity of Instilled Silver Nanoparticles: Influence of Size, Coating and Rat Strain." PLOS ONE **10**(3): e0119726.

Threadgill, D. W. and G. A. Churchill (2012). "Ten Years of the Collaborative Cross." Genetics **190**(2): 291-294.

Threadgill, D. W., D. R. Miller, G. a. Churchill and F. P.-M. de Villena (2011). "The collaborative cross: a recombinant inbred mouse population for the systems genetic era." ILAR journal / National Research Council, Institute of Laboratory Animal Resources **52**: 24-31.

Visscher, P. M., W. G. Hill and N. R. Wray (2008). "Heritability in the genomics era - concepts and misconceptions." Nature Reviews Genetics **9**(4): 255-266.

Walters, D. M., K. M. White, U. Patel, M. J. Davis, R. M. Veluci-Marlow, S. R. Bhupanapadu Sunkesula, . . . S. R. Kleeberger (2014). "Genetic susceptibility to interstitial pulmonary fibrosis in mice induced by vanadium pentoxide (V2O5)." The FASEB Journal **28**(3): 1098-1112.

Weldy, C. S., C. C. White, H.-W. Wilkerson, T. V. Larson, J. A. Stewart, S. E. Gill, . . . T. J. Kavanagh (2011). "Heterozygosity in the glutathione synthesis gene Gclm increases sensitivity to diesel exhaust particulate induced lung inflammation in mice." Inhalation Toxicology **23**(12): 724-735.

Wickham, H. (2009). ggplot2: Elegant Graphics for Data Analysis, Springer Publishing Company, Incorporated.

Wu, X., H. Liu, J. Liu, K. N. Haley, J. A. Treadway, J. P. Larson, . . . M. P. Bruchez (2003). "Immunofluorescent labeling of cancer marker Her2 and other cellular targets with semiconductor quantum dots." Nature Biotechnology **21**(1): 41-46.

Yang, C., X. Yang, J. Du, H. Wang, H. Li, L. Zeng, . . . J. Jiang (2015). "Retinoic acid promotes the endogenous repair of lung stem/progenitor cells in combined with simvastatin after acute lung injury: a stereological analysis." Respiratory Research **16**(1): 140.

Zhong, H., X. Yang, L. M. Kaplan, C. Molony and E. E. Schadt (2010). "Integrating Pathway Analysis and Genetics of Gene Expression for Genome-wide Association Studies." The American Journal of Human Genetics **86**(4): 581-591.

Zou, F. (2009). "QTL mapping in intercross and backcross populations." Methods in Molecular Biology **573**: 157-173.

Table 1.

Broad sense heritability of RI Mouse strain QD phenotypes.

Phenotype	h^2	
	QD	Sal
% Neutrophils in BALF	0.58	0.67
BALF KC	0.30	0.42
BALF Total Protein	0.74	0.57
BALF LDH	0.35	0.59
Lung GSH	0.04	<0.01
Lung HMOX1	0.29	0.21

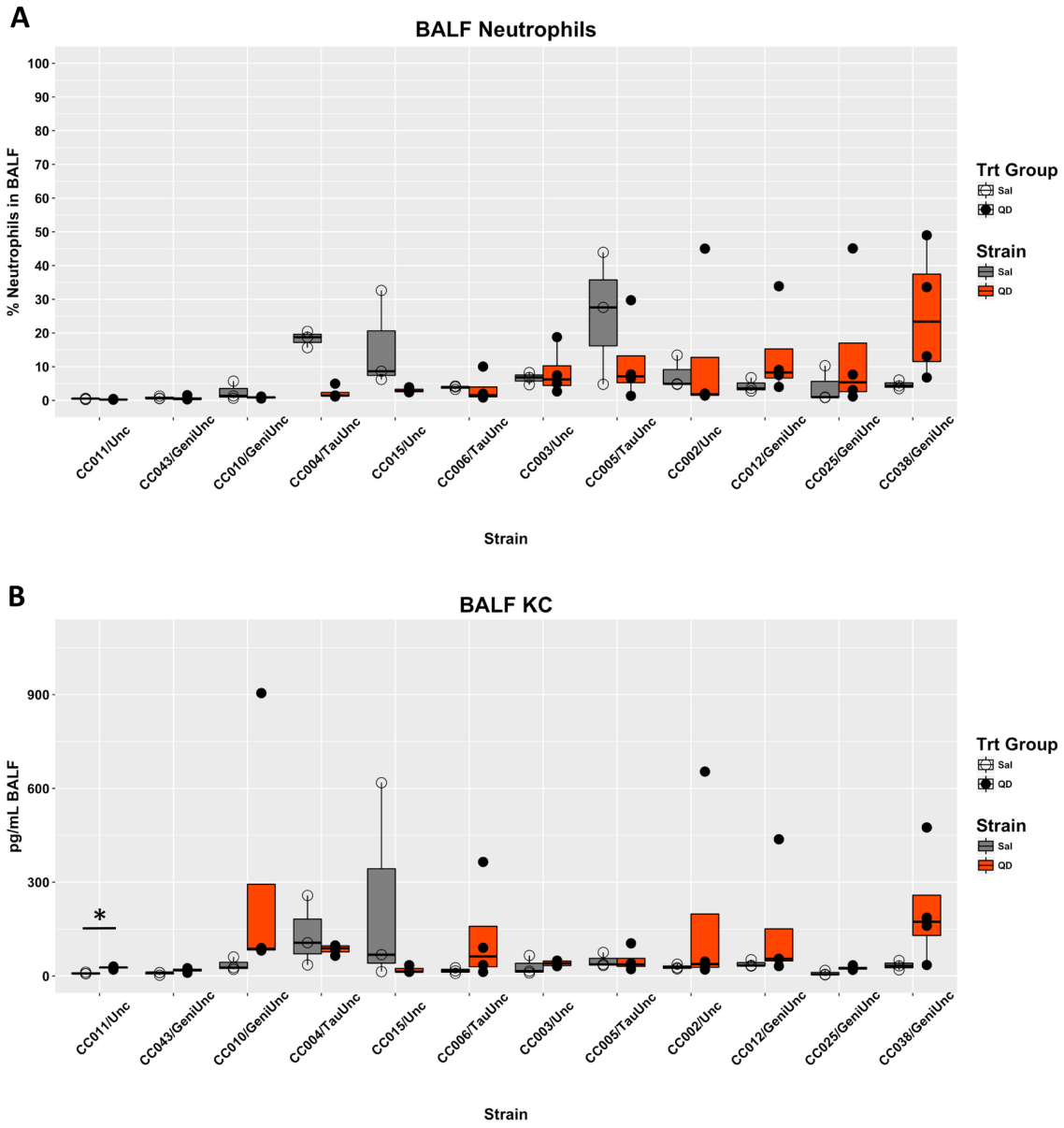

Figure 1. Percent neutrophils in BALF (A) and KC levels in BALF(B) for each QD and Saline treated mouse from 12 CC RI strains are shown overlaid on box plots.

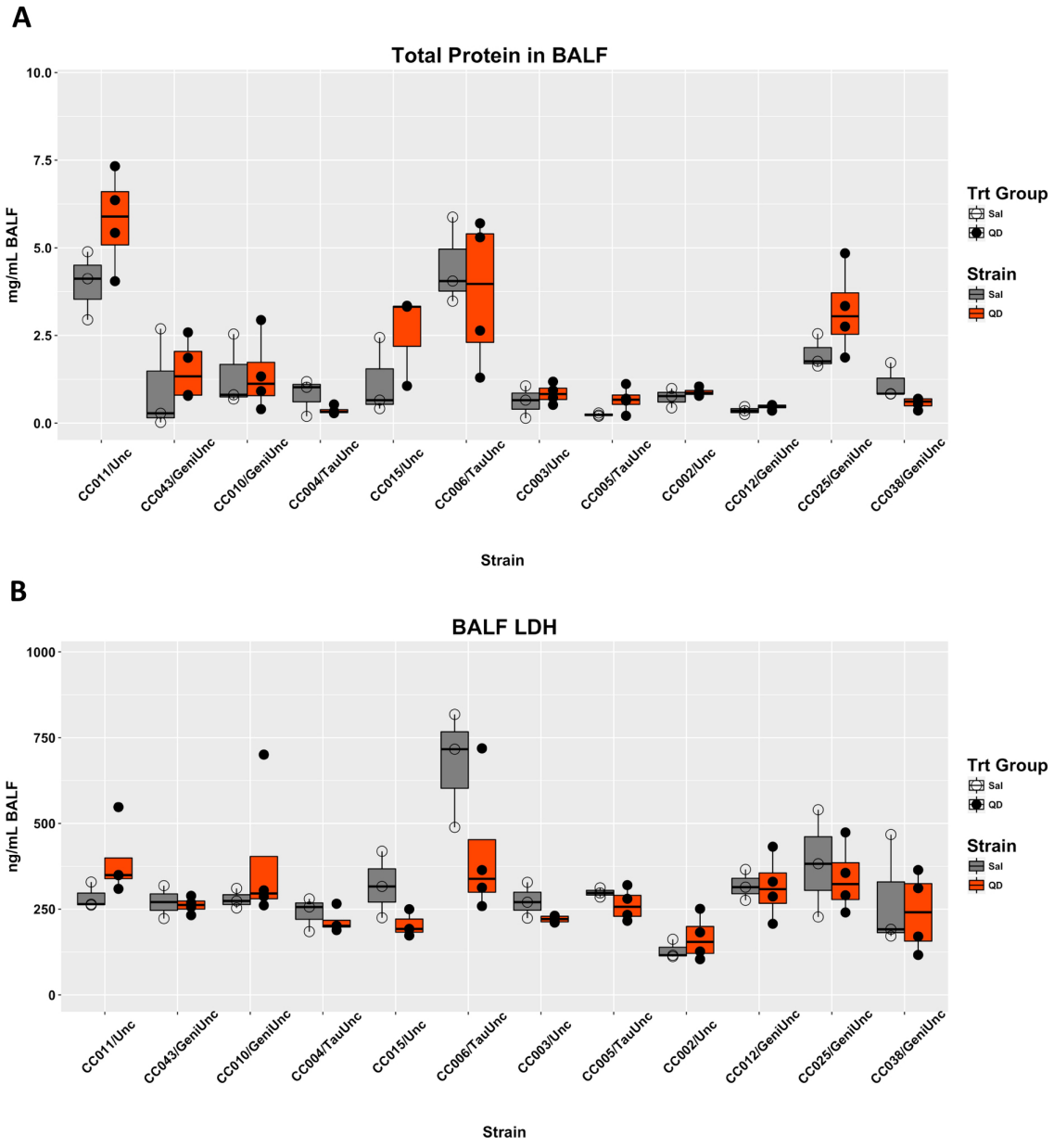

Figure 2. Total protein in BALF(A) and LDH levels in BALF (B) for each QD and Saline treated mouse from 12 CC RI strains are shown overlaid on box plots.

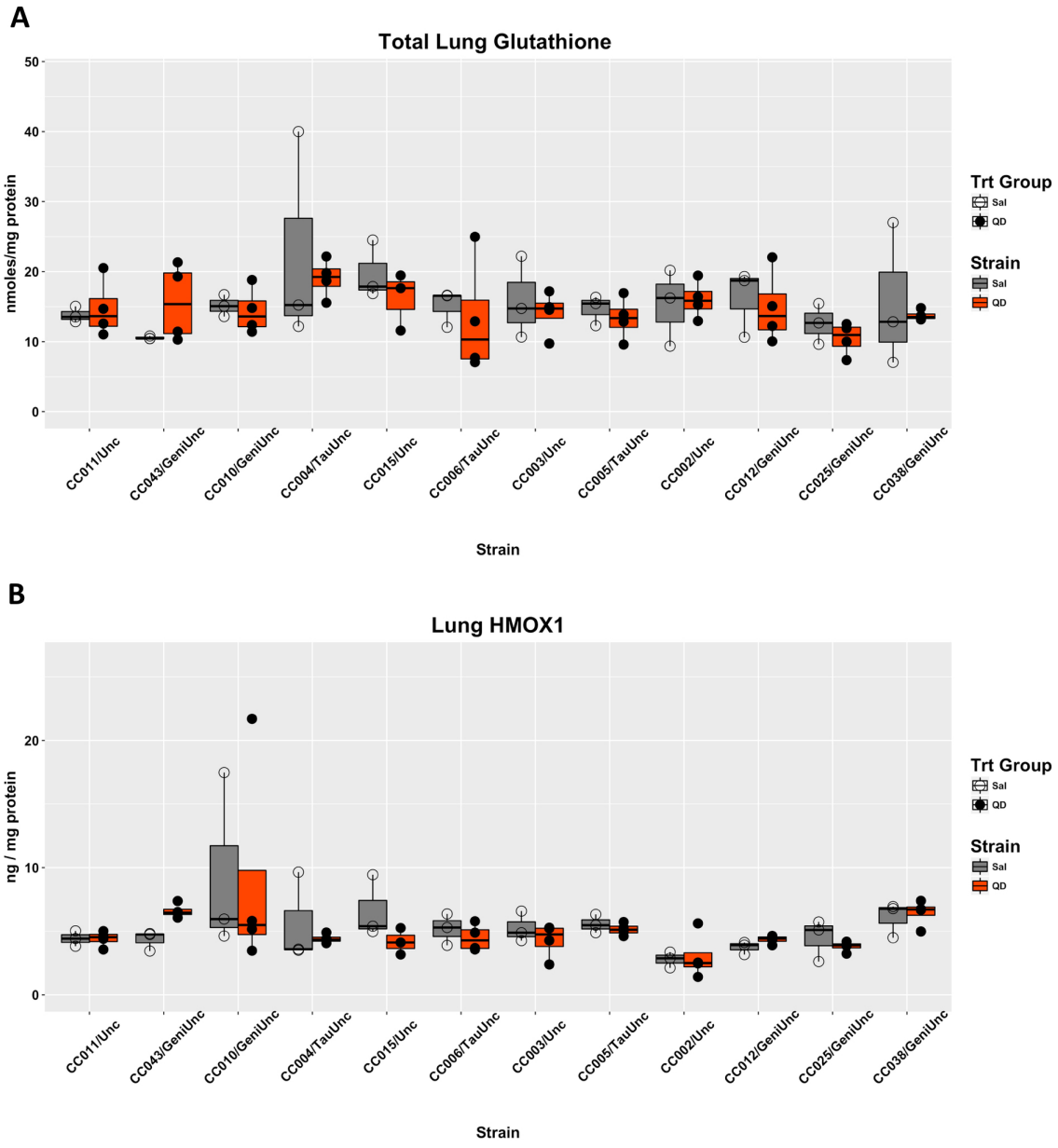

Figure 3. Total lung glutathione (A) and HMOX1 in BALF (B) for each QD and Saline treated mouse from 12 CC RI strains are shown overlaid on box plots.

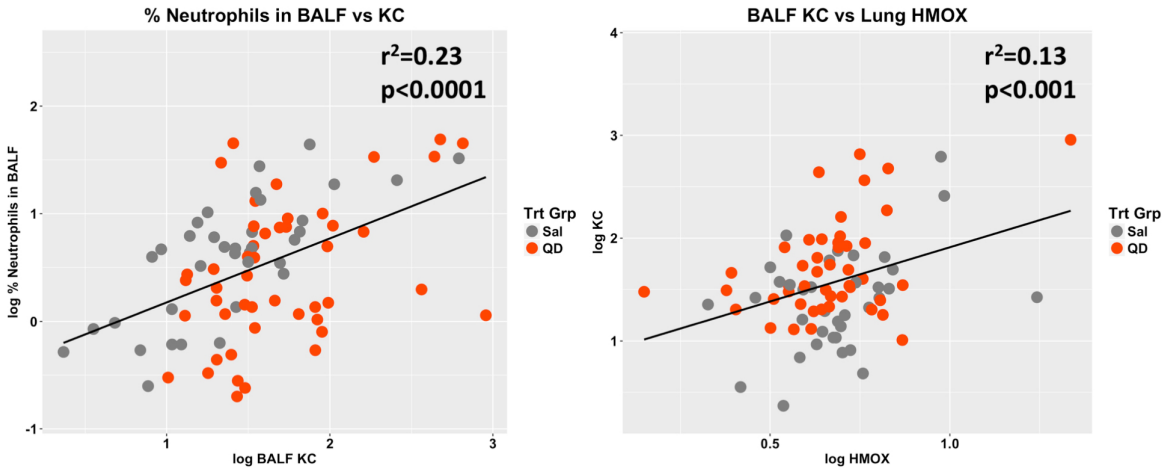

Figure 4. Scatter plots compare % neutrophils in BALF to levels of BALF KC (A), levels of BALF KC to HMOX1 (B). The linear regression line is plotted along with the r^2 and p-value of the association.

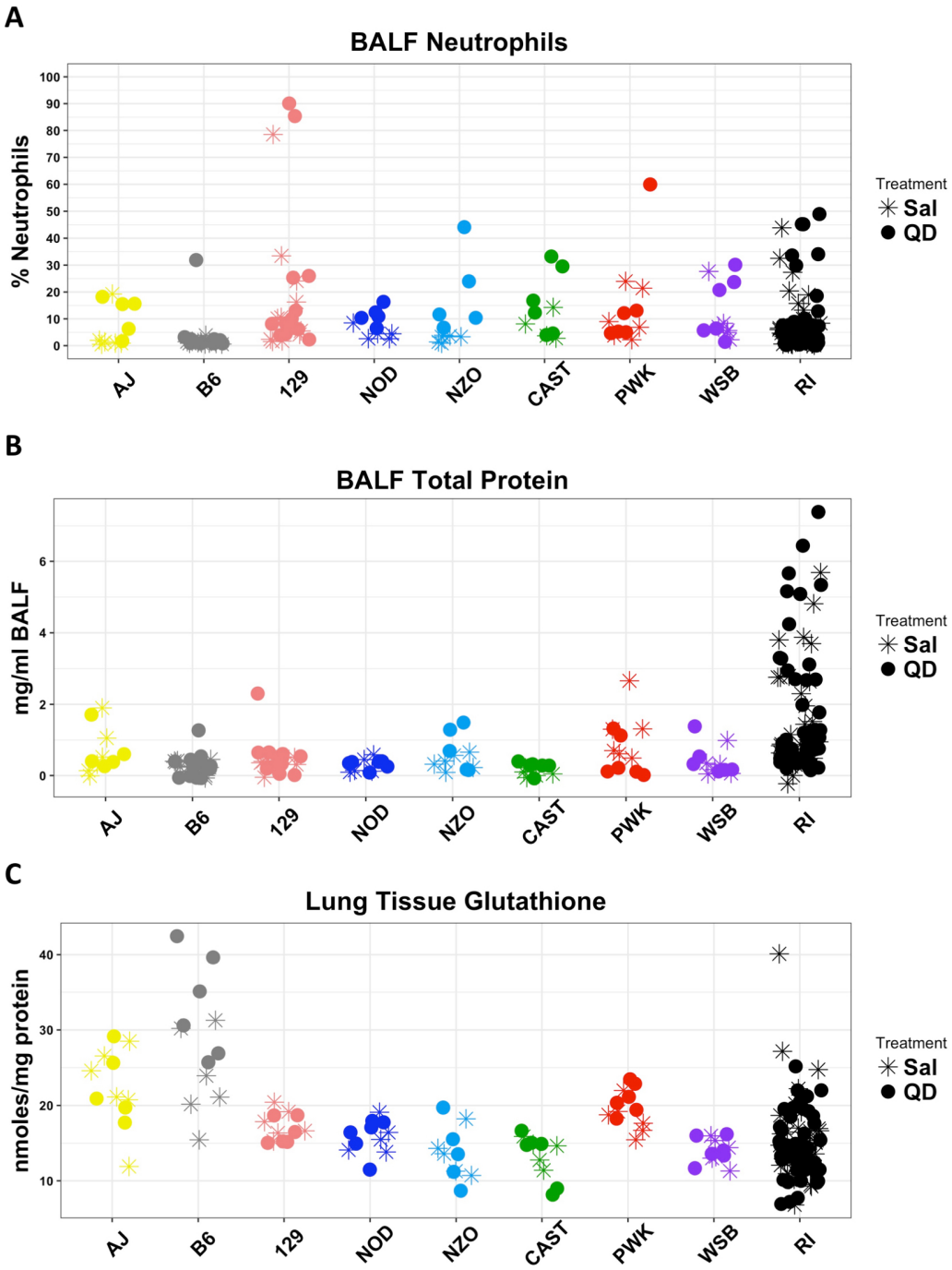

Figure 5. CC founder strain and RI strain % neutrophils in BALF (A), total protein in BALF (B), and lung glutathione (C). The CC founder strains are abbreviated: (AJ-A/J, B6-C57L/6J, 129-129S1/SvImJ, NOD- NOD/ShiLtJ, NZO- NZO/HlLtJ, CAST-CAST/EiJ, PWK-PWK/PhJ, WSB-WSB/EiJ).

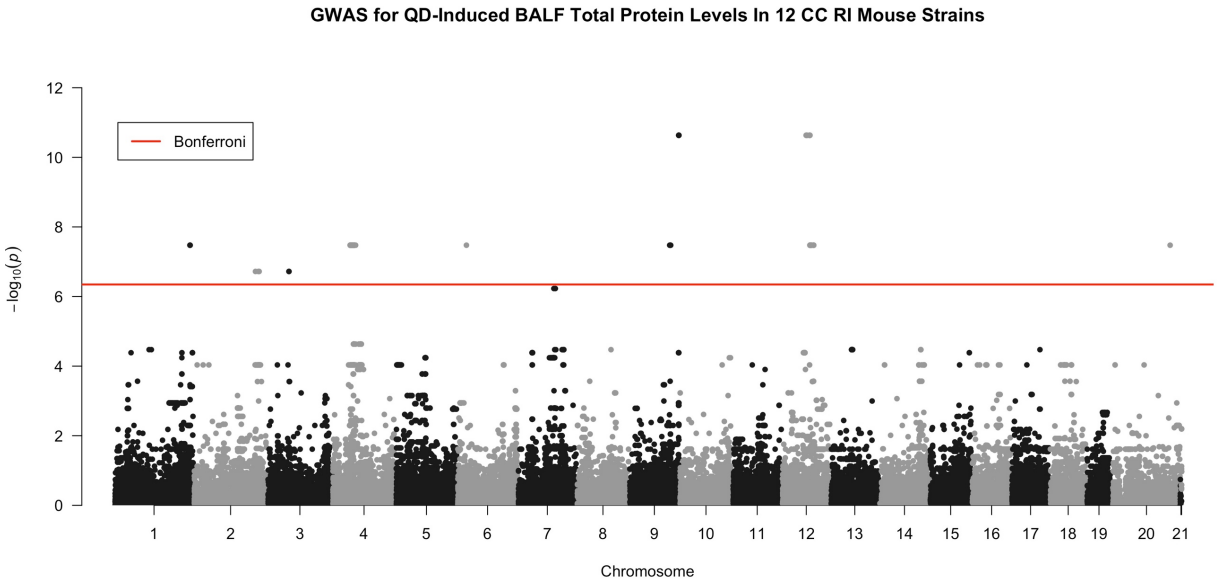

Figure 6. Manhattan plot with chromosomes and SNP location on the x-axis and -$\log_{10}$(p) for SNP associations with levels of total BALF Protein on the y-axis. The red line shows the cutoff for SNP -$\log_{10}$(p) values to be considered significant after Bonferroni correction. In this study, 110,852 SNPs were tested for association so p-values must be less than 0.45×10^{-7}, equating to a $-\log_{10}$(p) cutoff at 6.34.

Supplemental Information

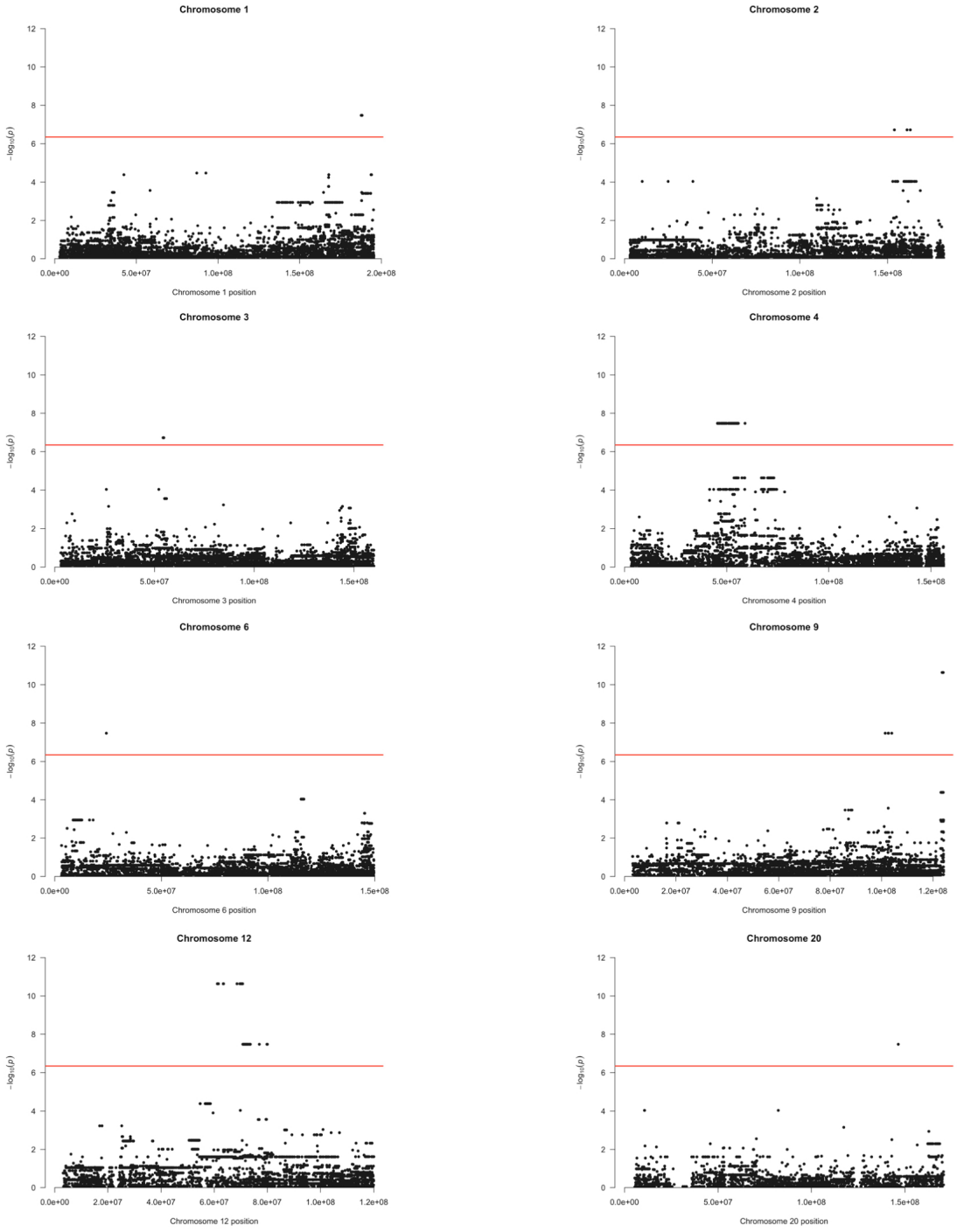

Figure S1. SNPs on chromosomes 1, 2, 3, 4, 6 ,9, 12, and X (shown on plot as 20) from the BALF total protein GWA mapping. Red lines represent Bonferroni cutoff.

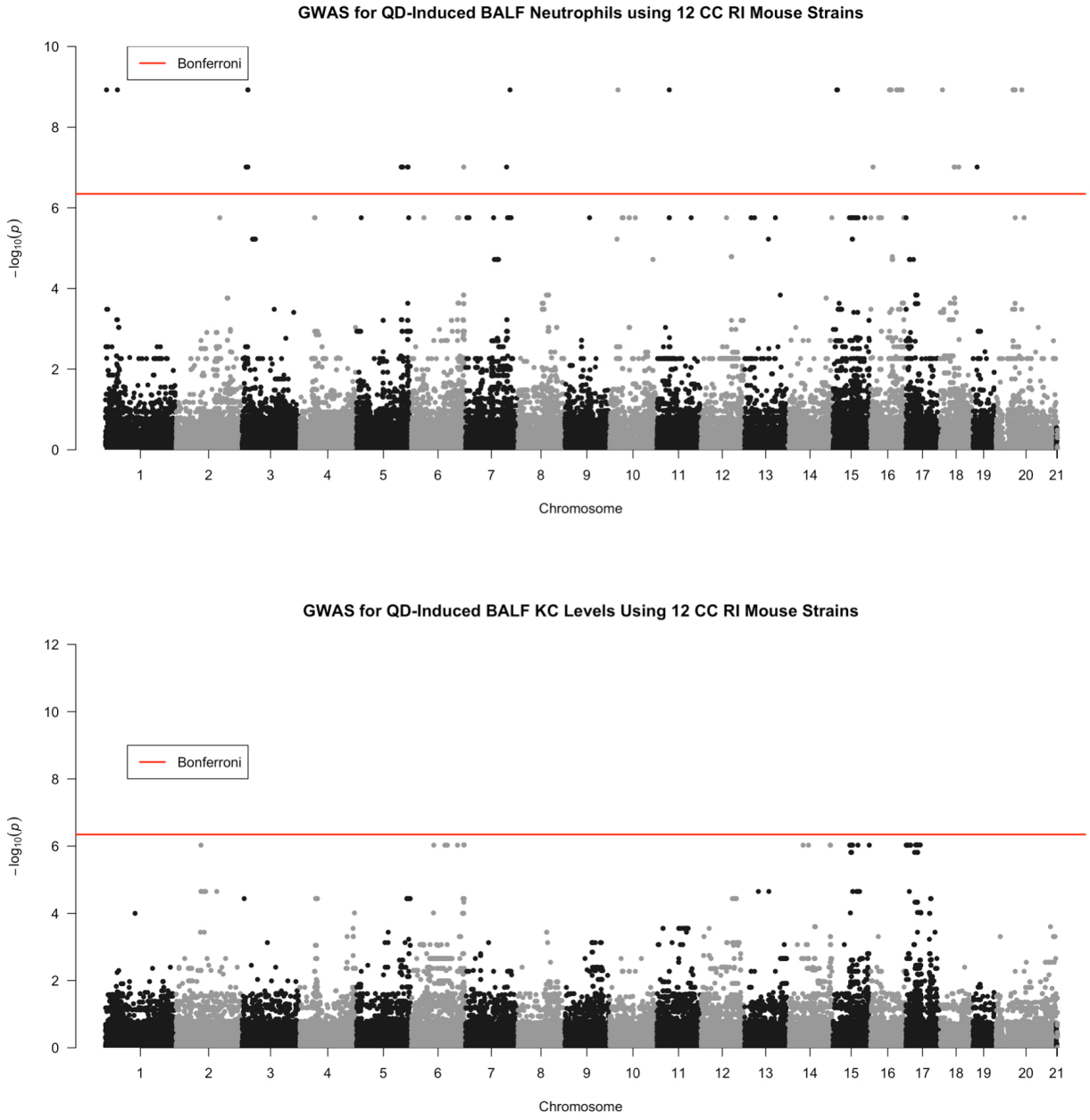

Figure S2. SNPs from GWA mapping for % neutrophils in BALF (A), and KC. The red line shows the cutoff for SNP -$\log_{10}$(p) values to be considered significant after Bonferroni correction.

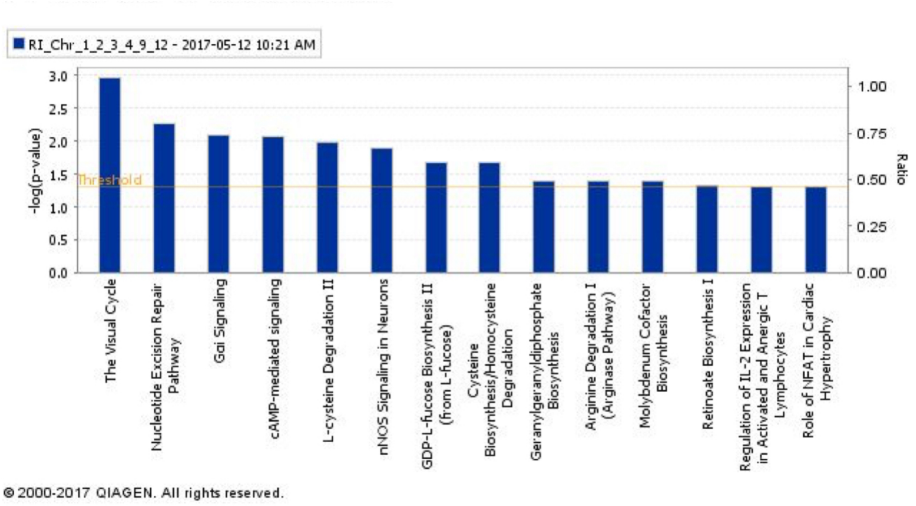

Figure S3. Significant IPA pathways are shown with bars representing the $-\log_{10}$ of the pathway p-values.

A The Visual Cycle

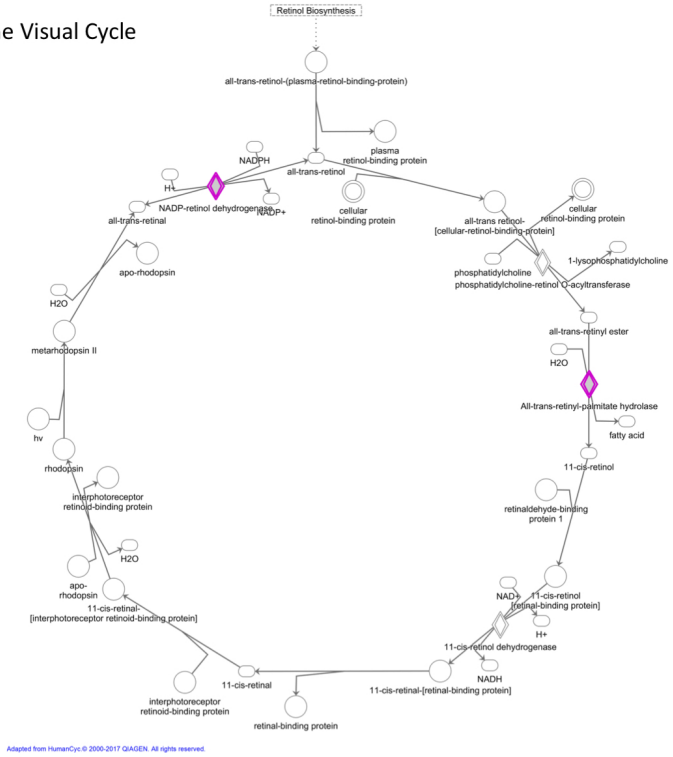

B Nucleotide Excision Repair

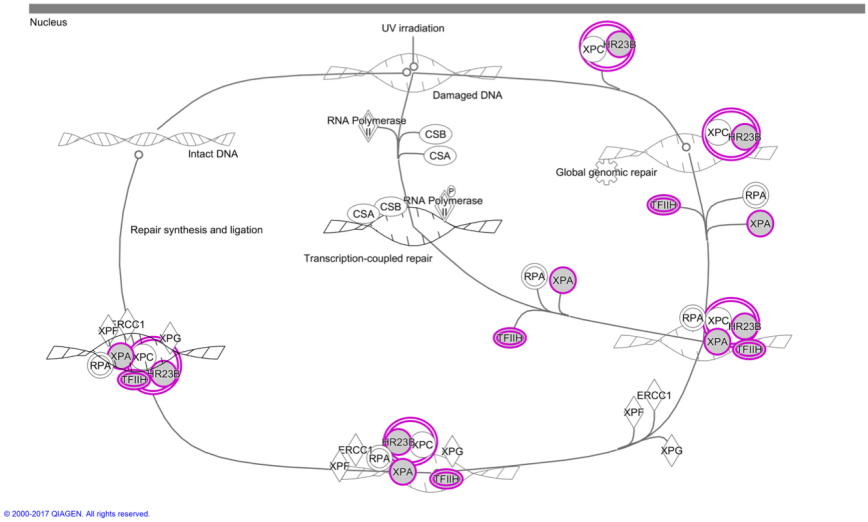

Figure S4. The IPA visual cycle (A) and nucleotide excision repair pathways (B). Genes from the GWA mapping generated gene list and protein complexes containing genes from this list are indicated in purple.

Chapter 4

Genetic Determinants of Susceptibility to Silver Nanoparticle-Induced Acute Lung Inflammation in Mice

David K. Scoville[1], Dianne Botta[1], Karen Galdanes[2], Stefanie C. Schmuck[1], Collin C. White[1], Patricia L. Stapleton[1], Theo K. Bammler[1], James W. MacDonald[1], William A. Altemeier[3], Michelle Hernandez[2], Steven R. Kleeberger[4], Lung-Chi Chen[2], Terry Gordon[2] and Terrance J. Kavanagh[1]

Departments of [1]Environmental and Occupational Health Sciences and [3]Medicine, University of Washington, Seattle, WA 98195
[2]Department of Environmental Medicine, New York University, Tuxedo, NY 10987
[4]Immunity, Inflammation, and Disease Laboratory, National Institute of Environmental Health Sciences, Research Triangle Park, NC 27709.

Corresponding Author:
Terrance J. Kavanagh, PhD
Department of Environmental and Occupational Health Sciences
Box 354695
University of Washington
Seattle, WA 98195, USA.
Tel: (206) 685-8479
Fax: (206) 685-4696
E-mail: tjkav@uw.edu
Running Title: Mouse GWAS for AgNP-Induced Lung Inflammation

Abstract

Silver nanoparticles (AgNPs) are employed in a variety of consumer products. However, *in vivo* rodent studies indicate that AgNPs can cause lung inflammation and toxicity in a strain- and particle type-dependent manner, but mechanisms of susceptibility remain unclear. The aim of this study was to assess variation in AgNP-induced lung inflammation and toxicity across multiple inbred mouse strains and use genome wide association (GWA) mapping to identify potential candidate susceptibility genes. We dosed mice with 0.25 mg/kg of either 20 nm citrate-coated AgNPs or citrate buffer using oropharyngeal aspiration (OPA). Neutrophils in bronchoalveolar lavage fluid (BALF) served as the marker of inflammation. We used the EMMA R package to perform GWA mapping. Quantitative RT-PCR was performed on candidate genes. We found significant strain and treatment dependent variation in neutrophils in BALF. GWA mapping identified 10 significant SNPs (FDR 15%) in 4 quantitative trait loci on mouse chromosomes 1, 4, 15, and 18, and *Nedd4l* (Chr 18), *Ano6* (Chr 15) and *Rnf220* (Chr 4) were considered candidate genes. qRT-PCR revealed significant inverse associations between mRNA levels of these genes and neutrophil influx. *Nedd4l*, *Ano6* and *Rnf220* are candidate susceptibility genes for AgNP-induced lung inflammation that warrant further exploration in future studies.

Introduction

Silver nanoparticles (AgNPs) are currently incorporated into a variety of consumer products ranging from athletic wear to toothbrushes (The Project on Emerging Nanotechnologies 2016). Because the number of AgNP containing products continues to grow, an increased likelihood of exposure to AgNPs among workers and consumers is expected. In facilities producing varied types of engineered nanoparticles (ENMs), there are indications that employees manufacturing ENMs may be at increased risk for adverse respiratory and cardiovascular outcomes (Cui 2013; Liao et al. 2014; Lee et al. 2015). The current OSHA permitted exposure limit (PEL) for silver dusts and soluble compounds is 0.01 mg/m^3 (The National Institute for Occupational Safety and Health 2014; Weldon et al. 2016). However, based on more recent inhalation studies in rats, Weldon et al propose an occupational exposure limit (OEL) of 0.19 ug/m^3 for AgNPs, based on bile duct hyperplasia. This OEL is also predicted to be protective of adverse lung effects caused by AgNP inhalation (Weldon et al. 2016).

In vitro studies have shown that AgNPs are cytotoxic in a cell-, dose-, size and coating-dependent manner. A study conducted in mouse embryonic fibroblast suggested oxidative stress, mitochondrial dysfunction, apoptosis, and autophagy as mechanisms of AgNP toxicity (Lee et al. 2014). In human lung cell lines BEAS-2B and A549, size, dose, and coating have been shown to modify AgNP induced cellular toxicity (Liu et al. 2010; Gliga et al. 2014; Wang et al. 2014). In BEAS-2B cells, 10 nm citrate coated AgNPs significantly reduced cell viability at 20 ug/mL and increased necrosis at 50 µg/mL compared to 40 and 75 nm citrate coated AgNPs (Gliga et al. 2014). Similar results were also found wherein 20nm citrate and polyvinylpyrrolidone (PVP) coated AgNP decreased BEAS-2B viability to a greater degree than 110 nm citrate coated AgNPs (Wang et al. 2014). In contrast, 110 nm PVP coated AgNP did not significantly decrease cell viability at doses up to 50 ï g/mL (Wang et al. 2014). Compared to 20 and 100 nm PVP coated AgNPs and 110 nm citrate coated AgNPs, 20 nm citrate coated AgNPs induced the highest levels of oxidative stress and

necrosis (Wang et al. 2014). Furthermore, particle coating (polyethylene glycol vs. branched polyethyleneimine) was also observed to modify the toxicity of AgNPs in the Hepa1c1c7 mouse liver cell line (Pang et al. 2016).

The size of AgNPs also modulates *in vivo* acute pro-inflammatory potential. In a recent study, 20 nm AgNPs induced higher numbers of neutrophils in BALF in Brown Norway (BN) rats than 110 nm AgNPs at 1 day after instillation, regardless of outer coating type (Seiffert et al. 2015). Neutrophils are a major component of the acute inflammatory response and are a commonly used marker of inflammation in ENM and other pulmonary toxicity studies (Kolaczkowska and Kubes 2013). Increases in total protein concentrations in BALF, indicative of compromised capillary/alveolar barrier function, were also observed in BN rats at 1 and 7 days after exposure to 20 nm citrate or PVP coated AgNPs, but not 110 nM AgNPs of either coating (Holter et al. 1986; Seiffert et al. 2015). Given that oxidative stress and cellular necrosis can trigger and exacerbate inflammation, *in vitro* observations of 20 nm citrate coated AgNPs inducing higher levels of oxidative stress and cellular necrosis are consistent with *in vivo* studies, where 20 nm citrate particles induced the highest levels of acute neutrophilic inflammatory responses (Morgan and Liu 2011; Wallach et al. 2014; Wang et al. 2014; Seiffert et al. 2015).

AgNP studies in SD rats provide additional evidence that size may also modify the timing of the inflammatory response and that size and coating affect the quantity and localization of AgNPs (Anderson et al. 2014; Anderson et al. 2015; Silva et al. 2015; Silva et al. 2016). Furthermore, in C57BL/6 mice, size modified the dose response and timing of citrate coated AgNP induced lung inflammation and surface coating and size altered AgNP effects on lung surfactant proteins and lung mechanics after instillation (Wang et al. 2014; Botelho et al. 2016).

Test animal strain has also been shown to impact AgNP induced inflammation and toxicity (Seiffert et al. 2015). Previous studies have shown that BN rats are more susceptible to ovalbumin (OVA) induced allergic or Th2-type inflammatory responses than

Sprague Dawley (SD) rats (Careau et al. 2002). BN rats also showed increases in markers of Th2 type inflammation compared to SD rats in response to AgNP exposure, characterized by increased numbers of eosinophils, and concentrations of eotaxin, IL-13, and total IgE in BALF (Seiffert et al. 2015). Additional strain differences included significant increases relative to control in total BALF protein and bronchial hyper-responsiveness in BN rats compared to SD rats following exposure to 20 nm citrate and PVP coated AgNPs. Thus, *in vivo* studies indicate that particle size, coating, and animal strain influence AgNP-induced lung inflammation and toxicity (Anderson et al. 2014; Wang et al. 2014; Anderson et al. 2015; Seiffert et al. 2015; Silva et al. 2015; Botelho et al. 2016; Silva et al. 2016).

Given the multitude of factors that can influence the toxicity of AgNPs, thorough mechanistic studies for all AgNP formulations would be a resource and time intensive undertaking. However, if genes and pathways associated with susceptibility to AgNP-induced lung inflammation and toxicity were identified using systems level unbiased methodologies such as genome wide association (GWA) mapping in model organisms, this could help to focus and prioritize those mechanistic studies. In addition, findings from such studies could provide information about human susceptibility and population variability for purposes of risk assessment and regulation of AgNPs, which is of importance given there is currently no unique regulatory standard for AgNP exposure.

GWA mapping studies using panels of multiple inbred mouse strains and primary cells from inbred mouse strains have succeeded in identifying novel susceptibility genes and regulatory mechanisms in a variety of toxicity and disease models (Harrill et al. 2009; Durrant et al. 2011; Church et al. 2014; Nichols et al. 2014; Rasmussen et al. 2014; Rutledge et al. 2014; Suzuki et al. 2014). Some examples of phenotypes for which candidate genes have been successfully identified using GWA mapping include susceptibility to acetaminophen and isoniazid induced liver injury (Harrill et al. 2009; Church et al. 2014), rotenone induced cytotoxicity (Suzuki et al. 2014), hyperoxia induced lung injury (Nichols et al. 2014), Aspergillus fumigatus and Ebola virus infection (Durrant et al. 2011; Rasmussen

et al. 2014), high-fat diet induced obesity and microbiota composition (Parks et al. 2013), atherosclerotic plaque formation (Colinayo et al. 2003), and identification of a novel regulatory protein for lung neutrophil influx (Rutledge et al. 2014). Variants in the human ortholog of the candidate gene CD44, discovered in a mouse GWAS of acetaminophen-induced liver toxicity, were associated with differences in susceptibility 2 separate human cohorts (Harrill et al. 2009). Identification of gene variants that explain differences in human susceptibility based on differential responses across mouse strains highlights the relevance of mouse GWA mapping studies.

In this study, we exposed mice from 25 different inbred strains to 20 nm citrate coated AgNPs or citrate buffer, measured neutrophils in BALF as a marker of lung inflammation, and used GWA mapping to identify novel candidate genes associated with AgNP-induced neutrophil influx into the lung.

Methods

AgNP Characterization

The AgNPs used in this study were nominally 20 nm and coated in citrate for stabilization. AgNPs were suspended in 1 mM citrate buffer. These particles are one of several nanomaterials available to the NIEHS Centers for Nanotechnology Health Implications Research (NCNHIR) Consortium and were initially characterized by the Nanotechnology Characterization Laboratories at the National Cancer Center. These particles have been thoroughly characterized by Shannahan and colleagues (Shannahan et al. 2013).

Animals and Dosing

All mice were males, and were purchased from The Jackson Laboratory (Bar Harbor, ME or Sacramento, CA). The Kavanagh laboratory phenotyped 11 inbred strains (CBA/J, C57L/J, MRL/MpJ, NOD/ShiLtJ, NZB/BlNJ, NZO/HlLtJ, NZW/LacJ, PL/J, PWD/PhJ, PWK/PhJ,

TALLYHO/JngJ, WSB/EiJ), and the Gordon/Chen laboratory phenotyped 10 different strains (BALB/cJ, BTBRT+tf/J, C3H/HeJ, C57BL/10J, DBA/2J, FVB/NJ, SJL/J, SM/J and SWR/J). Both labs also assayed an additional 4 strains (129S1/SvImJ, A/J, AKR/J, and C57BL/6J mice) for inter-laboratory comparison purposes. The number of replicates for each strain and treatment group are outlined in Table 1S. Mice were housed in polycarbonate cages, at least 2 mice per cage, with corn-cob bedding in temperature (20-23° C) and humidity controlled rooms with a 12 hr light/dark cycle. Animals were provided standard rodent chow and water *ad libitum*. All animal procedures and handling were performed under the National Institutes of Health and Animal Welfare Act guidelines for the ethical treatment of animals, and under protocols approved by the University of Washington and NYU School of Medicine Institutional Animal Care and Use Committees. Mice were anesthetized using Isoflurane and dosed with 0.25 mg/kg BW of either 20 nm citrate-coated AgNPs or 1 mM citrate buffer alone using oropharyngeal aspiration (OPA). Mice were sacrificed 24 hr after OPA.

Bronchoalveolar lavage fluid (BALF)

BAL was performed on the whole lung in each mouse twice sequentially (1.2 mL followed by 0.6 mL) with phosphate buffered saline (PBS). For strains with small body weights (PWK/PhJ, WSB/EiJ), lavage volumes were adjusted to 0.7 mL followed by 0.35 mL.

Cytospins

Lavage aliquots of 100 µL were deposited onto microscope slides using a Shandon Cytospin (Thermo Fisher Scientific, Waltham, MA) and stained with Diff-Quik (Siemens - Thermo Fisher Scientific, Waltham, MA). The percentage of neutrophils in BALF was determined by the number of neutrophils present in either 500 counted cells (Kavanagh Lab) or 100 counted cells (Gordon/Chen Lab).

Tissue Collection

Tissues were either flash frozen in liquid nitrogen and stored at -80^{o} C or fixed in 10% neutral buffered formalin. Prior to freezing, a portion of the right lung was preserved in 150 µL RNAlater (Ambion - Thermo Fisher Scientific) and stored at -80^{o} C.

RNA Isolation

Lung tissue was thawed, removed from RNAlater and homogenized at 50 Hz for 5 min in 700 µL of Qiazol (Qiagen, Hilden, Germany) using 5 mm stainless steel beads (Qiagen) in 2 mL Eppendorf tubes in a TissueLyser LT (Qiagen). Total RNA was extracted using the miRNEasy kit (Qiagen) according to the manufacturer's instructions for total RNA.

qRT-PCR

A PCR mixture (12 µl) consisting of the cDNA, primers, a labeled TaqMan probe, 1x TaqMan Gene Expression Master Mix and water underwent a quantitative real-time PCR reaction. The species/gene specific primers and probes were designed by Applied Biosystems Inc. (Thermo Fisher Scientific, Waltham, MA). Amplification and fluorescence detection were measured using the ABI 7900HT Fast Real-Time PCR System with the following PCR reaction profile: 1 cycle of 95° C for 10 min followed by 40 cycles of 95° C for 20s and 62° C for 1 min. The cycle number at which the concentration reached the threshold for fluorescence detection (Ct number) was calculated using SDS 2.4 software. The delta delta Ct method was used to calculate differences in expression of *Nedd4l*, *Ano6*, and *Rnf220* mRNA between AgNP and citrate treated mice after normalizing to the average expression of reference genes β-actin and GAPDH within each sample. The anti-log base 2 of the delta delta Ct values was then used to derive fold-change in mRNA expression.

Genome Wide Association Mapping and Other Statistical Analyses

Two-way analysis of variance (ANOVA) was used to determine the impact of AgNP treatment and mouse strain on BALF neutrophils in the 25 inbred strains and whether there

was an interaction between the two factors. We also calculated the broad sense heritability for % neutrophils in BALF using variance component analysis with a linear mixed model. We used R packages nlme and ape to calculate between and within-strain variance components, while adjusting for AgNP treatment (Paradis et al. 2004; Visscher et al. 2008; Almasy and Blangero 2010; Felix et al. 2012; Pinheiro et al. 2016). The EMMA (efficient mixed-model association) R package was used for genome wide association mapping (Kang et al. 2008). Single nucleotide polymorphisms (SNPs) for the 25 strains (NCBI build 37/ UCSC build mm9) were obtained from the Mouse Haplotype Project (Broad Institute, Harvard, MIT, Cambridge MA). A linear regression forced through the origin derived from the mean values in AgNP and citrate treated mice from the 4 strains that the two laboratories had in common was used to derive an adjustment factor (0.4592) to % neutrophil values from the Kavanagh Laboratory to account for inter-laboratory differences. All associations between BALF neutrophils and genotype were adjusted by the EMMA program for genetic relatedness among strains (Figure 1S). The purpose of this adjustment is to account for population structure and reduce the number of false-positives (Kang et al. 2008). Individual animal data were run using the emma.REML.t algorithm, and AgNP or citrate treatments were incorporated as covariates. Significance of associations was determined using a false discovery rate (FDR) of 15%. The size effects of candidate SNPs were calculated using Cohen's d-statistic (Cohen 1977; Harrill et al. 2009; Labots et al. 2016). To account for control mice, we first subtracted the mean % neutrophils in control mice from the mean of AgNP treated mice within each strain and then assessed allele specific differences in mean % neutrophils. The pooled standard deviation was also calculated after subtraction of control values from AgNP mice. The UCSC genome browser was used to explore candidate genes in regions indicated by significant SNPs (Kent et al. 2002). The Manhattan plots in Figures 2 and 3 were generated using modified source code from the qqman R package (Turner 2014). Other plots were created using base R, lattice or ggplot2 packages (Deepayan 2008; Wickham 2009; R Core Team 2014)

To determine if our candidate genes were differentially expressed in lung tissue between AgNP and control mice, we used a one-sided t-test to determine if strain specific mean delta delta Ct values were different than 0. Resulting p-values from the t-tests for each gene were adjusted using the Bonferroni method. Simple linear regression was used to investigate relationships between candidate gene mRNA expression and BALF neutrophils. Correlations with p-values ≤ 0.05 were considered statistically significant.

Results

Lung Inflammation

Neutrophils are key cells in acute inflammatory responses and accordingly we have used neutrophil influx as a primary marker of ENM induced lung inflammation in previously published studies (McConnachie et al. 2013; Scoville et al. 2015). Accordingly, we used neutrophil influx as the phenotype of interest in this study, which was focused on identifying genetic determinants of AgNP-induced lung inflammation. We found significant strain dependent increases in % neutrophils in BALF in AgNP-treated mice compared to citrate-treated strain-matched controls (Figure 1). There was a wide range of responses in AgNP treated mice across the 25 inbred strains, ranging from 0 (SWR/J) to 60% (BALB/c) neutrophils in BALF with coefficients of variation (CV) of 166% for AgNP treated mice and 49% for citrate controls. Importantly, statistically significant AgNP-induced lung inflammation was found in most strains, the exceptions being SWR/J, DBA/2J, SM/J, BTBRT^{+} tf/J, and C57BL/10J. AgNP treatment- and strain-related effects along with a significant interaction between them (by two-way ANOVA) strongly suggest a role for genetic background in determining susceptibility to AgNP induced acute lung inflammation.

Heritability of AgNP Induced Lung Inflammation

We calculated the broad sense heritability for % neutrophils in BALF to determine the genetic contribution to the large amount of variability we found across the strains. We found that heritability for % BALF neutrophils was 0.37 when AgNP was included and adjusted for treatment in the mixed model. When evaluated separately, heritability estimates were 0.43 for citrate treated animals and 0.73 in AgNP-treated animals. These results also show that genetic background is an important determinant of inter-strain variation in AgNP-induced lung inflammation.

GWA Mapping

We performed GWA mapping to identify specific genomic regions and candidate genes that may contribute to inter-strain differences in sensitivity to AgNPs. After filtering for SNPs with missing genotype calls, 65,493 SNPs were used in EMMA to their associations with % BALF neutrophils (Figure 2). We found 6 significant SNPs in QTL peaks on chromosomes 4, 15, and 18 (Figure 3, Table 1). The strongest QTL spanned 3 megabases (Mb) in the qE1 region of chromosome 18. This region held 3 of the 6 significant SNPs with -$\log_{10}$(p) rank orders #1 (rs29865915-close to *St8sia3*), #2 (rs29959933-close to *Nedd4l*), #4 (rs29778747-close to *Nedd4l*) (Figure 3A, Table 1). This region also contained 17 other known genes and 2 micro-RNAs (Figure 3A). The QTL on chromosome 15 spanned 10 Mb across the distal qE3 and proximal qF1 regions; contained 1 significant SNP with rank order #3 (rs31581766 – intragenic in *Ano6*) and a SNP with rank order #6 (rs3688273 –not close to a gene). This QTL region also contained over 100 other known genes (Figure 3B, Table 1). The QTL peak region on chromosome 4 was 62.5 Mb wide and covered the qC3 region through part of the proximal portion of qD3; contained 1 significant SNP with rank order #5 (rs27482013-intragenic in *Rnf220*); and also contained well over 100 known genes (Figure 3C, Table 1). QTL boundaries and -$\log_{10}$(p-values) for the 6 significant SNPs are also listed in Table 1.

We also looked at the distribution of % BALF neutrophils by treatment group and SNP allele for the 6 significant SNPs to visualize the effects that alleles and AgNP had on BALF neutrophils. Plots for the 5 out of 6 SNPs that were either in or near a gene are shown in Figure 4. Cohen's effect size d-statistics for these same 5 SNPs were ≥ 0.9, indicating moderate to large effects on AgNP-induced neutrophil influx (Table 1) (Labots et al. 2016). The allele distributions by strain were also examined and were all different for these 5 SNPs (Figure 3S).

Candidate Gene Exploration Using the Mouse Phenome Database

As an initial screening step for potential candidate genes, mRNA expression values for the potential candidate genes identified in the chromosome 18 QTL and for *Ano6* and *Rnf220* were obtained from a 9-strain microarray-based gene expression study on untreated female mice (n=3 per strain) submitted by Stearns et al. to the Mouse Phenome Database (MPD) (Berndt and Stearns 2011). Since the QTL regions on chromosome 15 and 4 contained over 100 genes, we focused on expression of *Ano6* and *Rnf220* given that the most significant SNPs in these regions were intragenic. These expression values from the MPD were then compared to strain means of % BALF neutrophils from AgNP treated mice from 8 overlapping strains used in our study. We found both positive and inverse correlations between reported baseline expression levels of some of the potential candidate genes and % BALF neutrophils from our study. The most inversely correlated genes were *Nedd4l* on chromosome 18 and *Ano6* on chromosome 15 (Figure 5, panels A and B). Despite containing a significant intragenic SNP, expression of *Rnf220* on chromosome 4 was not correlated with % BALF neutrophils (Figure 5, panel C). The most positively correlated genes were *Ccbe1* and *Cplx4,* which are both on chromosome 18 (Figures 5, panels D and E). *St8sia3*, which is also on chromosome 18, was moderately correlated but it was not statistically significant (Figure 5, panel F).

qRT-PCR on Candidate Genes

To determine whether the candidate genes were differentially expressed in lungs exposed to AgNP, we performed qRT-PCR on the right lung tissue from a subset of our strains that represented low (C57BL/6J, 129S1/SvImJ), and moderate/high (MRL/MpJ, A/J) neutrophilia (Figure 6, panel A). In addition to the list of genes with significant intra-genic SNPs and/or those that are significantly correlated or inversely correlated with % BALF neutrophils using the data from Berndt and Stearns (Berndt and Stearns 2011), we also performed qRT-PCR on *St8sia3*, as it is adjacent to the most significant SNP (rs26865915).

We found that the fold-changes in mRNA expression of *Nedd4l*, *Ano6*, and *Rnf220* between AgNP and control mice were all significantly inversely correlated with % BALF neutrophils in AgNP treated mice (Figures 6, panels B-D). Interestingly, we found that three of the genes from the chromosome 18 QTL that were either significantly correlated with % BALF neutrophils using mRNA expression data from the mouse phenome database (*Ccbe1* and *Cplx4)* (Berndt and Stearns 2011), or adjacent to a highly significant SNP (*St8sia3*) were not expressed in lung tissue taken from either AgNP or citrate treated mice.

Discussion

In this study, we used GWA mapping with a panel of 25 inbred mouse strains to identify 3 candidate genes in QTLs on chromosomes 4, 15, and 18 associated with a 0.25 mg/kg dose of 20 nm citrate coated AgNP-induced lung inflammation. Mouse strains were chosen to maximize genetic diversity to improve resolution of GWA-mapping (Petkov et al. 2004; Valdar et al. 2006; Aylor et al. 2011). As such, we included members of the Collaborative Cross founder mouse strains in our panel (Threadgill and Churchill 2012). Some strains were selected due to their genetic similarity (ex. C57BL10/J and C57BL/6J mice) to determine how closely related strains would respond to AgNP exposure. Dose selection was focused on maximizing contrast in % neutrophils in BALF across mouse strains

to increase power for GWA mapping. Preliminary dose response data, in genetically divergent BALB/cJ, FVB/NJ, and C57BL/6J mouse strains, showed that a dose of 0.25 mg/kg resulted in the greatest variability across these 3 mouse strains (Figure 4S). Using a calculation published by Wang and colleagues to translate human airborne AgNP exposures to bolus doses, 0.25 mg/kg in mice is equivalent to a human aggregate dose of 219 ug/m3 air for 8 hr/day, 5 days/week for 4 weeks; this is within the 5 - 289 ug/m3 air observed for occupational exposures (Wang et al. 2014). While inhalation exposures are different than bolus doses, intratracheal instillation has been acknowledged as a valid screening tool (Driscoll et al. 2000). Oropharyngeal aspiration, which was the exposure method used in this study, has been shown to have superior distribution in the lungs compared to intratracheal instillation (Lakatos et al. 2006). Furthermore, equivalent doses of multi-walled carbon nanotubes delivered using aspiration and inhalation produced similar pathologies in mice (Kinaret et al. 2017).

Using EMMA allowed us to reduce the number of false positives by adjusting association values for genetic relatedness between the strains. We gained statistical power through the capacity of EMMA to incorporate individual animal measures within a strain. Another advantage with EMMA was the ability to incorporate AgNP treatment as a covariate and use all of our data rather than adjusting for controls by using fold change or ignoring control animals entirely.

We found 3 significant SNPs and 20 potential candidate genes in the chromosome 18 QTL. We used the presence of intragenic SNPs, proximity to significant SNPs, and the correlation of the expression data from the data published by Berndt and Stearns (2011) with % BALF neutrophils to further refine the list of candidate genes. We performed qRT-PCR on *St8sia3* based on its proximity to the most significant SNP. We chose *Nedd4l* as it had close proximity to the 2nd and 4th most significant SNPs (Table 1). In addition, *Nedd4l* expression from the Stearns et al. dataset at the MPD had the strongest correlation coefficient with % BALF neutrophils. *Ccbe1* and *Cplx4* were chosen as candidates for qRT-

PCR solely based on high correlation of expression in the with % BALF neutrophils. We found that of the 4 genes assessed, only *Nedd4l* mRNA was significantly expressed in the lungs of our mice. We found a significant inverse correlation with *Nedd4l* mRNA levels and % BALF neutrophils. Nedd4l is an E3 ubiquitin ligase that is known to target the epithelial sodium channel (ENAC) for ubiquitination (Kamynina et al. 2001). Interestingly, overexpression of ENAC in mice is known to result in severe lung inflammation in mice with phenotypic similarities to cystic fibrosis (Mall et al. 2004). ENAC overexpressing mice experience increased mucus obstruction, decreased airway surface liquid volume, increased neutrophils, and reduced bacterial clearance (Mall et al. 2004). Mice that lack Nedd4l in lung epithelial cells also develop severe lung inflammation (Kimura et al. 2011). Given that Nedd4l has been shown to inhibit ENAC, and that increased expression of ENAC is associated with lung inflammation, it is reasonable that *Nedd4l* could modulate susceptibility to AgNP-induced lung inflammation. Decreased levels of Nedd4l leading to increased ENAC could result in a lung that is more prone to inflammation following a toxic insult, consistent with the inverse association we found between *Nedd4l* mRNA and % BALF neutrophils. Furthermore, human GWA studies have suggested that *NEDD4L* may be associated with variability in asthma susceptibility ($p<1x10^{-6}$), blood neutrophils ($p<1x10^{-5}$), and lung function ($p<1x10^{-4}$) (Ramos et al. 2014).

On chromosome 15, *Ano6* was considered a candidate gene since it contained an intragenic statistically significant SNP (rs31581766), and lung mRNA expression levels for *Ano6* published by Berndt and Stearns (2011) were inversely correlated with % BALF neutrophils we found (Figure 5B). Our qRT-PCR results confirmed an inverse association between *Ano6* mRNA and % BALF neutrophils. Ano6 is a transmembrane protein that has been shown to have ion channel activity and to influence phospholipid scrambling (Pedemonte and Galietta 2014; Rysavy et al. 2014; Ousingsawat et al. 2015). The ion channel activity of Ano6 has been illustrated in several studies, but its ion selectivity is not completely understood (Pedemonte and Galietta 2014). Phospholipid scramblases mediate

the bi-directional transport of phospholipids between the inner and outer leaflets of the cell membrane lipid bi-layer (Rysavy et al. 2014). Asymmetrical distribution of specific phospholipids to either the inner or outer leaflet is mediated by flippase and floppase proteins, respectively (Rysavy et al. 2014). Scramblase mediated relocation of phosphatidylserine (PS) to the outer leaflet of the cell membrane serves in diverse signaling mechanisms in multiple cell types (Pedemonte and Galietta 2014; Rysavy et al. 2014). In Ano6, the region between amino acids 529 and 559, which spans transmembrane domains 4 and 5, is thought to be responsible for phospholipid scramblase activity (Yu et al. 2015). Loss of function mutations in *ANO6* have been associated with Scott Syndrome, which is a condition wherein individuals have defective PS scrambling and associated reductions in blood clotting (Toti et al. 1996; Suzuki et al. 2010). *Ano6* knockout mice recapitulate symptoms of Scott Syndrome (Yang et al. 2012).

The presence of PS in the outer leaflet can also signal for phagocytosis of apoptotic cells, a process known as efferocytosis (Pedemonte and Galietta 2014; Rysavy et al. 2014). It is known that efferocytosis of apoptotic cells is important for the resolution of inflammation. Many chronic lung diseases are associated with ineffective efferocytosis (Morimoto et al. 2012). Furthermore, recognition of dying cells is thought to influence the polarization of alveolar macrophage towards a more M2 or inflammation resolving state (Korns et al. 2011; Mares et al. 2011). In human kidney HEK293 cells, over expression of *ANO6* increased PS on the cell surface (Yu et al. 2015). If reduced expression of *ANO6* has the opposite effect, then apoptotic inflammatory cells with lower *ANO6* expression could have less surface PS and be more resistant to efferocytosis, potentially leading to prolonged and more severe inflammation. This hypothesis is in keeping with our observed inverse association of *Ano6* mRNA and BALF neutrophils and with recently reported evidence indicating that peritoneal macrophages from *Ano6* knockout mice have reduced phagocytic capacity, which could work in conjunction with reduced apoptotic neutrophil PS scrambling (Ousingsawat et al. 2015). There is also some evidence that Ano6 may also participate in PS

scrambling in the context of mast cell degranulation (Rysavy et al. 2014). In addition, human GWA studies have suggested that *ANO6* may be associated with variability in levels of C-reactive protein, a biomarker of inflammation ($p<3x10^{-6}$).

Given the many demonstrated functions of Ano6, AgNP-induced lung inflammation could be impacted by a number of different mechanisms including ion transport induced changes in airway surface fluid volume and viscosity, changes in PS signaling related apoptosis and phagocytosis, and/or mast cell function (Mall et al. 2004; Martins et al. 2011; Rysavy et al. 2014).

In the QTL on chromosome 4, *Rnf220* was considered a candidate gene because the most significant SNP (rs27482013) is intragenic in this gene. In addition, we found that among 8 strains in common between our study and those in the microarray dataset published on the Mouse Phenome Database by Berndt and Stearns (2011), lung *Rnf220* mRNA was inversely correlated with % BALF neutrophils (Figure 5C). We also found that when we performed qRT-PCR for *Rnf220* mRNA in lung tissue from a subset of 4 strains in our study, mRNA levels again were significantly inversely correlated with % BALF neutrophils (Figure 5C). Rnf220 is an E3 ubiquitin ligase with a RING finger domain that has been shown to stabilize β-catenin and therefore enhance canonical Wnt signaling (Ma et al. 2014). β-catenin stabilization was shown to occur through deubiquitination by a complex of Rnf220 and the ubiquitin-specific protease 7 (USP7) (Ma et al. 2014). Promotion of Wnt/ β-catenin signaling by canonical ligand Wnt3a and inhibition of Wnt antagonist Dkk1 has been shown to decrease LPS-induced neutrophil influx and cytokine production (Guo et al. 2015). In addition, ghrelin has been shown to rescue LPS-induced inhibition of β-catenin, LPS induced apoptosis in alveolar macrophages, and improve ARDS outcomes in rats (Li et al. 2015). Thus, it is plausible that Rnf220 could modulate susceptibility to AgNP-induced lung inflammation through increased stabilization of β-catenin and increased Wnt/β-catenin signaling leading to a less severe inflammatory response. The inverse association we observed between *Rnf220* mRNA and % BALF neutrophils supports this hypothesis. In

addition, human GWA studies have suggested that *RNF220* may be associated with variability in lung function ($p=<1x10^{-4}$) (Ramos et al. 2014).

Acknowledging that GWA study results may be influenced by model assumptions and the choice of mouse strains, we performed a sensitivity analysis. Since the phenotype data in our study was collected in two laboratories, we explored an alternate method for inter-laboratory adjustment in our sensitivity analysis than in our initial analysis. Instead of adjusting the Kavanagh lab data using linear regression with the 4 strains that the two laboratories had in common, we tried using un-scaled phenotype data in the EMMA model and included laboratory as an additional covariate. We also explored the effects of running the data from the Gordon/Chen and Kavanagh labs separately as well as excluding different combinations of wild derived strains WSB/EiJ, PWK/PhJ and PWD/PhJ. PWK/PhJ and PWD/PhJ are highly genetically related to each other but divergent from the other strains. The influence of closely related classical inbred strains was also explored by excluding C57BL/10J from the primary analysis since they are closely related to C57BL/6J mice. (Figure 1S). After running the alternate analyses, we compared the 6 SNPs with the highest –log(p) values from the initial and alternate analyses (Figure 2S). We found that the most significant SNPs on chromosomes 18 (rs29865915 – near *St8sia3*, rs29778747– near *Nedd4l*, rs29959933 – near *Nedd4l*) from the initial analysis were among the top 6 SNPs in all analyses combining strains from both laboratories, regardless of inter-laboratory adjustment method or whether different combinations of wild-derived strains or C57BL/10J mice were included in the analysis. we adjusted between labs using laboratory as a covariate; and when different combinations of wild WSB/EiJ and PW (PWK/PhJ and PWD/PhJ) strains were excluded, regardless of how we adjusted between labs. The most significant SNP on chromosome 15 (rs31581766 – intragenic in *Ano6*) from the initial analysis was also among the top 6 SNPs in the analysis when laboratory was adjusted for as a co-variate and PW strains were excluded and all alternate analyses where linear regression was used to adjust for inter-laboratory differences. The most significant SNP on

chromosome 4 (rs27482013 – intragenic in *Rnf220*) from the primary analysis was also among the top 6 SNPs of all alternate analyses where linear regression was used to adjust for inter-laboratory differences. The other significant SNP on chromosome 15 (rs3688273 – not close to any genes) from the initial analysis also appeared in the top 6 SNPs in analyses where linear regression adjustment was used for inter-laboratory adjustment when either PW or C57BL/10J mice were excluded. In general, the importance of the significant SNPs and associated candidate genes identified in the initial analysis appear relatively robust to choice of mouse strain and methods for inter-laboratory adjustment of % BALF neutrophils. In conclusion, our study evaluated AgNP-induced lung inflammation in 25 inbred strains of mice and used GWA mapping to search for susceptibility genes that corresponded with the large range of observed responses.

In conclusion, we found 3 promising candidate genes: *Nedd4l*, *Rnf220*, and *Ano6* for which mRNA levels were inversely correlated with AgNP-induced lung inflammation, which is likely a complex polygenic trait. To varying degrees, *Nedd4l* and *Rnf220* have also been associated with human variation in lung function in human GWA studies; *Ano6* has been has been moderately associated with C-reactive protein and thus overall inflammation (Pepys and Hirschfield 2003; Ramos et al. 2014). Since differences in human susceptibility to drug exposure have been associated with polymorphisms in genes identified using mouse GWA mapping, the role of these genes in modulating susceptibility to AgNP induced lung inflammation need to be further explored. By showing that genetic background contributes to variation in the inflammatory response observed across our 25 inbred mouse strains and identifying candidate susceptibility genes for further studies, we have generated information that should guide future AgNP mechanistic studies. However, such experiments are beyond the scope of the current study. In addition, information on inter-strain variation in mice that differ in sensitivity to AgNP induced lung inflammation could be useful for gauging intra-species uncertainty factors in AgNP risk assessments, thus assuring adequate protection for

vulnerable individuals who may be genetically predisposed to AgNP-induced lung inflammation.

Acknowledgements

This work was supported by NIH/NIEHS grants U01ES019545, U01ES0200126, T32ES015459, P30ES007033 and P30ES000260. SRK was supported by the Intramural Research Program, NIEHS, National Institutes of Health, U.S. Department of Health and Human Services. The silver nanomaterials used in these studies were procured, characterized and provided by the NCNHIR consortium.

Chapter 4 References

Almasy, L. and J. Blangero (2010). "Variance Component Methods for Analysis of Complex Phenotypes." Cold Spring Harbor protocols **2010**(5).

Anderson, D. S., E. S. Patchin, R. M. Silva, D. L. Uyeminami, A. Sharmah, T. Guo, . . . L. S. Van Winkle (2015). "Influence of particle size on persistence and clearance of aerosolized silver nanoparticles in the rat lung." Toxicological Sciences **144**(2): 366-381.

Anderson, D. S., R. M. Silva, D. Lee, P. C. Edwards, A. Sharmah, T. Guo, . . . L. S. Van Winkle (2014). "Persistence of silver nanoparticles in the rat lung: Influence of dose, size, and chemical composition." Nanotoxicology **9**(5): 591- 602.

Aylor, D. L., W. Valdar, W. Foulds-Mathes, R. J. Buus, R. A. Verdugo, R. S. Baric, . . . G. A. Churchill (2011). "Genetic analysis of complex traits in the emerging Collaborative Cross." Genome Research **21**(8): 1213-1222.

Berndt, A. and T. M. Stearns. (2011). " Lung gene expression in females of 9 inbred strains of mice. MPD:Stearns1." Mouse Phenome Database web resource (RRID:SCR_003212), The Jackson Laboratory, Bar Harbor, Maine USA., 2016, from http://phenome.jax.org/

Botelho, D. J., B. F. Leo, C. B. Massa, S. Sarkar, T. D. Tetley, K. F. Chung, . . . A. J. Gow (2016). "Low-dose AgNPs reduce lung mechanical function and innate immune defense in the absence of cellular toxicity." Nanotoxicology **10**(1): 118-127.

Careau, E., J. Sirois and E. Y. Bissonnette (2002). "Characterization of Lung Hyperresponsiveness, Inflammation, and Alveolar Macrophage Mediator Production in Allergy Resistant and Susceptible Rats." American Journal of Respiratory Cell and Molecular Biology **26**(5): 579-586.

Church, R. J., H. Wu, M. Mosedale, S. J. Sumner, W. Pathmasiri, C. L. Kurtz, . . . A. H. Harrill (2014). "A Systems Biology Approach Utilizing a Mouse Diversity Panel Identifies Genetic Differences Influencing Isoniazid-Induced Microvesicular Steatosis." Toxicological Sciences **140**(2): 481-492.

Cohen, J. (1977). Statistical Power Analysis for the Behavioral Sciences. New York, New York, Academic Press**:** 19-27.

Colinayo, V. V., J. H. Qiao, X. Wang, K. L. Krass, E. Schadt, A. J. Lusis and T. A. Drake (2003). "Genetic loci for diet-induced atherosclerotic lesions and plasma lipids in mice." Mammlian Genome **14**(7): 464-471.

Cui, L. (2013). Exposure assessment and inflammatory response among workers producing calcium carbonate nanomaterials Dissertation, University of Washington.

Deepayan, S. (2008). "Lattice: Multivariate Data Visualization with R.".

Driscoll, K. E., D. L. Costa, G. Hatch, R. Henderson, G. Oberdorster, H. Salem and R. B. Schlesinger (2000). "Intratracheal Instillation as an Exposure Technique for the Evaluation of Respiratory Tract Toxicity: Uses and Limitations." Toxicological Sciences **55**(1): 24-35.

Durrant, C., H. Tayem, B. Yalcin and J. Cleak (2011). "Collaborative Cross mice and their power to map host susceptibility to Aspergillus fumigatus infection." Genome **21**(8): 1239-1248.

Felix, T. M., K. A. Hughes, E. A. Stone, J. M. Drnevich and J. Leips (2012). "Age-Specific Variation in Immune Response in Drosophila melanogaster Has a Genetic Basis." Genetics **191**(3): 989-1002.

Gliga, A. R., S. Skoglund, I. O. Wallinder, B. Fadeel and H. L. Karlsson (2014). "Size-dependent cytotoxicity of silver nanoparticles in human lung cells: the role of cellular uptake, agglomeration and Ag release." Particle and Fibre toxicology **11**: 11.

Guo, Y., A. Mishra, E. Howland, C. Zhao, D. Shukla, T. Weng and L. Liu (2015). "Platelet-derived Wnt antagonist Dickkopf-1 is implicated in ICAM-1/VCAM-1-mediated neutrophilic acute lung inflammation." Blood **126**(19): 2220-2229.

Harrill, A. H., P. B. Watkins, S. Su, P. K. Ross, D. E. Harbourt, I. M. Stylianou, . . . D. W. Threadgill (2009). "Mouse population-guided resequencing reveals that variants in CD44 contribute to acetaminophen-induced liver injury in humans." Genome Research **19**(9): 1507-1515.

Holter, J. F., J. E. Weiland, E. R. Pacht, J. E. Gadek and W. B. Davis (1986). "Protein permeability in the adult respiratory distress syndrome. Loss of size selectivity of the alveolar epithelium." Journal of Clinical Investigation **78**(6): 1513-1522.

Kamynina, E., C. Debonneville, M. Bens, A. Vandewalle and O. Staub (2001). "A novel mouse Nedd4 protein suppresses the activity of the epithelial Na+ channel." The FASEB Journal **15**(1): 204-214.

Kang, H. M., N. A. Zaitlen, C. M. Wade, A. Kirby, D. Heckerman, M. J. Daly and E. Eskin (2008). "Efficient Control of Population Structure in Model Organism Association Mapping." Genetics **178**(3): 1709-1723.

Kent, W. J., C. W. Sugnet, T. S. Furey, K. M. Roskin, T. H. Pringle, A. M. Zahler, . . . David (2002). "The Human Genome Browser at UCSC." Genome Research **12**(6): 996-1006 -- http://genome.ucsc.edu/.

Kimura, T., H. Kawabe, C. Jiang, W. Zhang, Y.-Y. Xiang, C. Lu, . . . D. Rotin (2011). "Deletion of the ubiquitin ligase Nedd4L in lung epithelia causes cystic fibrosis-like disease." Proceedings of the National Academy of Sciences of the United States of America **108**(8): 3216-3221.

Kinaret, P., M. Ilves, V. Fortino, E. Rydman, P. Karisola, A. Lähde, . . . H. Alenius (2017). "Inhalation and Oropharyngeal Aspiration Exposure to Rod-Like Carbon Nanotubes Induce Similar Airway Inflammation and Biological Responses in Mouse Lungs." ACS Nano **11**(1): 291-303.

Kolaczkowska, E. and P. Kubes (2013). "Neutrophil recruitment and function in health and inflammation." Nature Reviews Immunology **13**(3): 159-175.

Korns, D. R., S. C. Frasch, R. Fernandez-Boyanapalli, P. M. Henson and D. L. Bratton (2011). "Modulation of Macrophage Efferocytosis in Inflammation." Frontiers in Immunology **2**.

Labots, M., M. C. Laarakker, F. Ohl and H. A. van Lith (2016). "Consomic mouse strain selection based on effect size measurement, statistical significance testing and integrated behavioral z-scoring: focus on anxiety-related behavior and locomotion." BMC Genetics **17**: 95.

Lakatos, H. F., H. A. Burgess, T. H. Thatcher, M. R. Redonnet, E. Hernady, J. P. Williams and P. J. Sime (2006). "Oropharyngeal aspiration of a silica suspension produces a superior model of silicosis in the mouse when compared to intratracheal instillation." Experimental Lung Research **32**(5): 181-199.

Lee, J. S., Y. C. Choi, J. H. Shin, J. H. Lee, Y. Lee, S. Y. Park, . . . I. J. Yu (2015). "Health surveillance study of workers who manufacture multi-walled carbon nanotubes." Nanotoxicology **9**: 802-811.

Lee, Y.-H., F.-Y. Cheng, H.-W. Chiu, J.-C. Tsai, C.-Y. Fang, C.-W. Chen and Y.-J. Wang (2014). "Cytotoxicity, oxidative stress, apoptosis and the autophagic effects of silver nanoparticles in mouse embryonic fibroblasts." Biomaterials **35**(16): 4706-4715.

Li, B., M. Zeng, W. He, X. Huang, L. Luo, H. Zhang and D. Y. Deng (2015). "Ghrelin protects alveolar macrophages against lipopolysaccharide-induced apoptosis through growth hormone secretagogue receptor 1a-dependent c-Jun N-terminal kinase and Wnt/beta-catenin signaling and suppresses lung inflammation." Endocrinology **156**(1): 203-217.

Liao, H.-Y., Y.-T. Chung, C.-H. Lai, S.-L. Wang, H.-C. Chiang, L.-A. Li, . . . S.-H. Liou (2014). "Six-month follow-up study of health markers of nanomaterials among workers handling engineered nanomaterials." Nanotoxicology **8**(sup1): 100-110.

Liu, W., Y. Wu, C. Wang, H. C. Li, T. Wang, C. Y. Liao, . . . G. B. Jiang (2010). "Impact of silver nanoparticles on human cells: Effect of particle size." Nanotoxicology **4**(3): 319-330.
Ma, P., X. Yang, Q. Kong, C. Li, S. Yang, Y. Li and B. Mao (2014). "The Ubiquitin Ligase RNF220 Enhances Canonical Wnt Signaling through USP7-Mediated Deubiquitination of β-Catenin." Molecular and Cellular Biology **34**(23): 4355-4366.
Mall, M., B. R. Grubb, J. R. Harkema, W. K. O'Neal and R. C. Boucher (2004). "Increased airway epithelial Na+ absorption produces cystic fibrosis-like lung disease in mice." Nature Medicine **10**(5): 487-493.
Mares, C. A., J. Sharma, Q. Li, E. L. Rangel, E. G. Morris, M. I. Enriquez and J. M. Teale (2011). "Defect in efferocytosis leads to alternative activation of macrophages in Francisella infections." Immunology and Cell Biology **89**(2): 167-172.
Martins, J. R., D. Faria, P. Kongsuphol, B. Reisch, R. Schreiber and K. Kunzelmann (2011). "Anoctamin 6 is an essential component of the outwardly rectifying chloride channel." Proceedings of the National Academy of Sciences of the United States of America **108**(44): 18168-18172.
McConnachie, L. A., D. Botta, C. C. White, C. S. Weldy, H. W. Wilkerson, J. Yu, . . . T. J. Kavanagh (2013). "The Glutathione Synthesis Gene Gclm Modulates Amphiphilic Polymer-Coated CdSe/ZnS Quantum Dot-Induced Lung Inflammation in Mice." PLOS ONE **8**(5): e64165.
Morgan, M. J. and Z.-g. Liu (2011). "Crosstalk of reactive oxygen species and NF-[kappa]B signaling." Cell Research **21**(1): 103-115.
Morimoto, K., W. J. Janssen and M. Terada (2012). "Defective efferocytosis by alveolar macrophages in IPF patients." Respiratory Medicine **106**(12): 1800-1803.
Nichols, J. L., W. Gladwell, K. C. Verhein, H.-Y. Cho, J. Wess, O. Suzuki, . . . S. R. Kleeberger (2014). "Genome-wide association mapping of acute lung injury in neonatal inbred mice." The FASEB Journal **28**(6): 2538-2550.
Ousingsawat, J., P. Wanitchakool, A. Kmit, A. M. Romao, W. Jantarajit, R. Schreiber and K. Kunzelmann (2015). "Anoctamin 6 mediates effects essential for innate immunity downstream of P2X7 receptors in macrophages." Nature Communications **6**: 6245.
Pang, C., A. Brunelli, C. Zhu, D. Hristozov, Y. Liu, E. Semenzin, . . . B. Zhao (2016). "Demonstrating approaches to chemically modify the surface of Ag nanoparticles in order to influence their cytotoxicity and biodistribution after single dose acute intravenous administration." Nanotoxicology **10**(2): 129-139.
Paradis, E., J. Claude and K. Strimmer. (2004). "A{PE}: analyses of phylogenetics and evolution in R language." 20, from https://cran.r-project.org/package=ape.
Parks, Brian W., E. Nam, E. Org, E. Kostem, F. Norheim, Simon T. Hui, . . . Aldons J. Lusis (2013). "Genetic Control of Obesity and Gut Microbiota Composition in Response to High-Fat, High-Sucrose Diet in Mice." Cell Metabolism **17**(1): 141-152.
Pedemonte, N. and L. J. V. Galietta (2014). "Structure and Function of TMEM16 Proteins (Anoctamins)." Physiological Reviews **94**(2): 419-459.
Pepys, M. B. and G. M. Hirschfield (2003). "C-reactive protein: a critical update." The Journal of Clinical Investigation **111**(12): 1805-1812.
Petkov, P. M., Y. Ding, M. A. Cassell, W. Zhang, G. Wagner, E. E. Sargent, . . . M. V. Wiles (2004). "An Efficient SNP System for Mouse Genome Scanning and Elucidating Strain Relationships." Genome Research **14**(9): 1806-1811.
Pinheiro, J., D. Bates, S. DebRoy, D. Sarkar and R. C. Team. (2016). "nlme: Linear and Nonlinear Mixed Effects Models." from http://cran.r-project.org/package=nlme.
R Core Team. (2014). "R: A language and environment for statistical computing, R Foundation for Statistical Computing, Vienna Austria." from http://www.r-project.org/.
Ramos, E. M., D. Hoffman, H. A. Junkins, D. Maglott, L. Phan, S. T. Sherry, . . . L. A. Hindorff (2014). "Phenotype-Genotype Integrator (PheGenI): synthesizing genome-

wide association study (GWAS) data with existing genomic resources." European Journal of Human Genetics **22**(1): 144-147.
Rasmussen, A. L., A. Okumura, M. T. Ferris, R. Green, F. Feldmann, S. M. Kelly, . . . M. G. Katze (2014). "Host genetic diversity enables Ebola hemorrhagic fever pathogenesis and resistance." Science **346**(6212): 987- 991.
Rutledge, H., D. L. Aylor, D. E. Carpenter, B. C. Peck, P. Chines, L. E. Ostrowski, . . . S. N. P. Kelada (2014). "Genetic Regulation of Zfp30, CXCL1, and Neutrophilic Inflammation in Murine Lung." Genetics **198**(2): 735-745.
Rysavy, N. M., L. M. N. Shimoda, A. M. Dixon, M. Speck, A. J. Stokes, H. Turner and E. Y. Umemoto (2014). "Beyond apoptosis: The mechanism and function of phosphatidylserine asymmetry in the membrane of activating mast cells." BioArchitecture **4**(4-5): 127-137.
Scoville, D. K., C. C. White, D. Botta, L. A. McConnachie, M. E. Zadworny, S. C. Schmuck, . . . T. J. Kavanagh (2015). "Susceptibility to quantum dot induced lung inflammation differs widely among the Collaborative Cross founder mouse strains." Toxicology and Applied Pharmacology **289**(2): 240-250.
Seiffert, J., F. Hussain, C. Wiegman, F. Li, L. Bey, W. Baker, . . . K. F. Chung (2015). "Pulmonary Toxicity of Instilled Silver Nanoparticles: Influence of Size, Coating and Rat Strain." PLOS ONE **10**(3): e0119726.
Shannahan, J. H., X. Lai, P. C. Ke, R. Podila, J. M. Brown and F. A. Witzmann (2013). "Silver nanoparticle protein corona composition in cell culture media." PLOS ONE **8**(9): e74001.
Silva, R. M., D. S. Anderson, L. M. Franzi, J. L. Peake, P. C. Edwards, L. S. Van Winkle and K. E. Pinkerton (2015). "Pulmonary Effects of Silver Nanoparticle Size, Coating, and Dose over Time upon Intratracheal Instillation." Toxicological Sciences **144**(1): 151-162.
Silva, R. M., D. S. Anderson, J. Peake, P. C. Edwards, E. S. Patchin, T. Guo, . . . K. E. Pinkerton (2016). "Aerosolized Silver Nanoparticles in the Rat Lung and Pulmonary Responses over Time." Toxicological Pathology **44**(5): 673-686.
Suzuki, J., M. Umeda, P. J. Sims and S. Nagata (2010). "Calcium-dependent phospholipid scrambling by TMEM16F." Nature **468**(7325): 834-838.
Suzuki, O. T., A. Frick, B. B. Parks, O. J. Trask Jr, N. Butz, B. Steffy, . . . T. Wiltshire (2014). "A cellular genetics approach identifies gene-drug interactions and pinpoints drug toxicity pathway nodes." Frontiers in Genetics **5**: 172.
The National Institute for Occupational Safety and Health. (2014). "Immediately Dangerous To Life or Health (IDLH)." 2016, from http://www.cdc.gov/niosh/idlh/7440224.html.
The Project on Emerging Nanotechnologies. (2016). "Consumer Products Inventory." 2016, from http://www.nanotechproject.org/cpi.
Threadgill, D. W. and G. A. Churchill (2012). "Ten Years of the Collaborative Cross." Genetics **190**(2): 291-294.
Toti, F., N. Satta, E. Fressinaud, D. Meyer and J. M. Freyssinet (1996). "Scott syndrome, characterized by impaired transmembrane migration of procoagulant phosphatidylserine and hemorrhagic complications, is an inherited disorder." Blood **87**(4): 1409-1415.
Turner, S. D. (2014). "qqman: an R package for visualizing GWAS results using Q-Q and manhattan plots." 2016, from https://cran.r-project.org/package=qqman.
Valdar, W., J. Flint and R. Mott (2006). "Simulating the Collaborative Cross: Power of Quantitative Trait Loci Detection and Mapping Resolution in Large Sets of Recombinant Inbred Strains of Mice." Genetics **172**(3): 1783.
Visscher, P. M., W. G. Hill and N. R. Wray (2008). "Heritability in the genomics era - concepts and misconceptions." Nature Reviews Genetics **9**(4): 255-266.

Wallach, D., T.-B. Kang and A. Kovalenko (2014). "Concepts of tissue injury and cell death in inflammation: a historical perspective." Nature Reviews Immunology **14**(1): 51-59.
Wang, X., Z. Ji, C. H. Chang, H. Zhang, M. Wang, Y.-P. Liao, . . . A. E. Nel (2014). "Use of Coated Silver Nanoparticles to Understand the Relationship of Particle Dissolution and Bioavailability to Cell and Lung Toxicological Potential." Small **10**(2): 385-398.
Weldon, B. A., M. F. E, G. Oberdorster, T. Workman, W. C. Griffith, C. Kneuer and I. J. Yu (2016). "Occupational exposure limit for silver nanoparticles: considerations on the derivation of a general health-based value." Nanotoxicology **10**(7): 945-956.
Wickham, H. (2009). ggplot2: Elegant Graphics for Data Analysis, Springer Publishing Company, Incorporated.
Yang, H., A. Kim, T. David, D. Palmer, T. Jin, J. Tien, . . . Lily Y. Jan (2012). "TMEM16F Forms a Ca2+-Activated Cation Channel Required for Lipid Scrambling in Platelets during Blood Coagulation." Cell **151**(1): 111-122.
Yu, K., J. M. Whitlock, K. Lee, E. A. Ortlund, Y. Yuan Cui and H. C. Hartzell (2015). "Identification of a lipid scrambling domain in ANO6/TMEM16F." eLife **4**: e06901.

Table 1. AgNP QTL Details

QTL Location	SNP rs number	SNP location	$-\log_{10}(p)$ & Rank Order	Effect Size (Cohen's d)
Chr 18: 63.5-66.5Mb	rs29865915	64292584	7.69 (1)	1.58
	rs29959933	64837330	6.30 (2)	1.67
	rs29778747	64837532	5.09 (4)	1.2
Chr 15: 90-100Mb	rs31581766	95827212	5.44 (3)	0.90
	rs3688273	96200660	4.87 (6)	1.06
Chr 4 72.5-135Mb	rs27482013	117407198	4.93 (5)	1.59

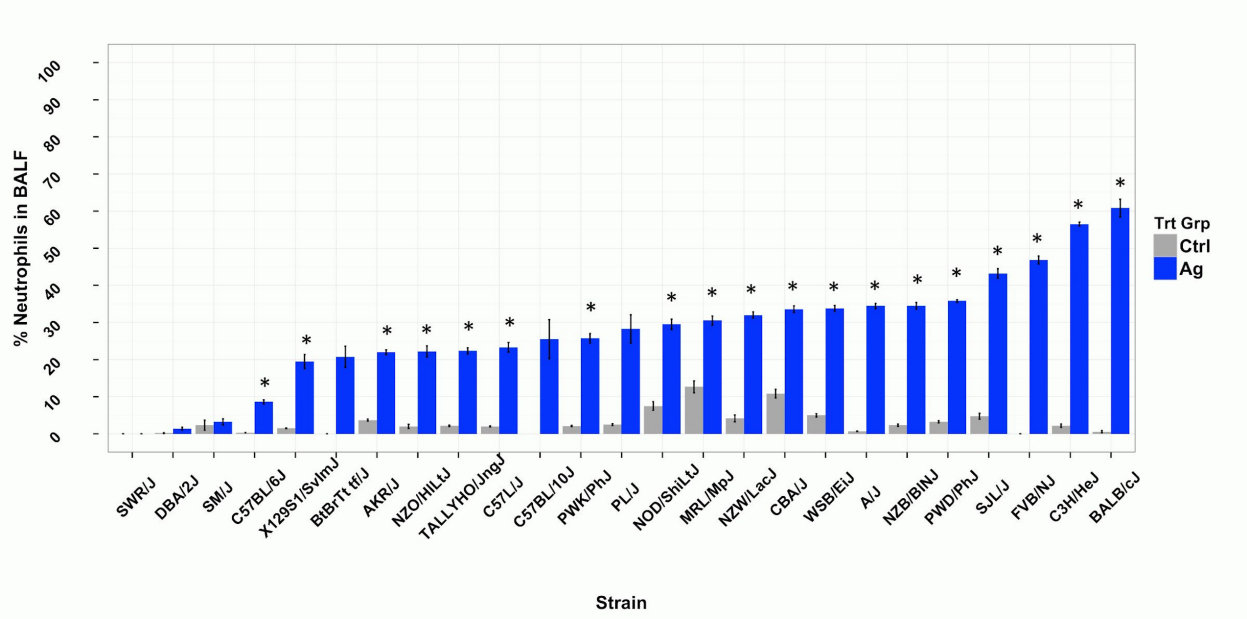

Figure 1. Plot of % BALF neutrophils for each strain for AgNP (Ag) and citrate buffer (Ctrl) treated mice. Bars are mean ± SEM. *Significant difference between AgNP treated and control for each strain by Student's t-test with correction for multiple comparisons ($p<0.05$), with the exception of the C57BL/10J strain, where n=1 for the control.

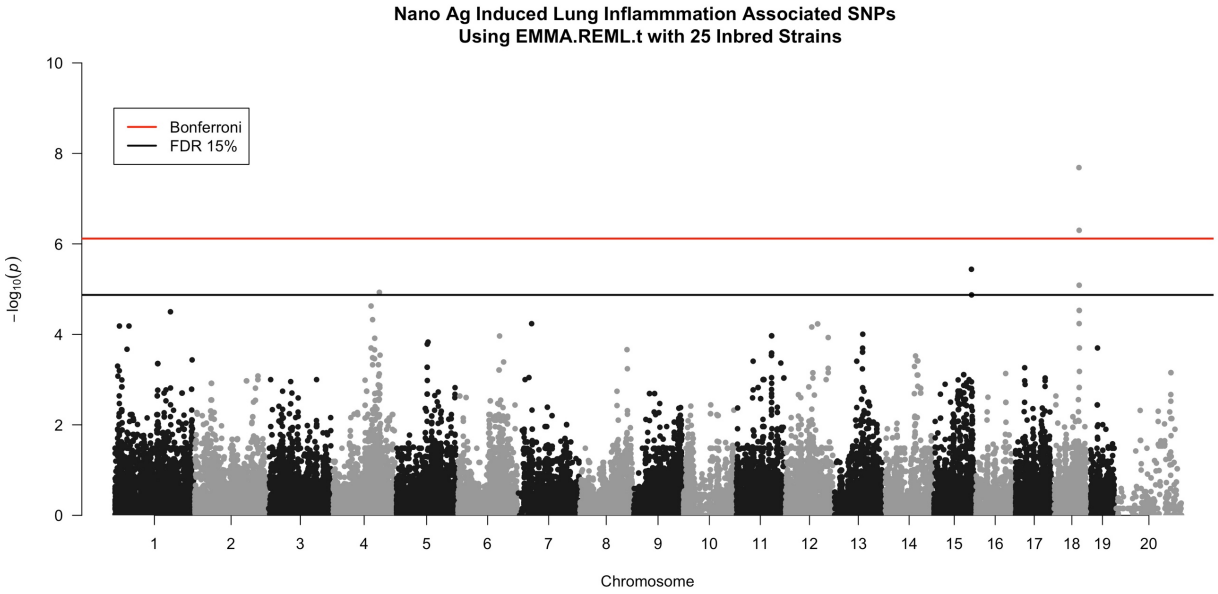

Figure 2. Manhattan plot showing the results from genome-wide analysis with EMMA. Each SNP tested is plotted by its chromosome and position on the x-axis. The y-axis shows the –log(p) value for each tested SNP. Significance lines for Bonferroni correction and for an FDR of 10 and 15% are also plotted.

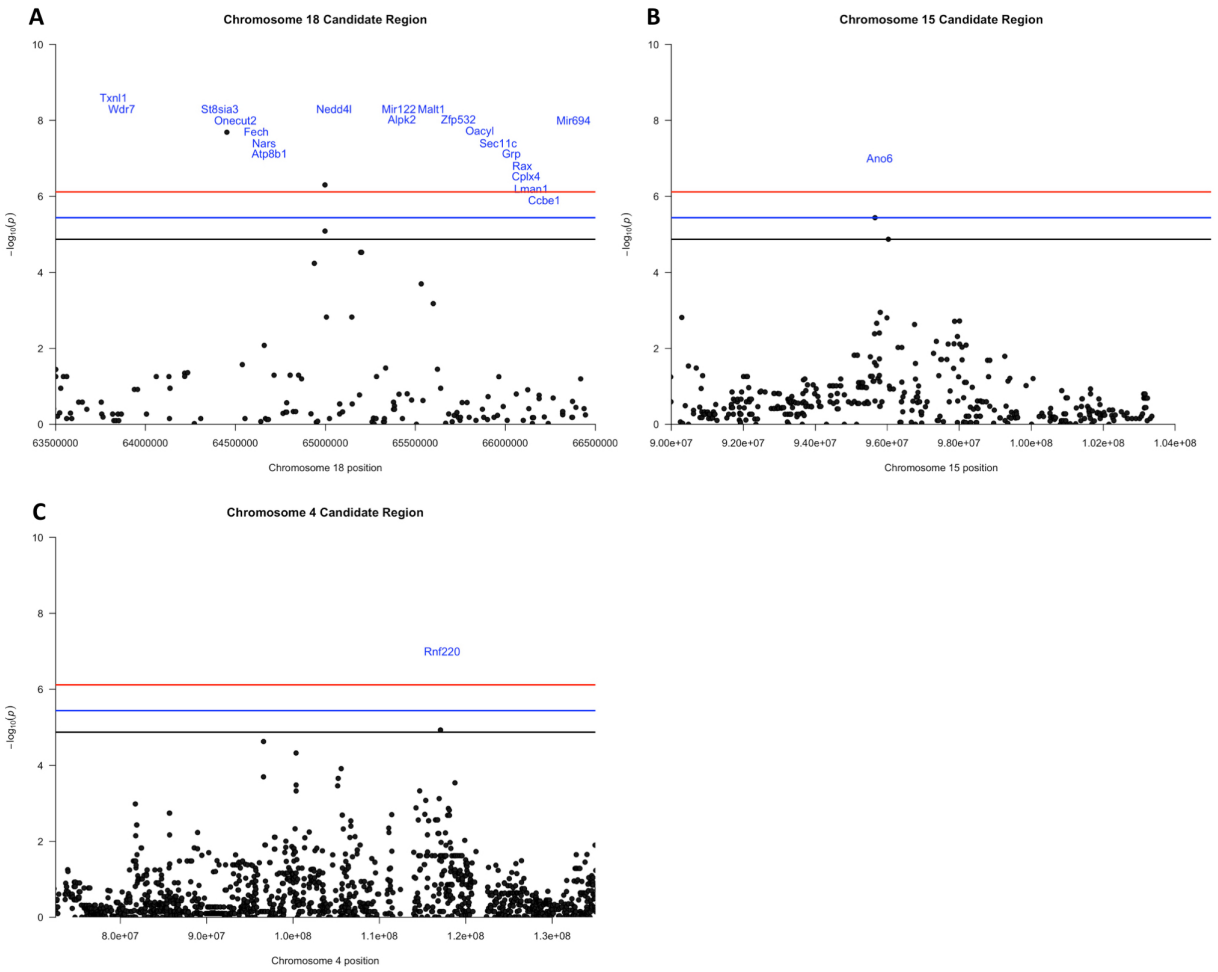

Figure 3. Candidate QTL regions on chromosomes 18, 15, and 4.

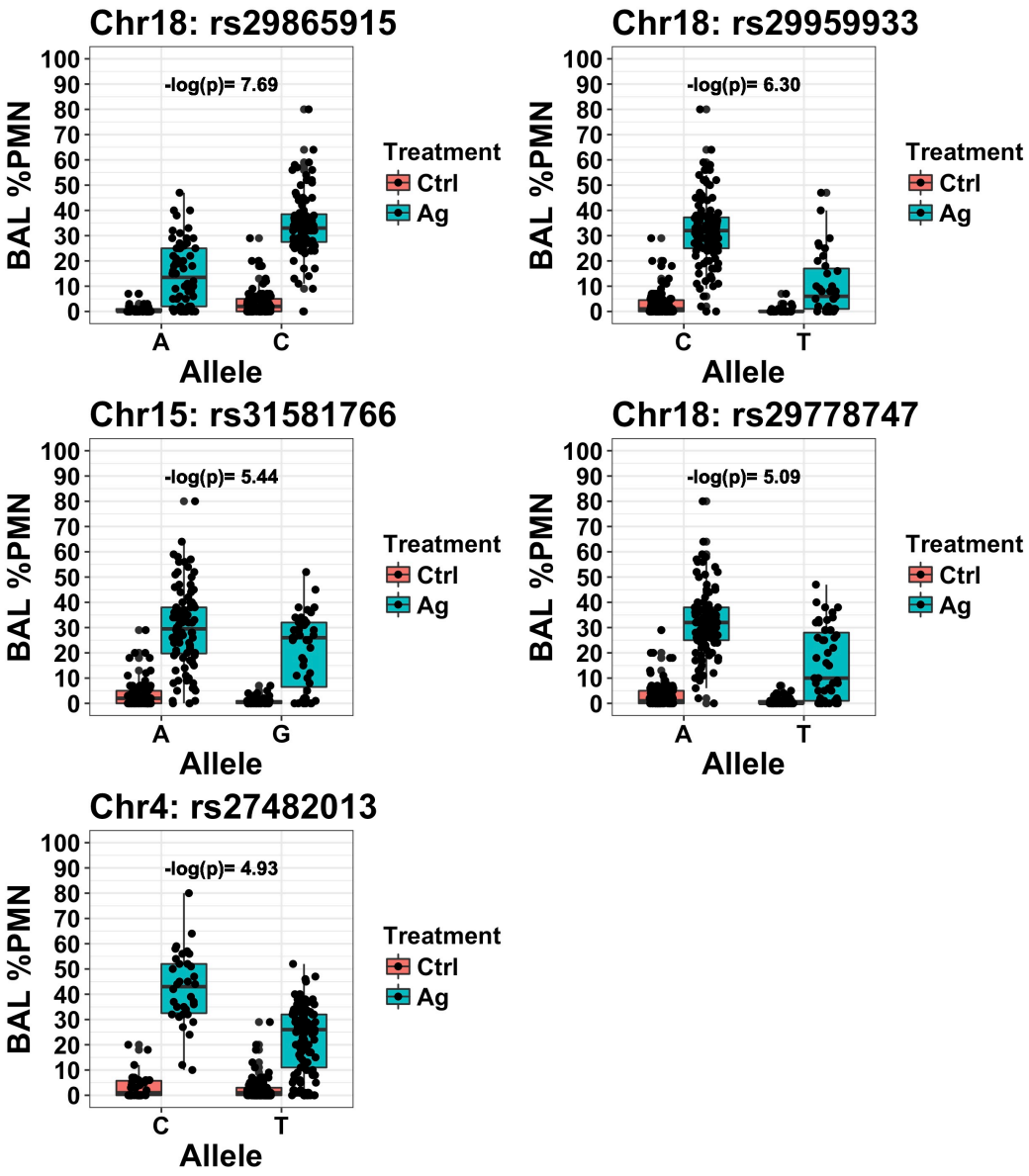

Figure 4. Plot of % BALF neutrophils for significant SNPs either in or near a candidate gene by allele and treatment group.

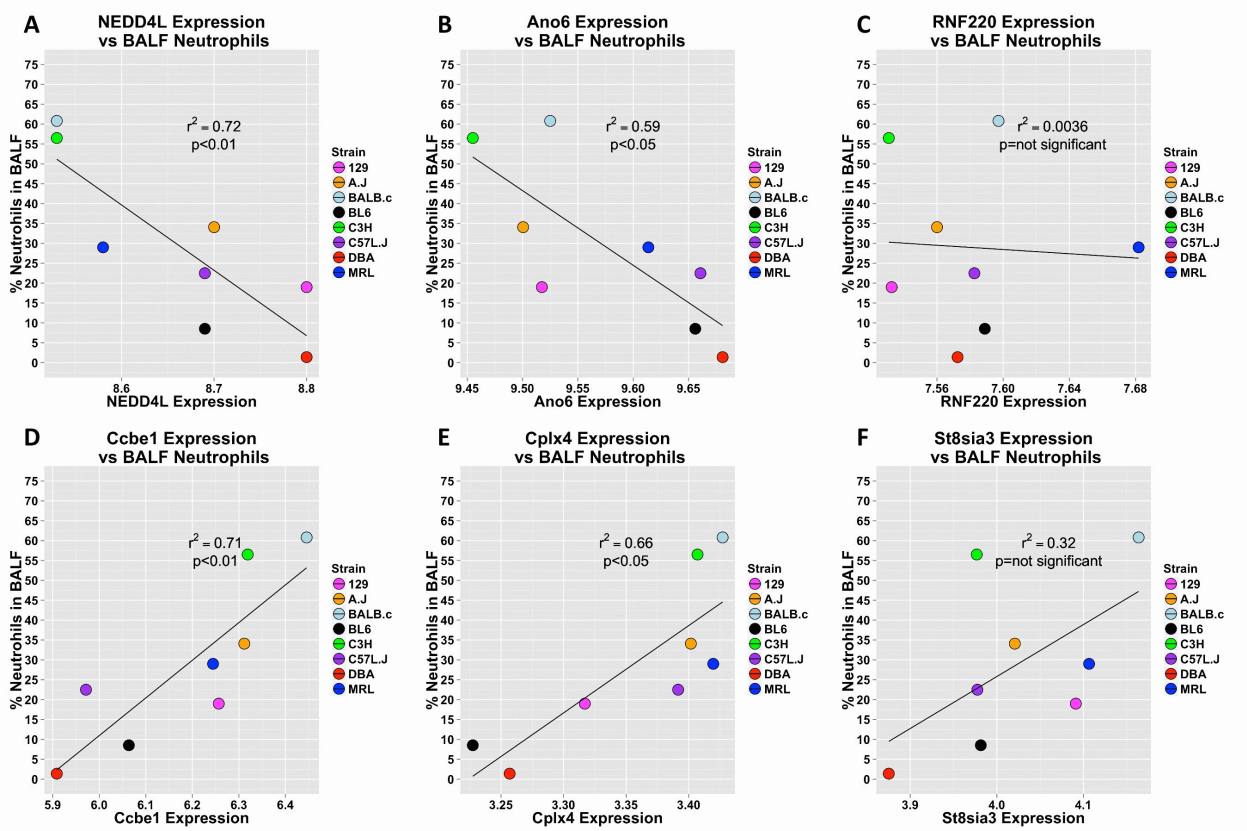

Figure 5. Correlations between % BALF neutrophils and mRNA levels from the Mouse Phenome Database for top candidate genes.

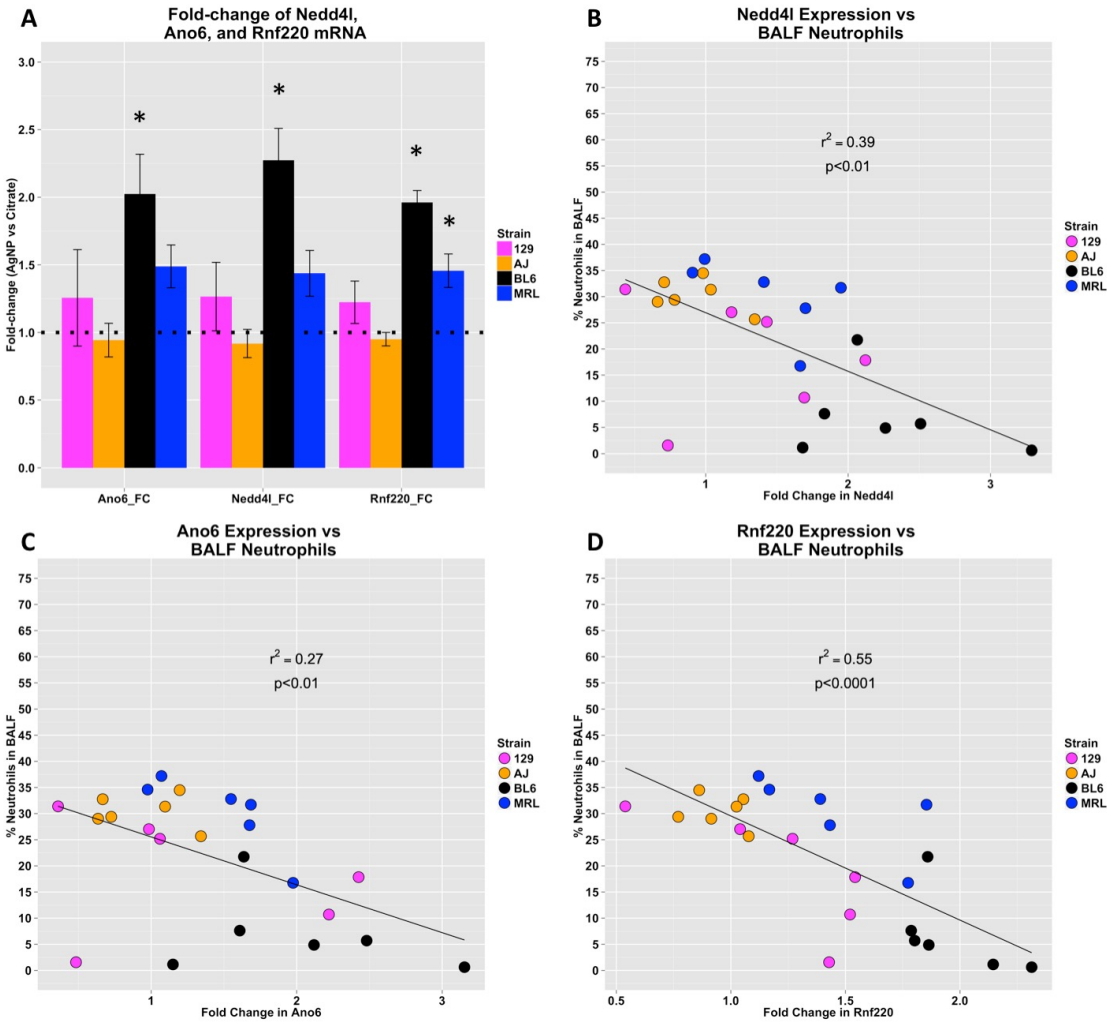

Figure 6. Expression of Nedd4l, Ano6 and Rnf220 mRNA (A) and correlations between % BALF neutrophils and fold change of mRNA levels between individual AgNP mice over the mean of strain matched control mice from qRT-PCR for top candidate genes (B-D). *=p<0.05 for one-sided t-test after Bonferroni adjustment.

Supplemental Information

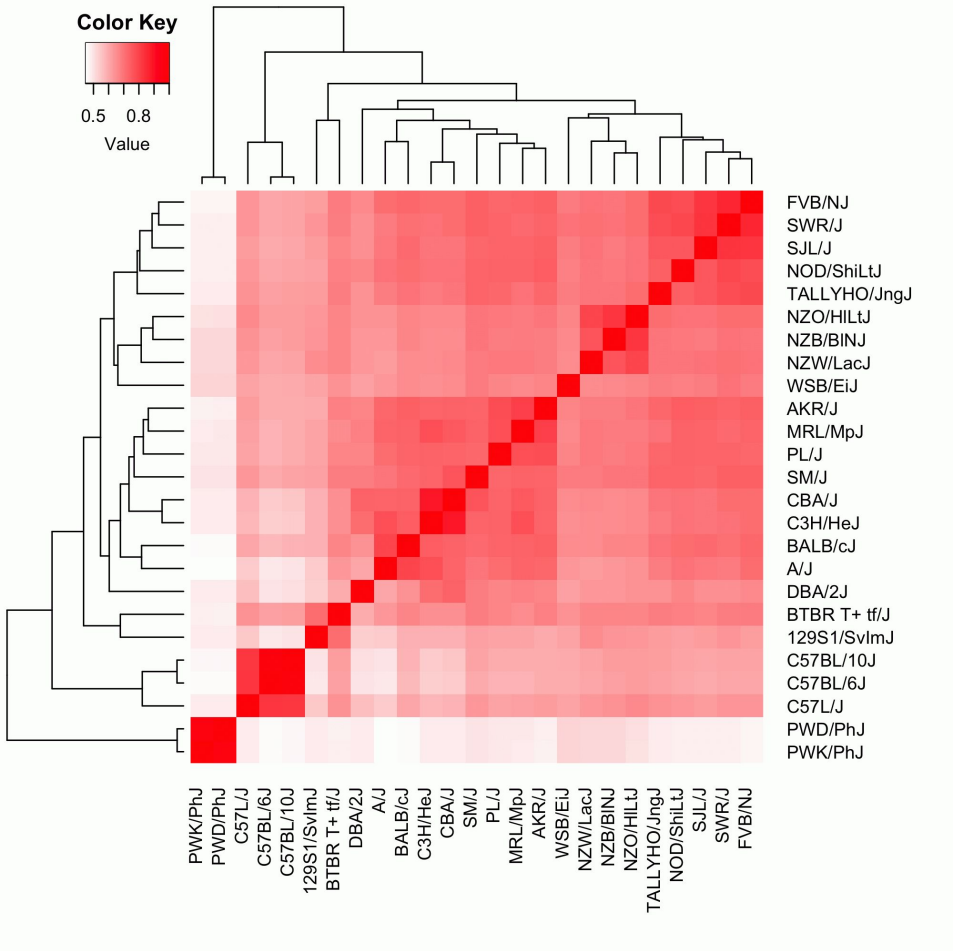

Figure 1S. Hierarchical clustering of kinship matrix showing genetic relatedness of the 25 strains based on their alleles at the 65,594 SNPs used in this study.

Mouse Strains Included In GWAS

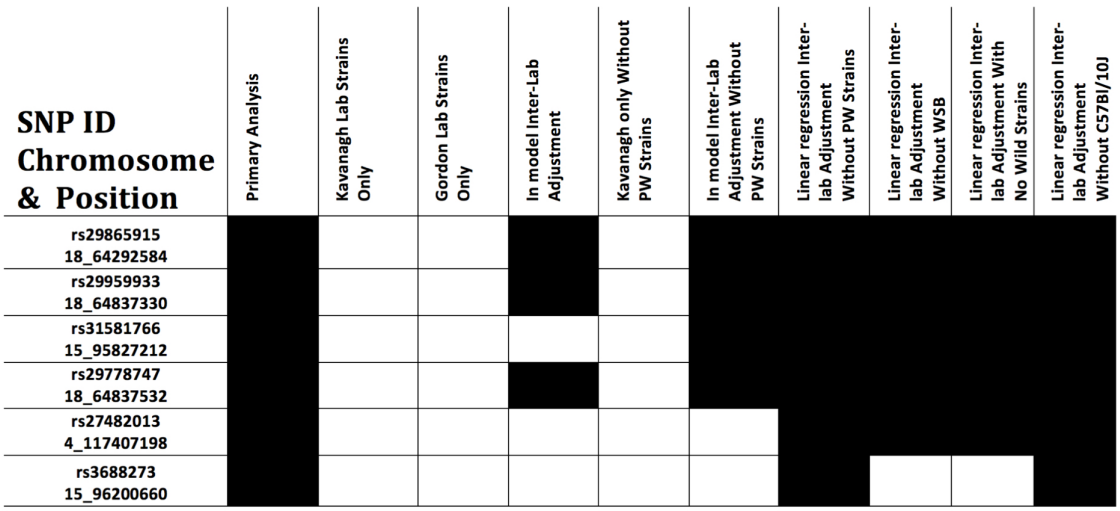

Figure 2S. SNPs that were among the top 6 in terms of –log(p) from different GWA studies performed using the initial and alternate analysis strategies. SNPs from alternate analyses shown where they appear more than once.

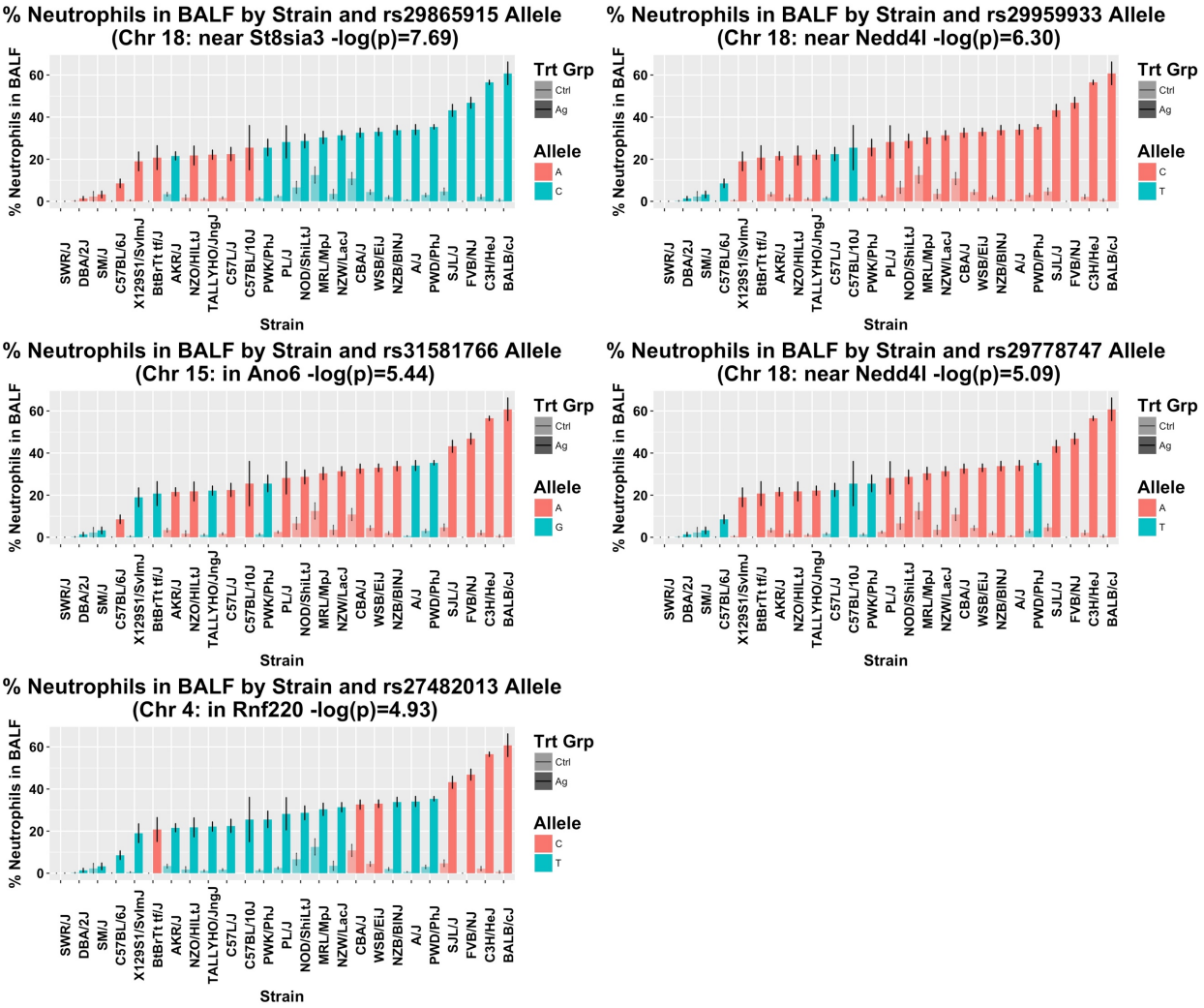

Figure 3S. Plot of % BALF neutrophils for the significant SNPs either in or near a candidate gene by strain, allele and treatment group illustrating allele distribution patterns.

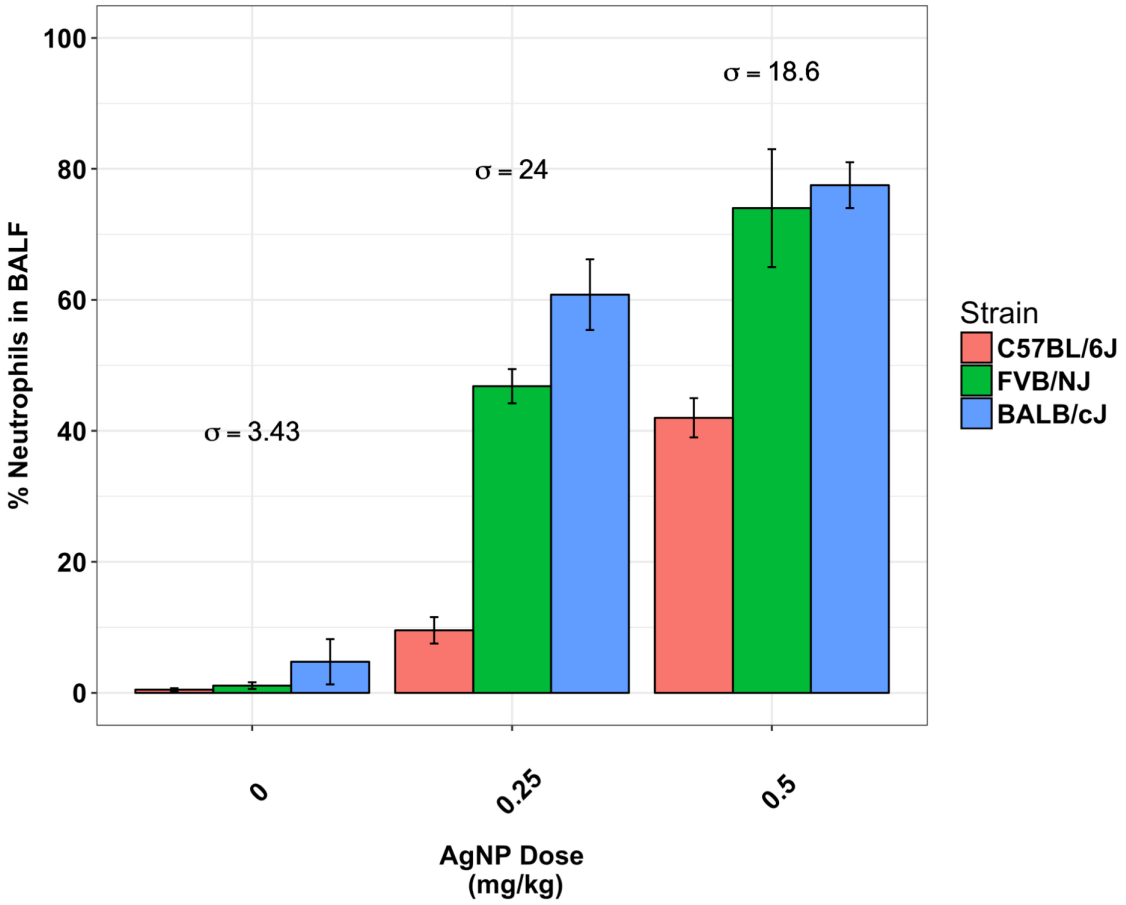

Figure 4S. AgNP dose response data in C57BL6/J, FVB/NJ, and BABL/c mice (0-0.5 mg/kg). Inset: Additional dose response for FVB/NJ mice (0-0.25 mg/kg).

Chapter 5

Quantum Dot Induced Acute Changes in Lung Mechanics are Mouse Strain Dependent

David K. Scoville[1], Collin C White[1], Dianne Botta[1], Dowon An[2], Zahra Afsharinejad[1], Theo K. Bammler[1], Xiaohu Gao[3], William A. Altemeier[2], Terrance J. Kavanagh[1]

Departments of [1]Environmental and Occupational Health Sciences, [2]Medicine and [3]Bioengineering, University of Washington, Seattle, WA 98195

Corresponding Author:
Terrance J. Kavanagh, PhD
Department of Environmental and Occupational Health Sciences
Box 354695
University of Washington
Seattle, WA 98195, USA.
Tel: (206) 685-8479
Fax: (206) 685-4696
E-mail: tjkav@uw.edu
Running Title: Mouse Strain Affects Quantum Dot Impact on Lung Mechanics

Abstract

Concerns have been raised over potential occupational exposure to engineered nanomaterials (ENMs). Potential impacts on lung function from inhalation exposures are of particular concern as the lung has proven to be a sensitive ENM target in animal studies. Emerging epidemiological data also suggest that occupational exposure to ENMs may impact respiratory and cardiovascular health. Quantum dots (QDs) are a type of ENM with outstanding semiconductor and fluorescent properties and thus have the potential for widespread use in biomedical research and in electronics. QDs have been shown in rodent models to induce inflammation and cytotoxicity. High dose exposures to QDs have been shown to impact lung function, measured two weeks after exposure. However, effects of mouse strain and the temporality of QD effects on lung function have not been established. In this study we extend our previous research on the acute effects of QD exposure to evaluate the impact on respiratory system mechanics in C57BL/6J and A/J mice. We have previously observed a greater initial inflammatory response to pulmonary QD exposure in A/J mice compared to C57BL/6J mice. We hypothesized that A/J mice would also be more sensitive to QD-induced acute effects on lung mechanics. Results from this study showed that lung mechanics in A/J mice were impacted by QD exposure and that both strains showed signs of QD-induced lung inflammation.

Introduction

The manufacturing of engineered nanomaterial (ENMs) and ENM enabled products has increased substantially in the last decade. However, data from rodent studies have demonstrated that a variety of ENMs can induce lung inflammation and toxicity by inhalation and other surrogate methods including intranasal and Intratracheal instillation, and oropharyngeal aspiration (Ma-Hock et al. 2009; Ma-Hock et al. 2012; Ma-Hock et al. 2013; McConnachie et al. 2013; Roberts et al. 2013; Seiffert et al. 2015; Silva et al. 2015; Cartwright et al. 2016). Emerging epidemiological data suggests that occupational ENM exposure can increase inflammatory cytokines in the respiratory tract (Cui 2013). Concerns over potential ENM impact on lung function (Liao et al. 2014; Liou et al. 2015) are relevant considering ENMs, including silver nanoparticles (AgNP) and single and multi-walled carbon nanotubes (SWCNTs, MWCNTs), have been shown to impact lung function in mice (Hsieh et al. 2012; Wang et al. 2012; Seiffert et al. 2015; Botelho et al. 2016) and potentially humans (Liao et al. 2014).

Quantum dots (QDs) are engineered semiconductor nanoparticles that are commonly composed of either a Cadmium/Selenium (CdSe), Cd/Tellurium (CdTe), or CdSeTe core that is surrounded by a Zinc/Sulfide (Zn/S) shell (Medintz et al. 2005). Additional outer coatings are frequently added for functionalization of QDs for a specific application (Michalet et al. 2005; Azzazy et al. 2007). *In vivo* studies in rodents have shown that pulmonary exposure to QDs can cause both acute and chronic inflammation characterized by neutrophil influx, cytokine production, compromised alveolar/capillary barrier function, and granuloma formation (Jacobsen et al. 2009; Ma-Hock et al. 2012; McConnachie et al. 2013; Roberts et al. 2013; Scoville et al. 2015). In some cases cytotoxicity and DNA damage were also observed (Jacobsen et al. 2009; Roberts et al. 2013). Changes in coatings have been shown to modify the toxic and inflammatory potential of QDs (Ma-Hock et al. 2013; Roberts et al. 2013). Furthermore, QDs have been shown to cause changes in lung mechanics when

measured 17 days after intratracheal installation of a high dose of QDs (Ho et al. 2013). However, the ability for QDs to impact lung mechanics in the acute setting has not been evaluated. The role of mouse strain has also not been evaluated for ENM effects on lung mechanics.

In this study, we sought to determine whether pulmonary exposure to QDs elicits changes in mouse lung mechanics in the acute setting and, if so, whether such effects would be influenced by mouse strain. We used forced oscillation techniques, thought to currently be the most accurate method for measuring mouse lung mechanics (Irvin and Bates 2003; Vanoirbeek et al. 2010). Since there is some concern over occupational health effects of ENM exposure, such as aggravation of asthma, and some ENMs have been shown to enhance models of allergic airway disease in mice, we used a methacholine challenge to assess airway hyperresponsiveness (AHR) (Hargreave et al. 1981; Postma and Kerstjens 1998; Nygaard et al. 2009; Golan et al. 2012; Brandenberger et al. 2013; Jonasson et al. 2013; Roy et al. 2013).

We have previously observed that C57BL6/J were more resistant than A/J mice to acute QD-induced lung inflammation (Scoville et al. 2015), and thus used these mouse strains to test the hypotheses that 1) QDs negatively impact mouse mechanics and 2) that responses are more pronounced in A/J mice. Results from this study showed that QDs induced lung inflammation in both C57L/6J and A/J mice and that A/J mice were more susceptible to the impact of QDs on lung mechanics. These mouse strain differences suggest that the potential for similar ENMs to affect lung function in humans could be influenced by an individual's genetics.

Materials and Methods

Ethics Statement

All procedures were approved by the University of Washington Institutional Animal Care and Use Committee (IACUC) on protocol #2384-08.

Animal Housing and Dosing

C57BL/6J and A/J mice (n=9 for QD and Saline groups for both strains) were ordered from Jackson Laboratories (Bar Harbor, ME) and housed in an Association for Assessment and Accreditation of Laboratory Animal Care (AAALAC)-approved vivarium under modified specific pathogen free (SPF) at the University of Washington. Food and water were available *ad libitum* during the 1-week acclimation period. Mice were dosed via oropharyngeal aspiration (OPA) with either 6 μg Cd equivalents/kg body weight of a 10 nM TOPO-PMAT QD solution or an equivalent volume of sterile saline.

Pulmonary Function Testing

At 24 hours after dosing, QD or saline treated C57BL/6J or A/J mice (N=6 for each category) were anesthetized with pentobarbital (90 mg/kg body weight), intubated via tracheotomy with an 18 gauge Luer stub that was secured in the trachea with a suture. The mice were then connected to a flexiVent 5.2 instrument (SCIREQ USA Inc., Tempe AZ). After an injection of pancuronium (0.1 mL) to eliminate reflexes from the mouse for breathing, pulmonary function was evaluated. The lungs were ventilated with a tidal volume of 10 mL/kg, at a rate of 180 breaths/min, with a positive end expiratory pressure of 3 cm H_2O. Subsequently, a total lung capacity maneuver was performed at 30 cm H_2O and baseline measurements were collected. To assess airway hyperresponsiveness, progressive doses of nebulized methacholine (MTCH) (0, 3.125, 12.5, and 50 mg/mL) were delivered to the lungs over 15 sec periods. At each dose of MTCH, a 3 sec multi-frequency forced oscillation maneuver was applied for determination of total lung impedance followed by a 1.5 sec single frequency oscillation for determination of Resistance (R), Elastance (E), and Compliance (C). Airway Resistance (Rn), Tissue Damping (G), and Tissue Elastance (H)

were calculated by the flexiVent software by applying the Constant Phase Model to the impedance measurement. Histerisivity (eta) is the ratio of G/H. Area under the curve was calculated for individual mice for comparisons between strain and treatment groups (Vanoirbeek et al. 2010).

Bronchoalveolar Lavage (BAL)

After pulmonary function testing, the animals were euthanized with an overdose of pentobarbital and BAL was performed. Mice that did not undergo lung mechanics testing were euthanized using CO_2 narcosis followed by cervical dislocation (N=3 for each category). Three 1 mL lavages were performed on each mouse using phosphate buffered saline (PBS). Aliquots of 100 µL from the 1st lavage were centrifuged onto microscope slides using a Cytospin 3 (Shandon Life Sciences International Ltd., Cheshire, England); these were later fixed and stained using Diff-Quik (Siemens - Thermo Fisher Scientific, Waltham, MA). Remaining BALF was centrifuged at 500g for 10 min and cells from the 3 lavages were pooled for flow cytometry. Supernatant from the 1st lavage was frozen at -80° C for measuring total protein and cytokines.

BALF Protein and Cytokine Analysis

BALF total protein was measured using the Bio-Rad Protein Assay (BioRad, Hercules, CA). Protein concentrations were interpolated from a standard curve created using dilutions of a BSA solution (0-0.35 mg/mL). BALF cytokines IFN-γ, IL-5, IL-17A, IL-33, KC (CXCL1), and IL-10 were measured in duplicate using a U-Plex assay (Meso Scale Discovery - Meso Scale Diagnostics, Rockville, MD). Samples below the lower limit of detection (LLOD) were replaced with the analyte-specific LLOD divided by the square root of 2.

Lung Tissue and Glutathione

The right lung was flash frozen in liquid nitrogen for determination of glutathione concentration, and the left lung was fixed in 10% Neutral Buffered Formalin (NBF) at 20 cm H_2O. Levels of total glutathione were measured as previously described (Weldy et al. 2011). Briefly, glutathione in lung tissue samples and standards (0-0.25 mM) was reduced with TCEP (tris(2-carboxyethyl) phosphine), and then derivatized with napthelene-2,3-dicarboxaldehyde. Relative fluorescence intensity was measured for samples and standards. Sample concentrations were interpolated from the GSH standard curve. Standards and samples were analyzed in triplicate and samples were normalized to total protein levels in the lung tissue sample measured using the Bradford method.

Flow Cytometry

Combined BALF cells were prepared and analyzed using flow cytometry as previously described (Weldy et al. 2011; Scoville et al. 2015). Briefly, cells were stained with an antibody cocktail containing a phycoerythrin conjugated primary antibody against Cd11b (AbCam, Cambridge,MA), a biotinylated primary antibody/ streptavidin/AlexaFluor350 secondary antibody combination against Ly-6G/Ly-6C (Gr1) (BioLegend, San Diego, CA), and an Alexafluor 488 conjugated primary antibody against F4/80 (eBioscience, San Diego, CA). Cells high in Cd11b and low in F4/80 fluorescence were classified as neutrophils.

Statistical Analysis

The data collected in this study were analyzed using Graphpad Prism (GraphPad Software, La Jolla, CA) and R (R Core Team 2014). Area under the methacholine dose-response curve was calculated for each animal, and a two-way analysis of variance (ANOVA) was used to assess mouse strain and QD treatment effects. If QD treatment effects were significant in the two-way ANOVA, post hoc t-tests were performed between saline and QD treated mice in both mouse strains. Two-way ANOVA was also used to determine if there were baseline differences in measures between mice that underwent lung mechanics testing

and those that did not. We included all mice in the study in our assessment of QD effects on % neutrophils in BALF and lung glutathione as lung mechanic testing did not affect % neutrophils in BALF or lung glutathione in saline control mice. However, baseline differences were observed with concentrations of total BALF protein. To allow for comparisons across measurements, we only further evaluated levels of total protein from mice that underwent lung mechanics testing. Cytokines were assessed in mice that underwent lung mechanics testing and that represented high, moderate and low % neutrophils in BALF. Pearson's correlation coefficients between endpoints were calculated using r.corr function in the Hmisc R package (Harrell et al. 2016). Data was managed in Microsoft Excel and R. Plots were generated using ggplot2 (Wickham 2009) and corrplot (Wei and Simko 2016).

Results

Lung Mechanics

Similar to a study by Nolin et al., we used total lung resistance (R) as our measure of AHR (Nolin et al. 2016). We observed that QD treatment and mouse strain significantly affected AHR overall (Figure 1A). Total lung elastance (E) was significantly affected by QD treatment overall but was not different between mouse strains (Figure 1B). Total lung compliance (C) was significantly affected by mouse strain but not QD treatment (Figure 1C). Airway resistance (Rn) was also significantly affected by mouse strain (Figure 1D). Tissue damping (G) was significantly increased by QD treatment in A/J mice but not in C57BL/6J mice (Figure 1E). Hysteresisivity (eta), the ratio of G/tissue elastance (H), was significantly affected by mouse strain overall but not by QD treatment (Figure 1F).

BALF Neutrophils, Total Protein, and Cytokines

We observed that % neutrophils in BALF were significantly increased in QD treated C57BL/6J and A/J mice compared to saline treated strain-matched controls (Figure 2 A). In

order to characterize potential drivers of the acute QD inflammatory response, we measured cytokines representative of Th1 (IFN- γ) and Th2 (IL-5, IL-33) immune responses as C57BL/6J are thought to be more Th1 response prone and A/J mice are thought to be more Th2 prone (Schroder et al. 2004; Sellers et al. 2011; Hallstrand et al. 2013). We also measured IL-17, which has been associated with neutrophil recruitment (Choy et al. 2015). IL-10, an anti-inflammatory cytokine, is released to prevent damage and is often increased in concert with pro-inflammatory cytokines (Saraiva and O'Garra 2010). Levels of total protein and IL-33 in BALF were not different between the two mouse strains or between treatment groups (Figure 2 B-C). Levels of the neutrophil chemokine KC were significantly increased in QD treated C57BL/6J mice compared to saline (Figure 2D). We also found a significant association between levels of KC and BALF neutrophils (Figure 2E). IL-17, IFN-γ, IL-5 and IL-10 were undetectable in virtually all mice (data not shown).

Lung Glutathione

Levels of lung glutathione were significantly different between the two mouse strains overall (Figure 3A). Additionally, we observed significant inverse correlations between total lung glutathione levels and the lung mechanics measures R and G in QD treated mice (Figure 3 B-C).

Discussion

In this study we investigated the impact of mouse strain and QD treatment on lung mechanics. The results indicate that QDs can influence mouse lung mechanics in a strain dependent manner. We observed that QD treatment significantly increased tissue damping (G), and lung elastance (E) in A/J mice but not in C57BL/6J mice. We also found that AHR was significantly affected by QD treatment and mouse strain. Other measures of lung

mechanics (Airway resistance (Rn), Compliance (C), and hysteresivity (eta)) were significantly affected by mouse strain, but not by QD treatment.

The results from measuring lung mechanics indicate that G and E are sensitive to QD treatment. Lung elastance (E) captures the elastic recoil properties of the lung. Increases in E were previously observed with silica nanoparticle instillation (Ferreira et al. 2013). Tissue damping (G) (referred to as G_{ti} by Tomioka) captures the dissipation of air pressure wave energy into the lung tissues (Tomioka 2002). True parenchymal tissue resistance to airflow (R_{ti}) can be measured directly using alveolar capsules, and although G and R_{ti} are not directly comparable, both parameters were significantly affected in a mouse ovalbumin (OVA) allergic airway model (Tomioka 2002). Furthermore, G was found to be a more sensitive measure than Rn (referred to as R_{AW} by Tokioka), highlighting the importance of the peripheral lung tissue to overall lung response. In a review article referencing the same OVA study by Tomioka it was suggested that changes in peripheral lung tissue and small airways may be related to changes in lung secretions (Tomioka 2002; Irvin and Bates 2003). The effects of lipopolysaccharide (LPS) on mouse lung mechanics and pulmonary surfactant have also been studied (Ingenito et al. 2001). Surfactant proteins are an essential component of the alveolar lining fluid, where they act to reduce surface tension. LPS was found to alter lung mechanics and change the expression and function of surfactant proteins (Ingenito et al. 2001). The authors suggested that inflammation in the lungs could damage surfactant proteins and lipids through neutrophil-derived proteases, reactive oxygen species, and lipid inflammatory mediators (Ingenito et al. 2001). In the context of these other studies that studied mouse lung mechanics and inflammation, we interpret our findings as evidence that acute exposure to QDs can adversely impact peripheral lung tissue mechanics and that A/J mice are more sensitive compared to C57BL/6J. A study comparing *Aspergillus fumigatus* allergic inflammation and airway hyperresponsiveness between C57BL/6J and BALB/c mice attributed resistance in C57BL/6J mice to increased levels of surfactant protein D (Atochina et al. 2003). Interestingly, a study investigating MWCNT

effects on lung mechanics in a non-allergic model found significant MWCNT associated increases in G in C57BL/6J mice suggesting that susceptibility to ENM-induced changes in lung mechanics are both particle and strain specific (Wang et al. 2011).

The observed inverse correlations of R and G with lung glutathione in QD treated mice in our study are consistent with previous reports indicating that glutathione supplementation improved LPS induced changes in lung mechanics and inflammation and that glutathione mediates lung permeability associated with cigarette smoke and air pollution PM_{10} (Rahman and MacNee 1999; Sharma et al. 2011).

We also observed a QD-induced inflammatory response characterized by significantly increased % neutrophils in BALF in both C57BL/6J and A/J mice and levels of KC in C57BL/6J mice. This is interesting in the context of our previous study showing that C57BL/6J did not exhibit QD associated significant increases in KC or in % neutrophils in BALF 8 hr after QD exposure (Scoville et al. 2015). In contrast, A/J mice showed significant increases in KC 8 hr after QD exposure, and, in a sensitivity analysis where potential outliers were removed, significant increases in BALF neutrophils (Scoville et al. 2015). These results suggest kinetics of QD-induced inflammatory response are also mouse strain dependent. The inability to detect IL-5, IFN-γ, IL-17, or IL-10 suggests that T-helper cells were not major contributors in the acute QD-induced immune response and that this response has not yet transitioned to the resolution phase. The relationship between % neutrophils and BALF KC in this study was comparable to that observed previously at 8 hr across all 8 Collaborative Cross founder strain mice (Scoville et al. 2015).

In conclusion, the results from this study suggest that QD effects on lung mechanics are mouse strain dependent (with A/J mice being more affected than C57BL/6 mice), and that peripheral lung tissue may be more sensitive to QDs than central airways. The observation of mouse strain differences in QD-induced changes in lung mechanics suggest that the potential for ENMs to affect lung function in humans could depend on genetics. Observations of QD-induced lung inflammation in this study and in previous studies could

have implications for predisposition to infection and other conditions. The results from this study showing that QDs enhanced AHR in general warrant future studies to investigate the impact of QDs on allergen-sensitized mice. Inverse associations between QD-induced AHR and glutathione warrant future studies to further investigate the biochemical and pathophysiological basis for this relationship.

Chapter 5 References

Atochina, E. N., M. F. Beers, Y. Tomer, S. T. Scanlon, S. J. Russo, R. A. Panettieri and A. Haczku (2003). "Attenuated allergic airway hyperresponsiveness in C57BL/6 mice is associated with enhanced surfactant protein (SP)-D production following allergic sensitization." Respiratory Research **4**(1): 15-15.

Azzazy, H. M. E., M. M. H. Mansour and S. C. Kazmierczak (2007). "From diagnostics to therapy: Prospects of quantum dots." Clinical Biochemistry **40**(13–14): 917-927.

Botelho, D. J., B. F. Leo, C. B. Massa, S. Sarkar, T. D. Tetley, K. F. Chung, . . . A. J. Gow (2016). "Low-dose AgNPs reduce lung mechanical function and innate immune defense in the absence of cellular toxicity." Nanotoxicology **10**(1): 118-127.

Brandenberger, C., N. L. Rowley, D. N. Jackson-Humbles, Q. Zhang, L. A. Bramble, R. P. Lewandowski, . . . J. R. Harkema (2013). "Engineered silica nanoparticles act as adjuvants to enhance allergic airway disease in mice." Particle and Fibre Toxicology **10**(1): 26.

Cartwright, M. M., S. C. Schmuck, C. Corredor, B. Wang, D. K. Scoville, C. R. Chisholm, . . . T. J. Kavanagh (2016). "The pulmonary inflammatory response to multiwalled carbon nanotubes is influenced by gender and glutathione synthesis." Redox Biology **9**: 264-275.

Choy, D. F., K. M. Hart, L. A. Borthwick, A. Shikotra, D. R. Nagarkar, S. Siddiqui, . . . P. Bradding (2015). "TH2 and TH17 inflammatory pathways are reciprocally regulated in asthma." Science Translational Medicine **7**(301): 301ra129.

Cui, L. (2013). Exposure assessment and inflammatory response among workers producing calcium carbonate nanomaterials Dissertation, University of Washington.

Ferreira, T. P., A. C. de Arantes, C. V. do Nascimento, P. C. Olsen, P. G. Trentin, P. R. Rocco, . . . P. M. Silva (2013). "IL-13 immunotoxin accelerates resolution of lung pathological changes triggered by silica particles in mice." J Immunol **191**(10): 5220-5229.

Golan, D., A. J. Tashjian, E. Armstrong and A. Armstrong (2012). Principles of Pharmacology: The Pathophysilogic Basis of Drug Therapy. Philadelphia PA, Lippincott Williams and Wilkins, Wolters Kluwer.

Hallstrand, T. S., T. L. Hackett, W. A. Altemeier, G. Matute-Bello, P. M. Hansbro and D. A. Knight (2013). "Airway epithelial regulation of pulmonary immune homeostasis and inflammation." Clinical Immunology **151**(1): 1-15.

Hargreave, F. E., G. Ryan, N. C. Thomson, P. M. O'Byrne, K. Latimer, E. F. Juniper and J. Dolovich (1981). "Bronchial responsiveness to histamine or methacholine in asthma: measurement and clinical significance." Journal of Allergy and Clinical Immunology **68**(5): 347-355.

Harrell, F. J. J., C. Dupont and e. al. (2016). "Hmisc." from https://cran.r-project.org/package=Hmisc.

Ho, C. C., H. Chang, H. T. Tsai, M. H. Tsai, C. S. Yang, Y. C. Ling and P. Lin (2013). "Quantum dot 705, a cadmium-based nanoparticle, induces persistent inflammation and granuloma formation in the mouse lung." Nanotoxicology **7**(1): 105-115.

Hsieh, W. Y., C. C. Chou, C. C. Ho, S. L. Yu, H. Y. Chen, H. Y. E. Chou, . . . P. Yang (2012). "Single-Walled Carbon Nanotubes Induce Airway Hyperreactivity and Parenchymal Injury in Mice." American Journal of Respiratory Cell and Molecular Biology **46**(2): 257-267.

Ingenito, E. P., R. Mora, M. Cullivan, Y. Marzan, K. Haley, L. Mark and L. A. Sonna (2001). "Decreased Surfactant Protein-B Expression and Surfactant Dysfunction in a Murine Model of Acute Lung Injury." American Journal of Respiratory Cell and Molecular Biology **25**(1): 35-44.

Irvin, C. and J. Bates (2003). "Measuring the lung function in the mouse: the challenge of size." Respiratory Research **4**(1): 4.
Jacobsen, N. R., P. Moller, K. A. Jensen, U. Vogel, O. Ladefoged, S. Loft and H. Wallin (2009). "Lung inflammation and genotoxicity following pulmonary exposure to nanoparticles in ApoE-/- mice." Particle and Fibre Toxicology **6**(2).
Jonasson, S., B. Gustafsson A Fau - Koch, A. Koch B Fau - Bucht and A. Bucht (2013). "Inhalation exposure of nano-scaled titanium dioxide (TiO2) particles alters the inflammatory responses in asthmatic mice." Inhalation Toxicology **25**(4): 1091-7691.
Liao, H.-Y., Y.-T. Chung, C.-H. Lai, S.-L. Wang, H.-C. Chiang, L.-A. Li, . . . S.-H. Liou (2014). "Six-month follow-up study of health markers of nanomaterials among workers handling engineered nanomaterials." Nanotoxicology **8**(sup1): 100-110.
Liou, S.-H., C. S. J. Tsai, D. Pelclova, M. K. Schubauer-Berigan and P. A. Schulte (2015). "Assessing the first wave of epidemiological studies of nanomaterial workers." Journal of Nanoparticle Research **17**: 413.
Ma-Hock, L., S. Brill, W. Wohlleben, P. M. A. Farias, C. R. Chaves, D. P. L. A. Tenório, . . . B. van Ravenzwaay (2012). "Short term inhalation toxicity of a liquid aerosol of CdS/Cd(OH)2 core shell quantum dots in male Wistar rats." Toxicology Letters **208**(2): 115-124.
Ma-Hock, L., P. M. Farias, T. Hofmann, A. C. Andrade, J. N. Silva, T. M. Arnaud, . . . B. van Ravenzwaay (2013). "Short term inhalation toxicity of a liquid aerosol of glutaraldehyde-coated CdS/Cd(OH) core shell quantum dots in rats." Toxicology Letters **225**(1): 20-26.
Ma-Hock, L., S. Treumann, V. Strauss, S. Brill, F. Luizi, M. Mertler, . . . R. Landsiedel (2009). "Inhalation Toxicity of Multiwall Carbon Nanotubes in Rats Exposed for 3 Months." Toxicological Sciences **112**(2): 468-481.
McConnachie, L. A., D. Botta, C. C. White, C. S. Weldy, H. W. Wilkerson, J. Yu, . . . T. J. Kavanagh (2013). "The Glutathione Synthesis Gene Gclm Modulates Amphiphilic Polymer-Coated CdSe/ZnS Quantum Dot-Induced Lung Inflammation in Mice." PLOS ONE **8**(5): e64165.
Medintz, I. L., H. T. Uyeda, E. R. Goldman and H. Mattoussi (2005). "Quantum dot bioconjugates for imaging, labelling and sensing." Nature Materials **4**: 435-446.
Michalet, X., F. F. Pinaud, L. A. Bentolila, J. M. Tsay, S. Doose, J. J. Li, . . . S. Weiss (2005). "Quantum dots for live cells, in vivo imaging, and diagnostics." Science **307**(5709): 538-544.
Nolin, J. D., H. L. Ogden, Y. Lai, W. A. Altemeier, C. W. Frevert, J. G. Bollinger, . . . T. S. Hallstrand (2016). "Identification of Epithelial Phospholipase A2 Receptor 1 (PLA2R1) as a Potential Target in Asthma." American Journal of Respiratory Cell and Molecular Biology.
Nygaard, U. C., J. S. Hansen, M. Samuelsen, T. Alberg, C. D. Marioara and M. Løvik (2009). "Single-Walled and Multi-Walled Carbon Nanotubes Promote Allergic Immune Responses in Mice." Toxicological Sciences **109**(1): 113-123.
Postma, D. S. and H. A. M. Kerstjens (1998). "Characteristics of Airway Hyperresponsiveness in Asthma and Chronic Obstructive Pulmonary Disease." American Journal of Respiratory and Critical Care Medicine **158**(supplement_2): S187-S192.
R Core Team. (2014). "R: A language and environment for statistical computing, R Foundation for Statistical Computing, Vienna Austria." from http://www.r-project.org/.
Rahman, I. and W. MacNee (1999). "Lung glutathione and oxidative stress: implications in cigarette smoke-induced airway disease." American Journal of Physiology - Lung Cellular and Molecular Physiology **277**(6): L1067.

Roberts, J. R., J. M. Antonini, D. W. Porter, R. S. Chapman, J. F. Scabilloni, S. H. Young, . . . R. R. Mercer (2013). "Lung toxicity and biodistribution of Cd/Se-ZnS quantum dots with different surface functional groups after pulmonary exposure in rats." Particle and Fibre Toxicology **10**: 5.

Roy, R., S. Kumar, A. K. Verma, A. Sharma, B. P. Chaudhari, A. Tripathi, . . . P. D. Dwivedi (2013). "Zinc oxide nanoparticles provide an adjuvant effect to ovalbumin via a Th2 response in Balb/c mice." International Immunology.

Saraiva, M. and A. O'Garra (2010). "The regulation of IL-10 production by immune cells." Nature Reviews Immunology **10**(3): 170-181.

Schroder, K., P. J. Hertzog, T. Ravasi and D. A. Hume (2004). "Interferon-γ: an overview of signals, mechanisms and functions." Journal of Leukocyte Biology **75**(2): 163-189.

Scoville, D. K., C. C. White, D. Botta, L. A. McConnachie, M. E. Zadworny, S. C. Schmuck, . . . T. J. Kavanagh (2015). "Susceptibility to quantum dot induced lung inflammation differs widely among the Collaborative Cross founder mouse strains." Toxicology and Applied Pharmacology **289**(2): 240-250.

Seiffert, J., F. Hussain, C. Wiegman, F. Li, L. Bey, W. Baker, . . . K. F. Chung (2015). "Pulmonary Toxicity of Instilled Silver Nanoparticles: Influence of Size, Coating and Rat Strain." PLOS ONE **10**(3): e0119726.

Sellers, R. S., C. B. Clifford, P. M. Treuting and C. Brayton (2011). "Immunological Variation Between Inbred Laboratory Mouse Strains." Veterinary Pathology **49**(1): 32-43.

Sharma, S., C. Dimitropoulou, S. Aggarwal, A. Smith, J. Catravas and S. M. Black (2011). "Glutathione Supplementation Attenuates Inflammation and Improves Lung Mechanics in a Murine Model of Acute Lung Injury." The FASEB Journal **25**(1 Supplement): 1101.1111.

Silva, R. M., D. S. Anderson, L. M. Franzi, J. L. Peake, P. C. Edwards, L. S. Van Winkle and K. E. Pinkerton (2015). "Pulmonary Effects of Silver Nanoparticle Size, Coating, and Dose over Time upon Intratracheal Instillation." Toxicological Sciences **144**(1): 151-162.

Tomioka, S. B. J. H. T. I. C. G. (2002). "Airway and tissue mechanics in a murine model of asthma: alveolar capsule vs. forced oscillations." Journal of Applied Physiology **93**(1): 263-270.

Vanoirbeek, J. A., M. Rinaldi, V. De Vooght, S. Haenen, S. Bobic, G. Gayan-Ramirez, . . . W. Janssens (2010). "Noninvasive and invasive pulmonary function in mouse models of obstructive and restrictive respiratory diseases." American Journal of Respiratory Cell and Molecular Biology **42**(1): 96-104.

Vanoirbeek, J. A. J., M. Rinaldi, V. De Vooght, S. Haenen, S. Bobic, G. Gayan-Ramirez, . . . W. Janssens (2010). "Noninvasive and Invasive Pulmonary Function in Mouse Models of Obstructive and Restrictive Respiratory Diseases." American Journal of Respiratory Cell and Molecular Biology **42**(1): 96-104.

Wang, X., J. Guo, T. Chen, H. Nie, H. Wang, J. Zang, . . . G. Jia (2012). "Multi-walled carbon nanotubes induce apoptosis via mitochondrial pathway and scavenger receptor." Toxicology in Vitro **26**(6): 799-806.

Wang, X., P. Katwa, R. Podila, P. Chen, P. C. Ke, A. M. Rao, . . . J. M. Brown (2011). "Multi-walled carbon nanotube instillation impairs pulmonary function in C57BL/6 mice." Particle and Fibre Toxicology **8**(1): 24.

Wei, T. and V. Simko. (2016). "corrplot: Visualization of a Correlation Matrix." 2016, from https://github.com/taiyun/corrplot.

Weldy, C. S., C. C. White, H.-W. Wilkerson, T. V. Larson, J. A. Stewart, S. E. Gill, . . . T. J. Kavanagh (2011). "Heterozygosity in the glutathione synthesis gene Gclm increases sensitivity to diesel exhaust particulate induced lung inflammation in mice." Inhalation Toxicology **23**(12): 724-735.

Wickham, H. (2009). ggplot2: Elegant Graphics for Data Analysis, Springer Publishing Company, Incorporated.

Figures.

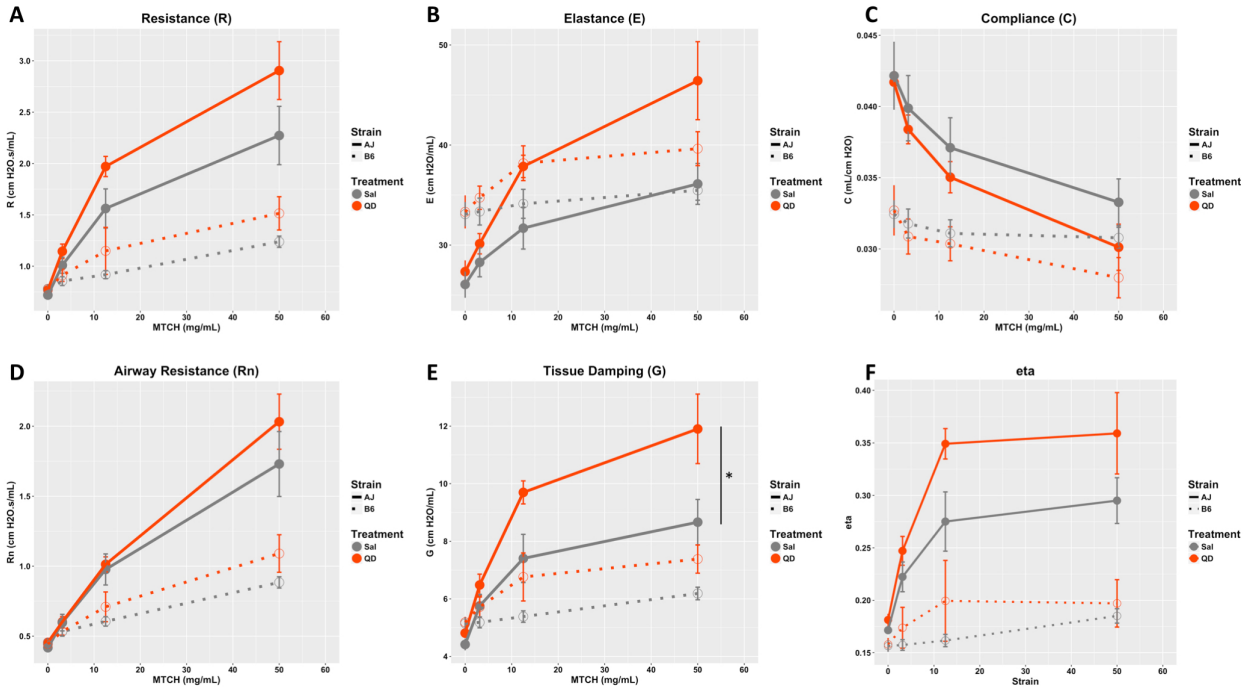

Figure 1. Lung Mechanics for QD and saline treated A/J and C57BL/6 mice plotted as mean ± SEM on the y-axes with MTCH dose on the x-axis. *p<0.05 after Bonferroni correction.

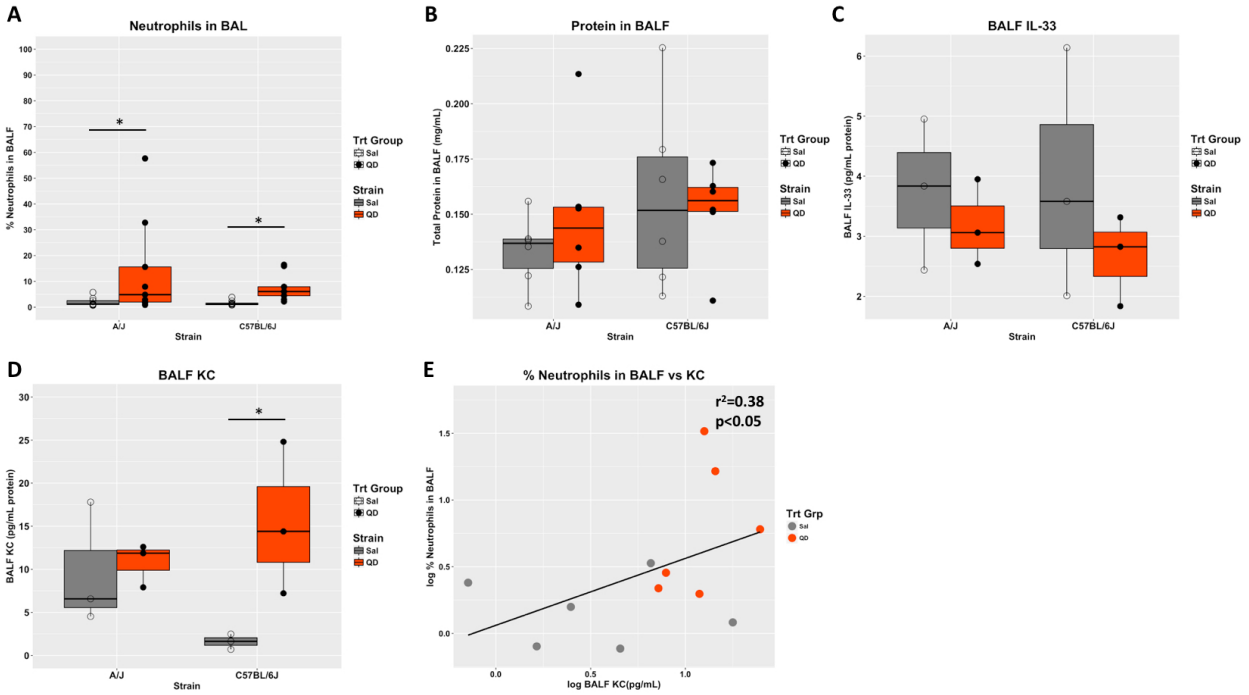

Figure 2. The % neutrophils (A) and concentrations of total protein (B), IL-33(C), and KC (D) in BALF for each mouse are shown overlaid on a box plot. *p<0.05 after Bonferroni correction. Correlations are shown between % neutrophils and KC levels in BALF (E). The linear regression line is plotted along with the r^2 and p-value of the association. *p<0.05 after Bonferroni correction.

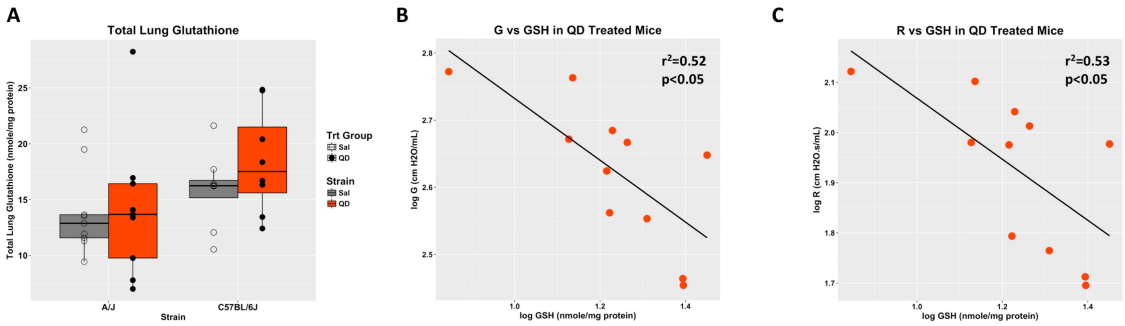

Figure 3. Lung glutathione levels for each mouse are shown overlaid on a box plot (A). Correlations are shown between G (B), R (C) and lung glutathione. The linear regression line is plotted along with the r^2 and p-value of the association.

Chapter 6

Quantum Dots and Mouse Strain Influence House Dust Mite-Induced Allergic Airway Disease

David K. Scoville[1], James D. Nolan[2], H. Luke Ogden[2], Dowon An[2], Zahra Afsharinejad[1], Theo K. Bammler[1], Xiaohu Gao[3], William A. Altemeier[2], Teal S. Hallstrand[2], Terrance J. Kavanagh[1]

Departments of [1]Environmental and Occupational Health Sciences, [2]Medicine and [3]Bioengineering, University of Washington, Seattle, WA 98195

Corresponding Author:
Terrance J. Kavanagh, PhD
Department of Environmental and Occupational Health Sciences
Box 354695
University of Washington
Seattle, WA 98195, USA.
Tel: (206) 685-8479
Fax: (206) 685-4696
E-mail: tjkav@uw.edu
Running Title: Quantum Dots and HDM, and Lung Inflammation

Abstract

Quantum dot nanoparticles (QDs) have utility in many industries including electronics, biomedical research, and medicine due to their semi-conductor and fluorescent properties. Evidence that pulmonary exposure to QDs induces acute lung inflammation and toxicity in mice and rats raises concerns about potential human health risks. Recent studies in mice showing that some ENMs can exacerbate allergic airway disease (AAD) suggest that individuals with AAD and/or other respiratory conditions may be especially sensitive to ENM exposure. However, QD enhancement of AAD and the potential for genetic background to modulate ENM effects on AAD have not been evaluated.

In this study, C57BL/6J and A/J mice were exposed to either saline, house dust mite (HDM), or a combination of HDM and QDs (7 nM QDs) on day 1 of the sensitization protocol. Mice were challenged on days 8, 9 and 10 with HDM or saline only. On day 11, airway hyperresponsiveness (AHR) was assessed, bronchoalveolar lavage (BAL) was performed, and lung tissue was collected. BAL fluid (BALF) supernatants were frozen and BAL and lung tissue cells were prepared for flow cytometry.

Significant changes in AHR related to HDM exposure or HDM+QD co-exposure were not observed. However, significant differences in several cellular and molecular markers of AAD induced by both HDM and HDM+QD were observed between C57BL/6J and A/J mice. In addition, HDM+QD co-exposure in A/J mice significantly increased levels of BALF IL-17, IL-33, and IL-10 compared to saline controls, whereas HDM exposure alone did not. BALF total protein levels in both mouse strains were also only significantly increased by HDM+QD co-exposure. We also found that A/J mice had significantly more lung type 2 innate lymphoid (ILC2) cells than C57BL/6J mice. In A/J mice ILC2s were significantly inversely correlated with lung glutathione and MHC-II^{high} macrophages, and positively correlated with dendritic cells and MHC-II^{low} resident macrophages.

The results from this study suggest that 1) QDs influence HDM-induced AAD by

potentiating and/or enhancing cytokine production; 2) that genetic background likely modulates the impact of QDs on HDM sensitization; and 3) that potential ILC2 contributions to HDM induced AAD are also likely to be modulated by genetic background.

Introduction

Quantum dot nanoparticles (QDs) are engineered nanomaterials (ENMs) with intriguing semiconductor and fluorescent properties including narrow emission spectra that can be modified by changing the size and composition of the particle core (Medintz et al. 2005). In this regard, QDs have promising applications in research, biomedical, and electronics industries (Wu et al. 2003; Kim et al. 2004; Hu et al. 2010; Jung et al. 2012). However, QDs and other ENMs have been shown to cause lung inflammation and toxicity in mice and rats following pulmonary exposures by inhalation and other surrogate methods including intranasal and intratracheal instillation and oropharyngeal aspiration (Ma-Hock et al. 2009; Wang et al. 2011; Ma-Hock et al. 2012; McConnachie et al. 2013; Roberts et al. 2013; Scoville et al. 2015; Seiffert et al. 2015; Silva et al. 2015; Cartwright et al. 2016). There is also emerging evidence that occupational exposures to ENMs may increase the risk of adverse respiratory and cardiovascular outcomes in humans (Cui 2013; Liao et al. 2014).

Currently, approximately 8% of people in the US are estimated to suffer from asthma, which is commonly characterized by chronic type 2 T-helper (Th2) cell associated airway inflammation and hyperresponsiveness (Kim and Mazza 2011; CDC 2017). Increased eosinophils and Th2 cell related cytokines including IL-4, IL-5, and IL-13 are common in asthma related airway inflammation (Choy et al. 2015). Type 2 innate lymphoid cells (ILC2s), which are negative for lymphoid lineage markers, have recently been identified as an additional source of traditional Th2 cytokines (Licona-Limon et al. 2013; Doherty and Broide 2015). ILC2s are regulated in part by IL-33 from epithelial cells, and have been suggested to be contributors to asthma (Hallstrand et al. 2013; Drake and Kita 2014). Neutrophils, which can be recruited by IL-17 via CXCL1/KC induction, are also elevated in many asthma cases (Choy et al. 2015; Lambrecht and Hammad 2015). Allergens and other environmental exposures are common triggers for asthma attacks (Kim and Mazza 2011). Furthermore, low glutathione levels have been shown to polarize the immune response to

antigen exposure in the Th2 direction and reduce type 1 T-helper cell (Th1) cytokine production (Peterson et al. 1998; Kim et al. 2007).

Recent studies using mouse models of allergic airway disease (AAD) suggest that some engineered nanomaterials (ENMs) including silica, titanium and zinc oxide nanoparticles, and carbon nanotubes, can enhance sensitization to allergens. Most studies have used the murine allergen ovalbumin (OVA) and have either tested the adjuvant potential of ENMs in place of a traditional adjuvant (such as alum), or tested the ability for ENMs to augment OVA challenge induced immune responses (Nygaard et al. 2009; Brandenberger et al. 2013; Jonasson et al. 2013; Roy et al. 2013). A few studies have used house dust mite extract (HDM), which is a murine and human allergen (Gregory and Lloyd 2011; Piyadasa et al. 2016). HDM does not require an additional adjuvant so these studies have either examined the impact of ENMs on existing AAD or examined whether co-exposure enhances sensitization resulting in more severe responses (Cates et al. 2004; Ronzani et al. 2014; Shipkowski et al. 2015). However, the potential of QDs to impact allergic sensitization in mice has not been evaluated. Genetic background, which can modulate susceptibility to QD-induced acute lung inflammation, has yet to be explored in the context of ENM enhancement of allergic sensitization (Scoville et al. 2015).

In this study, we tested the hypotheses that pulmonary exposure to QDs enhances allergic sensitization to HDM, and that genetic background is a modulator of these enhancement effects. We also sought to explore the effect of HDM and QDs on glutathione levels. We used C57BL/6J and A/J mice because these two strains have genetically distinct responses to QDs, as A/J mice 1) have been shown to be less susceptible than A/J mice to QD-induced acute lung inflammation (Scoville et al. 2015), and 2) have naturally higher levels of lung glutathione.

Mice were sensitized to either HDM, HDM + QDs, or saline using oropharyngeal aspiration. After 1 week, mice were challenged once a day for 3 consecutive days with either HDM (HDM and HDM+QD sensitized mice) or saline. On the day following the final

challenge, AHR was assessed and bronchoalveolar lavage was performed to enumerate eosinophils, neutrophils, other leukocyte populations, cytokines, and BALF protein as a measure of lung epithelial/vascular barrier function. We also quantified ILC2s and measured glutathione in lung tissue.

We found that HDM+QD co-exposure during sensitization elevated levels of cytokines that were not significantly increased by HDM sensitization alone and that this response was strain specific. Significant increases in total BALF protein in both strains were also significantly increased with HDM+QD co-exposure during sensitization but not by HDM alone. Sensitization to both HDM alone and HDM+QD co-exposure during sensitization increased multiple BALF CD45+ subpopulations and lung ILC2s in a strain specific manner. Associations with glutathione, ILC2s, and multiple leukocyte populations were also strain dependent. To our knowledge, this is the first study to enumerate lung ILC2s in A/J mice and compare them across different mouse strains. The results from this study suggest that QDs may affect sensitization to HDM in a strain dependent manner by enhancing cytokine production, and that ILC2s contributions to these phenotypes are also likely strain dependent.

Methods

Mice and Sensitization

All procedures were approved by the University of Washington Institutional Animal Care and Use Committee (IACUC) on protocol # 2384-08. Seven-week old male C57BL/6J and A/J mice were purchased from Jackson Laboratories (Bar Harbor, ME). Mice were housed either 2 or 3 mice per cage in a specific pathogen free (SPF) vivarium at the University of Washington and acclimated for a week prior to sensitization. Mice were on a 12 hr light/dark cycle and food and water were available *ad libitum*. Groups of 6 mice from each strain were anesthetized with Isoflurane (4%, 2L/min O_2 flow rate) and either

sensitized on Day 0 to 50 µL of saline, 0.2 µg/µL HDM (Greer Laboratories, Lenoir NC – lot# 27533) in saline (100 µg HDM), or co-exposed to HDM+QDs (100 µg HDM + 140 ng Cd equivalents of QDs) using oropharyngeal aspiration (OPA). On Days 8, 9, and 10, mice dosed on day 1 with saline were challenged with 50 µL saline and HDM and HDM+QD exposed mice received 50 µL of 0.5 µg/µL (25 µg HDM) via OPA. One C57BL/6J HDM treated mouse was euthanized after day 8 OPA due to behavioral signs of distress. However, given that no other mice from any of the treatment groups showed any signs of distress after multiple OPA exposures, the distress in the euthanized C57BL/6J mouse was not considered HDM related. The dose of QDs in this study is virtually the same as that which C57BL/6J and A/J mice received in our previous studies (Scoville et al. 2015).

Quantum Dots

QDs used in this study were synthesized and characterized in the laboratory of Dr. Xiaohu Gao in the Department of Bioengineering at the University of Washington as previously described (Pellegrino et al. 2004; Bagalkot and Gao 2011; McConnachie et al. 2012; McConnachie et al. 2013). The QDs are composed of a Cadmium/Selenium core and a Zinc Sulfide shell, with an outer amphiphilic polymer coating of tri-n-octylphosphine oxide, poly(maleic anhydride-alt-1-tetradecene (TOPO-PMAT).

Lung Mechanics

On Day 11, mice were anesthetized with pentobarbital (90 mg/kg body weight) and intubated via tracheotomy with an 18 gauge Luer stub secured in the trachea with a suture. The mice were then ventilated using a flexiVent apparatus (SCIREQ Inc., Montreal, QC, Canada) to assess lung function. After an injection of pancuronium (0.1 mL) to eliminate breathing reflexes, pulmonary function was evaluated. The lungs were ventilated with a tidal volume of 10 mL/kg, at a rate of 180 breaths/minute, with a positive end expiratory pressure of 3 cm H_2O. After a total lung capacity maneuver was performed at 30 cm H_2O,

baseline measurements were collected. In order to assess airway hyper-reactivity, progressive doses of nebulized methacholine (0, 3.125, 12.5, and 50 mg/mL) were delivered to the lungs. At each dose of methacholine (MTCH), a 3 second multi-frequency forced oscillation maneuver was applied for determination of total lung impedance followed by a 1.5 sec single frequency oscillation for determination of Resistance (R), Elastance (E), and Compliance (C). Airway Resistance (Rn), Tissue Damping (G), and Tissue Elastance (H) were calculated by the flexiVent software by applying the Constant Phase model to the impedance measurement. Area under the curve was calculated for each animal to allow for strain and treatment comparisons (Vanoirbeek et al. 2010).

Bronchoalveolar Lavage (BAL)

Three lavages were performed in each mouse using 1 mL phosphate buffered saline (PBS). Cells were collected by centrifugation of the recovered BAL fluid (BALF) at 300g for 5 min at 4°C. The supernatant from the 1st lavage in each mouse was stored at -80°C for measuring total BALF protein and cytokines. Cells from all three lavages were combined in 500 µL RPMI media with 10% fetal bovine serum (FBS) and counted using a Cellometer Auto 2000 (Nexcelom Bioscience, Lawrence, MA). Aliquots of BAL cells (20,000 cells/slide) were centrifuged at 750 RPM for 5 min using a Cytopro model 7620 cytocentrifuge (Wescor Inc., Logan, UT) and later stained with Diff-Quik (Siemens - Thermo Fisher Scientific, Waltham, MA).

Lung Tissue Collection and Processing

Following lavage, the lungs were perfused with HBSS and right superior and inferior lobes were collected and placed on ice in RPMI medium with 10% FBS. After removal of medium, lung tissue was minced with scissors. A small portion was frozen for future protein analysis and another was placed into Trizol (Invitrogen, Carlsbad, CA) and frozen for future mRNA extraction. Digestion media (RPMI, 5% FBS, 0.5 mg/mL Liberase (Roche,

Indianapolis, IN), 40 U/ml DNase 1 (Qiagen, Germantown, MD) was added to the remaining minced lung tissue. Following a 30 min incubation at 37°C, the digested lung solution was filtered through a 40 µm filter (Corning-Falcon, Corning Inc., Corning, NY) to obtain a single-cell suspension. The accessory and middle right lobes were flash frozen for measurement of glutathione.

Multi-Color Flow Cytometry for BALF Cell Differentials

BALF single cell suspensions were stained for enumeration of inflammatory cell populations as previously described (Nolin et al. 2016). Briefly, cells were blocked using Fc block (BD Biosciences, San Jose, CA). BALF cells were then labeled with an anti-mouse antibody cocktail (CD45-APC/Cy7[1], CD3-PerCP-Cy5.5[2], MHC-II -BV605[3], SiglecF-PE[3], Cd11c-FITC[2], and Gr1-APC[2] -- [1]Biolegend, San Diego, CA [2]eBiosciences, San Diego, CA [3]BD Biosciences, San Jose, CA). Cells were then incubated with eFluor 450 fixable viability dye (eBioscience). Single stained controls used for color compensation were obtained using ArC amine reactive beads (Thermo-Fisher, Waltham, MA) and viability single stained control was obtained using OneComp eBeads (eBioscience). Stained cells were analyzed using a FACS LSR II flow cytometer (Becton Dickinson Instrument Systems, Franklin Lakes, NJ) and gating and compensation were performed using FlowJo software (TreeStar, Ashland, OR).

Multi-Color Flow Cytometry for Lung ILC2s

For detection of ILC2s, lung single cell suspensions were labeled with an anti-mouse antibody cocktail (Mouse Hematopoietic Lineage FITC Cocktail (CD3, CD45R/B220, CD11b, Ter119, Gr-1), CD45 (AlexaFluor 700[2] or APC/Cy7[1]), CD90.2 (APC[2]), CD25(BV421[1]), and ST2 (PE[3]) -- [1]Biolegend, San Diego, CA [2]eBiosciences, San Diego, CA [3]MD Biosciences, St Paul, MN). Cells were blocked with Fc Block (BD Bioscience) and subsequently incubated with the primary antibody cocktail for 30 min at 4°C in the dark. After washing, cells were then resuspended in PBS containing eFluor 455UV fixable viability dye (eBioscience) and

incubated for 15 min at 4°C in the dark. Cells were then fixed in 10% NBF and stored at 4°C in MACS buffer until analyzed via flow cytometry. ArC amine reactive beads and OneComp eBeads were used for single stain compensation controls as described above. Fluorescence minus one (FMO) controls for CD90.2, CD25, and ST2 were also used for compensation. All FMOs contained the lineage cocktail and the CD45 antibody with the omission of only CD90.2, CD25 or ST2 to allow for accurate gating. All samples were analyzed using a BD FACS LSR II flow cytometer and subsequent gating and compensation were performed using FlowJo.

BALF Total Protein and Cytokine Analysis

Total protein levels in BALF were measured in triplicate using the Bio-Rad Protein Assay (BioRad, Hercules, CA) according to manufacturer's instructions. Absorbance was read at 590 nm using a SpectraMax 190 spectrophotometric plate reader (Molecular Devices, Sunnyvale, CA). Protein concentrations were interpolated from a standard curve created using dilutions of a BSA solution (0-0.35 mg/mL). BALF cytokines IFN-γ, IL-5, IL-17A, IL-33, KC, and IL-10 were measured in duplicate using a U-Plex assay (Meso Scale Discovery - Meso Scale Diagnostics, Rockville, MD). Samples below the lower limit of detection (LLOD) were replaced with the analyte specific LLOD divided by the square root of 2.

Lung Total Glutathione

Approximately 20-40 mg of lung tissue was homogenized in 400 µL of TES/SB buffer (TES/SB (20 mM Tris, pH 7.4, 1 mM EDTA, 250 mM sucrose, 20 mM serine, and 1 mM boric acid with 10 µL/mL protease inhibitor (Roche, Indianapolis, IN)) using 5 mm steel beads (Qiagen, Germantown, MD) in a 2 mL micro-tube for 5 min at 50 Hz using a TissueLyser (Qiagen). Levels of glutathione were measured as previously described (Weldy et al. 2011). Briefly, glutathione in lung tissue samples and standards (0-0.25 mM) was reduced with

TCEP (tris(2-carboxyethyl) phosphine), and then derivatized with napthelene-2,3-dicarboxaldehyde. Relative fluorescence intensity was measured for samples and standards. Sample concentrations were interpolated from the GSH standard curve. Standards and samples were analyzed in triplicate and samples were normalized to total protein levels in the lung tissue sample measured using the Bradford method.

Statistical Analysis

Differences between strains and treatment groups were analyzed using two-way ANOVA on log transformed data. If a significant QD treatment effect was seen using two-way ANOVA then a one-way ANOVA was performed in each strain and post-hoc comparisons were made using Tukey's HSD test. Pearson's correlation coefficients between endpoints were calculated using r.corr function in the Hmisc R package (Harrell et al. 2016). Data was managed in Microsoft Excel and R. All analyses were done using R and plots were generated using ggplot2 (Wickham 2009) and corrplot (Wei and Simko 2016).

Results

AHR and Lung Permeability

Similar to Nolin et al. (Nolin et al. 2016), AHR was assessed using total lung resistance (R) (Figure 1A). AHR, defined here as an increase in R in HDM sensitized or HDM+QD co-exposed mice compared to saline treated mice, was not observed. However, A/J mice were observed to be significantly more responsive to MTCH than C57BL/6J mice. While our main focus was on AHR, differences in other lung mechanics measures were also observed between the C57BL/6J and A/J mice. A/J mice were observed to have significant increases in tissue elastance (H) in HDM sensitized and HDM+ QD co-exposed mice although there was not a significant difference between HDM and HDM+QD exposures (Figure S1). In A/J mice, hysteresivity (eta) was significantly decreased in HDM sensitized

compared to saline treated mice (Figure S1). Lung permeability was assessed by measuring total protein levels in BALF (Figure 1B). Significant increases in total BALF protein were observed in HDM+QD co-exposed C57BL/6J and A/J mice but not in mice exposed to HDM alone. In C57BL/6J mice, a weak but significant association between levels of BALF protein and R were observed (Figure 1C).

BALF Inflammatory Cells

To characterize lung inflammatory cells, multiple CD45+ BALF cell populations were enumerated using flow cytometry (Figure 2). Total CD45+ cells, T-cells, eosinophils, granulocytes, and neutrophils, were all significantly induced by HDM sensitization and HDM+QD co-exposure in both C57BL/6J and A/J mice (Figure 2 A, E, F-H). MHC-II^{high} resident macrophages and dendritic cells were only significantly induced by HDM sensitization and HDM+QD co-exposure in C57BL/6J mice (Figures 2B and 2C).

BALF Cytokines

To further characterize HDM and QD+HDM-induced inflammatory responses, BALF cytokines IL-5, IL-33, IFN-γ, IL-17, IL-10, and KC were measured using a MSD U-plex assay (Figure 3). IL-17, IL-10, and IL-33, and in A/J mice were significantly induced by HDM+QD co-exposure but not by HDM alone (Figure 3A-C). IL-5 and KC were significantly induced by both HDM and HDM+QD co-exposure in both C57BL/6J and A/J mice (Figure 3D and 3E). IFN-γ was detectable in HDM sensitized and QD+HDM co-exposed C57BL/6J mice but was undetectable in A/J mice (Figure 3F). Significant positive associations were observed between total lung resistance (R) and KC and IL-33 in C57BL/6J mice (Figure 3 G and H).

Lung ILC2 cells

ILC2 cells are recently identified lymphoid cells that lack traditional lineage markers. ILC2s

are thought to be innate sources of Th2 cytokines, and may contribute to allergic inflammation (Doherty and Broide 2015). ILC2 cells were identified by gating for CD45+, CD90.2+ CD25+ and ST2+ (IL-33 receptor). While neither HDM or HDM+QD co-exposure changed numbers of ILC2 cells, A/J mice were observed to have significantly more lung ILC2 cells than C57BL/6J mice (Figure 4A). In A/J mice, a significant positive association was observed between ILC2 cells and MHC-II^{low} resident macrophages (Figure 4B). An inverse association was observed between ILC2 cells and MHC-II^{high} resident macrophages in A/J mice (Figure 4C).

Lung Glutathione

Glutathione is essential for redox homeostasis and redox status has been associated with immune response polarization. We measured total lung glutathione using derivatization with 2,3-naphthalenedicarboxaldehyde. No significant differences among saline, HDM sensitized or HDM+QD co-exposed mice in either strain were found (Figure 5A). However, significant inverse associations between levels of glutathione and lung ILC2 cells and MHC-II low resident macrophages were observed in A/J mice (Figure 5 B, C).

Discussion

While recent studies have shown that some ENMs can enhance allergic sensitization in mouse models of AAD, the potential for QDs to act in a similar manner has not been evaluated. Genetic background as a susceptibility factor to ENM enhancement of allergic sensitization has also not yet been explored. Thus, in this study we sensitized C57BL/6J and A/J mice to the murine and human allergen HDM and HDM + QDs to test the hypotheses that QDs would enhance allergic sensitization to HDM and that genetic background would modulate susceptibility.

While AHR was not observed, we did find significant increases in BALF eosinophils

and IL-5 in HDM sensitized mice of both strains, indicative of Th2 airway inflammation. Levels of IL-5, eosinophils and neutrophils in BALF in mice from our study were comparable to levels in another recent study investigating HDM sensitization in BALB/c mice (Piyadasa et al. 2016). While not significant, there is a suggestion that levels of lung resistance R may be increased by HDM sensitization in C57BL/6J mice, and levels of total protein, IL-33 and KC in C57BL/6J mice were significantly correlated with R. This may suggest that in addition to IL-33, which is known to contribute to AHR, lung permeability, and KC are also contributing to total lung resistance (R) in C57BL/6J mice (Barlow et al. 2013).

Interestingly, we found that levels of total protein in BALF were significantly elevated in mice from both mouse strains co-exposed to HDM+QD during sensitization but not in mice sensitized to HDM alone, suggesting that QDs may have enhanced HDM effects on lung permeability. Furthermore, in A/J mice, BALF cytokines IL-17, IL-33, and IL-10 were significantly increased by HDM+ QD co-exposure during sensitization but not with HDM alone, suggesting that QDs may enhance the HDM cytokine response in a strain dependent manner. While levels of IL-17 appear higher in C57BL/6J mice, high variability in both HDM sensitized and HDM+QD sensitized mice lead to a lack of statistical significance. The scenario is similar for IL-33. Levels of IL-5 and KC were significantly increased in HDM sensitized and HDM+QD co-exposed mice in both mouse strains. IL-10 was significantly increased by sensitization to HDM and HDM+QDs in C57BL/6J mice. IFN-γ was detectable in HDM sensitized and HDM+QD co-exposed C57BL/6J mice whereas it was undetectable in all A/J mice. Collectively, the cytokine data suggest that both strains mounted a Th2 response to HDM (IL-5). It also suggests that HDM+QD co-exposure potentiated a Th17 response (IL-17) in A/J mice in the absence of a significant increase with HDM alone. Silica nanoparticles have also been shown to induce IL-17 in a different Th2 prone mouse strain (BALB/c) compared to allergen alone (Sellers et al. 2011; Brandenberger et al. 2013). Detectable levels of IFN-γ in HDM-sensitized and HDM+QD co-exposed C57BL/6J mice, although not significantly different from saline mice where IFN-γ was not detected, suggests a potential

low-grade C57BL/6J specific Th1 response. This would be consistent with C57BL/6J mice being more prone to Th1 immune responses than A/J mice (Sellers et al. 2011). The significant increases in the anti-inflammatory cytokine IL-10 in HDM-sensitized C57BL/6J mice and QD-HDM co-exposed C57BL/6J and A/J mice suggests that both strains are attempting to keep inflammatory responses in check (Saraiva and O'Garra 2010).

We also found that A/J mice have significantly higher numbers of lung ILC2 cells overall than C57BL/6J mice. In A/J mice, levels of ILC2s were significantly positively correlated with levels of MHC-II^{low} resident macrophages and inversely correlated with levels of MHC-II^{high} resident macrophages and total MHC-II^{high} cells. The direction of these correlations between ILC2s and macrophages are consistent with evidence that ILC2s play a role in supporting M2 macrophages and with current thinking that increased expression of MHC-II is associated with macrophages in the M2 state, and the opposite for M1 macrophages (Bouchery et al. 2015; Chávez-Galán et al. 2015). While we did not see significant differences between treatment groups in ILC2s, to our knowledge this is the first study to enumerate ILC2s in A/J mice and compare their numbers across different mouse strains.

Although we did not observe any significant differences in glutathione levels across treatment groups, or between mouse strains, a significant inverse correlation was observed between lung glutathione levels and ILC2s in A/J mice. Glutathione levels were also inversely correlated in A/J mice with MHC-II low resident macrophages. Both correlations are in keeping with previous studies showing that lower glutathione levels are associated with altered Th1 and Th2 immune responses (Peterson et al. 1998; Chan et al. 2006; Kim et al. 2007).

In conclusion, the results from this study suggest that 1) QDs influence HDM induced AAD by potentiating and/or enhancing cytokine production; 2) that genetic background likely modulates the impact of QDs on HDM sensitization; and 3) that potential ILC2 contributions to HDM induced AAD are also likely to be modulated by genetic background.

Future studies are needed to further elucidate the influence of ILC2s and to formally evaluate the role of glutathione in HDM induced AAD.

Chapter 6 References

Bagalkot, V. and X. Gao (2011). "siRNA-Aptamer Chimeras on Nanoparticles: Preserving Targeting Functionality for Effective Gene Silencing." ACS Nano **5**(10): 8131-8139.

Barlow, J. L., S. Peel, J. Fox, V. Panova, C. S. Hardman, A. Camelo, . . . A. N. McKenzie (2013). "IL-33 is more potent than IL-25 in provoking IL-13-producing nuocytes (type 2 innate lymphoid cells) and airway contraction." Journal of Allergy and Clinical Immunology **132**(4): 933-941.

Bouchery, T., R. Kyle, M. Camberis, A. Shepherd, K. Filbey, A. Smith, . . . G. Le Gros (2015). "ILC2s and T cells cooperate to ensure maintenance of M2 macrophages for lung immunity against hookworms." Nature Communications **6**: 6970.

Brandenberger, C., N. L. Rowley, D. N. Jackson-Humbles, Q. Zhang, L. A. Bramble, R. P. Lewandowski, . . . J. R. Harkema (2013). "Engineered silica nanoparticles act as adjuvants to enhance allergic airway disease in mice." Particle and Fibre Toxicology **10**(1): 26.

Cartwright, M. M., S. C. Schmuck, C. Corredor, B. Wang, D. K. Scoville, C. R. Chisholm, . . . T. J. Kavanagh (2016). "The pulmonary inflammatory response to multiwalled carbon nanotubes is influenced by gender and glutathione synthesis." Redox Biology **9**: 264-275.

Cates, E. C., R. Fattouh, J. Wattie, M. D. Inman, S. Goncharova, A. J. Coyle, . . . M. Jordana (2004). "Intranasal Exposure of Mice to House Dust Mite Elicits Allergic Airway Inflammation via a GM-CSF-Mediated Mechanism." The Journal of Immunology **173**(10): 6384-6392.

CDC. (2017). "CDC - Asthma - Data and Surveillance - Asthma Surveillance Data ", from http://www.cdc.gov/asthma/asthmadata.htm

Chan, R. C.-F., M. Wang, N. Li, Y. Yanagawa, K. Onoé, J. J. Lee and A. E. Nel (2006). "Pro-oxidative diesel exhaust particle chemicals inhibit LPS-induced dendritic cell responses involved in T-helper differentiation." Journal of Allergy and Clinical Immunology **118**(2): 455-465.

Chávez-Galán, L., M. L. Olleros, D. Vesin and I. Garcia (2015). "Much More than M1 and M2 Macrophages, There are also CD169+ and TCR+ Macrophages." Frontiers in Immunology **6**(263).

Choy, D. F., K. M. Hart, L. A. Borthwick, A. Shikotra, D. R. Nagarkar, S. Siddiqui, . . . P. Bradding (2015). "TH2 and TH17 inflammatory pathways are reciprocally regulated in asthma." Science Translational Medicine **7**(301): 301ra129.

Cui, L. (2013). Exposure assessment and inflammatory response among workers producing calcium carbonate nanomaterials Dissertation, University of Washington.

Doherty, T. A. and D. H. Broide (2015). "Group 2 Innate Lymphoid Cells: New Players in Human Allergic Diseases." Journal of investigational allergology & clinical immunology **25**(1): 1-11.

Drake, L. Y. and H. Kita (2014). "Group 2 Innate Lymphoid Cells in the Lung." Advances in Immunology **124**: 1-16.

Gregory, L. G. and C. M. Lloyd (2011). "Orchestrating house dust mite-associated allergy in the lung." Trends in Immunology **32**(9): 402-411.

Hallstrand, T. S., T. L. Hackett, W. A. Altemeier, G. Matute-Bello, P. M. Hansbro and D. A. Knight (2013). "Airway epithelial regulation of pulmonary immune homeostasis and inflammation." Clinical Immunology **151**(1): 1-15.

Harrell, F. J. J., C. Dupont and e. al. (2016). "Hmisc." from https://cran.r-project.org/package=Hmisc.

Hu, X., H. Han, L. Hua and Z. Sheng (2010). "Electrogenerated chemiluminescence of blue emitting ZnSe quantum dots and its biosensing for hydrogen peroxide." Biosensors and Bioelectronics **25**(7): 1843-1846.

Jonasson, S., B. Gustafsson A Fau - Koch, A. Koch B Fau - Bucht and A. Bucht (2013). "Inhalation exposure of nano-scaled titanium dioxide (TiO2) particles alters the inflammatory responses in asthmatic mice." Inhalation Toxicology **25**(4): 1091-7691.

Jung, H., W. Chung, C. H. Lee and S. H. Kim (2012). "Fabrication of white light-emitting diodes based on UV light-emitting diodes with conjugated polymers-(CdSe/ZnS) quantum dots as hybrid phosphors." Journal of Nanoscience and Nanotechnology **12**(7): 5407-5411.

Kim, H. and J. Mazza (2011). "Asthma." Allergy, Asthma & Clinical Immunology **7**(1): S2.

Kim, H.-J., B. Barajas, R. C.-F. Chan and A. E. Nel (2007). "Glutathione depletion inhibits dendritic cell maturation and delayed-type hypersensitivity: Implications for systemic disease and immunosenescence." Journal of Allergy and Clinical Immunology **119**(5): 1225-1233.

Kim, S., Y. T. Lim, E. G. Soltesz, A. M. De Grand, J. Lee, A. Nakayama, . . . J. V. Frangioni (2004). "Near-infrared fluorescent type II quantum dots for sentinel lymph node mapping." Nature Biotechnology **22**(1): 93-97.

Lambrecht, B. N. and H. Hammad (2015). "The immunology of asthma." Nature Immunology **16**(1): 45-56.

Liao, H.-Y., Y.-T. Chung, C.-H. Lai, S.-L. Wang, H.-C. Chiang, L.-A. Li, . . . S.-H. Liou (2014). "Six-month follow-up study of health markers of nanomaterials among workers handling engineered nanomaterials." Nanotoxicology **8**(sup1): 100-110.

Licona-Limon, P., L. K. Kim, N. W. Palm and R. A. Flavell (2013). "TH2, allergy and group 2 innate lymphoid cells." Nature Immunology **14**(6): 536-542.

Ma-Hock, L., S. Brill, W. Wohlleben, P. M. A. Farias, C. R. Chaves, D. P. L. A. Tenório, . . . B. van Ravenzwaay (2012). "Short term inhalation toxicity of a liquid aerosol of CdS/Cd(OH)2 core shell quantum dots in male Wistar rats." Toxicology Letters **208**(2): 115-124.

Ma-Hock, L., S. Treumann, V. Strauss, S. Brill, F. Luizi, M. Mertler, . . . R. Landsiedel (2009). "Inhalation Toxicity of Multiwall Carbon Nanotubes in Rats Exposed for 3 Months." Toxicological Sciences **112**(2): 468-481.

McConnachie, L. A., D. Botta, C. C. White, C. S. Weldy, H. W. Wilkerson, J. Yu, . . . T. J. Kavanagh (2013). "The Glutathione Synthesis Gene Gclm Modulates Amphiphilic Polymer-Coated CdSe/ZnS Quantum Dot-Induced Lung Inflammation in Mice." PLOS ONE **8**(5): e64165.

McConnachie, L. A., C. C. White, D. Botta, M. E. Zadworny, D. P. Cox, R. P. Beyer, . . . T. J. Kavanagh (2012). "Heme oxygenase expression as a biomarker of exposure to amphiphilic polymer-coated CdSe/ZnS quantum dots." Nanotoxicology **7**(2): 181-191.

Medintz, I. L., H. T. Uyeda, E. R. Goldman and H. Mattoussi (2005). "Quantum dot bioconjugates for imaging, labelling and sensing." Nature Materials **4**: 435-446.

Nolin, J. D., H. L. Ogden, Y. Lai, W. A. Altemeier, C. W. Frevert, J. G. Bollinger, . . . T. S. Hallstrand (2016). "Identification of Epithelial Phospholipase A2 Receptor 1 (PLA2R1) as a Potential Target in Asthma." American Journal of Respiratory Cell and Molecular Biology.

Nygaard, U. C., J. S. Hansen, M. Samuelsen, T. Alberg, C. D. Marioara and M. Løvik (2009). "Single-Walled and Multi-Walled Carbon Nanotubes Promote Allergic Immune Responses in Mice." Toxicological Sciences **109**(1): 113-123.

Pellegrino, T., L. Manna, S. Kudera, T. Liedl, D. Koktysh, A. L. Rogach, . . . W. J. Parak (2004). "Hydrophobic Nanocrystals Coated with an Amphiphilic Polymer Shell: A General Route to Water Soluble Nanocrystals." Nano Letters **4**(4): 703-707.

Peterson, J. D., L. A. Herzenberg, K. Vasquez and C. Waltenbaugh (1998). "Glutathione levels in antigen-presenting cells modulate Th1 versus Th2 response patterns."

Proceedings of the National Academy of Sciences of the United States of America **95**(6): 3071-3076.
Piyadasa, H., A. Altieri, S. Basu, J. Schwartz, A. J. Halayko and N. Mookherjee (2016). "Biosignature for airway inflammation in a house dust mite-challenged murine model of allergic asthma." Biology Open.
Roberts, J. R., J. M. Antonini, D. W. Porter, R. S. Chapman, J. F. Scabilloni, S. H. Young, . . . R. R. Mercer (2013). "Lung toxicity and biodistribution of Cd/Se-ZnS quantum dots with different surface functional groups after pulmonary exposure in rats." Particle and Fibre Toxicology **10**: 5.
Ronzani, C., A. Casset and F. Pons (2014). "Exposure to multi-walled carbon nanotubes results in aggravation of airway inflammation and remodeling and in increased production of epithelium-derived innate cytokines in a mouse model of asthma." Archives of Toxicology **88**(2): 489-499.
Roy, R., S. Kumar, A. K. Verma, A. Sharma, B. P. Chaudhari, A. Tripathi, . . . P. D. Dwivedi (2013). "Zinc oxide nanoparticles provide an adjuvant effect to ovalbumin via a Th2 response in Balb/c mice." International Immunology.
Saraiva, M. and A. O'Garra (2010). "The regulation of IL-10 production by immune cells." Nature Reviews Immunology **10**(3): 170-181.
Scoville, D. K., C. C. White, D. Botta, L. A. McConnachie, M. E. Zadworny, S. C. Schmuck, . . . T. J. Kavanagh (2015). "Susceptibility to quantum dot induced lung inflammation differs widely among the Collaborative Cross founder mouse strains." Toxicology and Applied Pharmacology **289**(2): 240-250.
Seiffert, J., F. Hussain, C. Wiegman, F. Li, L. Bey, W. Baker, . . . K. F. Chung (2015). "Pulmonary Toxicity of Instilled Silver Nanoparticles: Influence of Size, Coating and Rat Strain." PLOS ONE **10**(3): e0119726.
Sellers, R. S., C. B. Clifford, P. M. Treuting and C. Brayton (2011). "Immunological Variation Between Inbred Laboratory Mouse Strains." Veterinary Pathology **49**(1): 32-43.
Shipkowski, K. A., A. J. Taylor, E. A. Thompson, E. E. Glista-Baker, B. C. Sayers, Z. J. Messenger, . . . J. C. Bonner (2015). "An Allergic Lung Microenvironment Suppresses Carbon Nanotube-Induced Inflammasome Activation via STAT6-Dependent Inhibition of Caspase-1." PLOS ONE **10**(6): e0128888.
Silva, R. M., D. S. Anderson, L. M. Franzi, J. L. Peake, P. C. Edwards, L. S. Van Winkle and K. E. Pinkerton (2015). "Pulmonary Effects of Silver Nanoparticle Size, Coating, and Dose over Time upon Intratracheal Instillation." Toxicological Sciences **144**(1): 151-162.
Vanoirbeek, J. A., M. Rinaldi, V. De Vooght, S. Haenen, S. Bobic, G. Gayan-Ramirez, . . . W. Janssens (2010). "Noninvasive and invasive pulmonary function in mouse models of obstructive and restrictive respiratory diseases." American Journal of Respiratory Cell and Molecular Biology **42**(1): 96-104.
Wang, X., P. Katwa, R. Podila, P. Chen, P. C. Ke, A. M. Rao, . . . J. M. Brown (2011). "Multi-walled carbon nanotube instillation impairs pulmonary function in C57BL/6 mice." Particle and Fibre Toxicology **8**(1): 24.
Wei, T. and V. Simko. (2016). "corrplot: Visualization of a Correlation Matrix." 2016, from https://github.com/taiyun/corrplot.
Weldy, C. S., C. C. White, H.-W. Wilkerson, T. V. Larson, J. A. Stewart, S. E. Gill, . . . T. J. Kavanagh (2011). "Heterozygosity in the glutathione synthesis gene Gclm increases sensitivity to diesel exhaust particulate induced lung inflammation in mice." Inhalation Toxicology **23**(12): 724-735.
Wickham, H. (2009). ggplot2: Elegant Graphics for Data Analysis, Springer Publishing Company, Incorporated.
Wu, X., H. Liu, J. Liu, K. N. Haley, J. A. Treadway, J. P. Larson, . . . M. P. Bruchez (2003). "Immunofluorescent labeling of cancer marker Her2 and other cellular targets with semiconductor quantum dots." Nature Biotechnology **21**(1): 41-46.

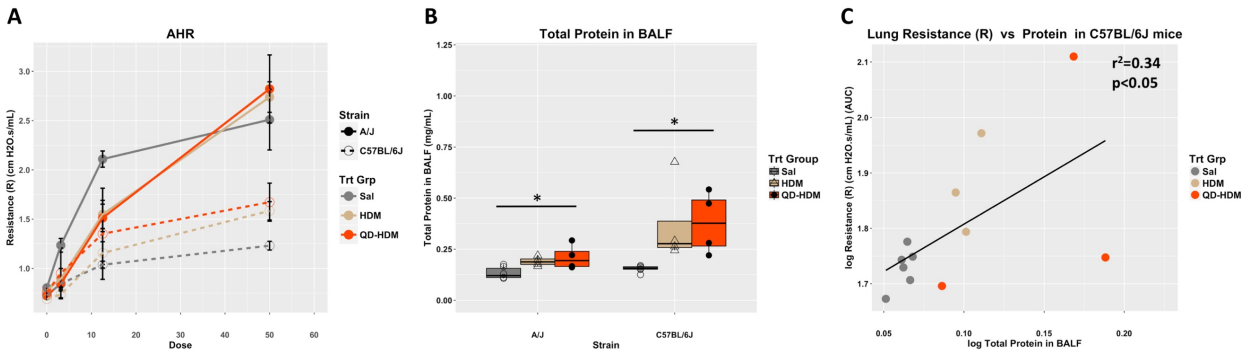

Figure 1. Levels of R in different strain and treatment groups are shown as means ± SEM (A). Concentrations of total BALF protein for each mouse are shown overlaid on a box plot (B). Correlations of R and total BALF protein (C). The linear regression line is plotted along with the r^2 and p-value of the association (C). *q<0.05 from Tukey's HSD test.

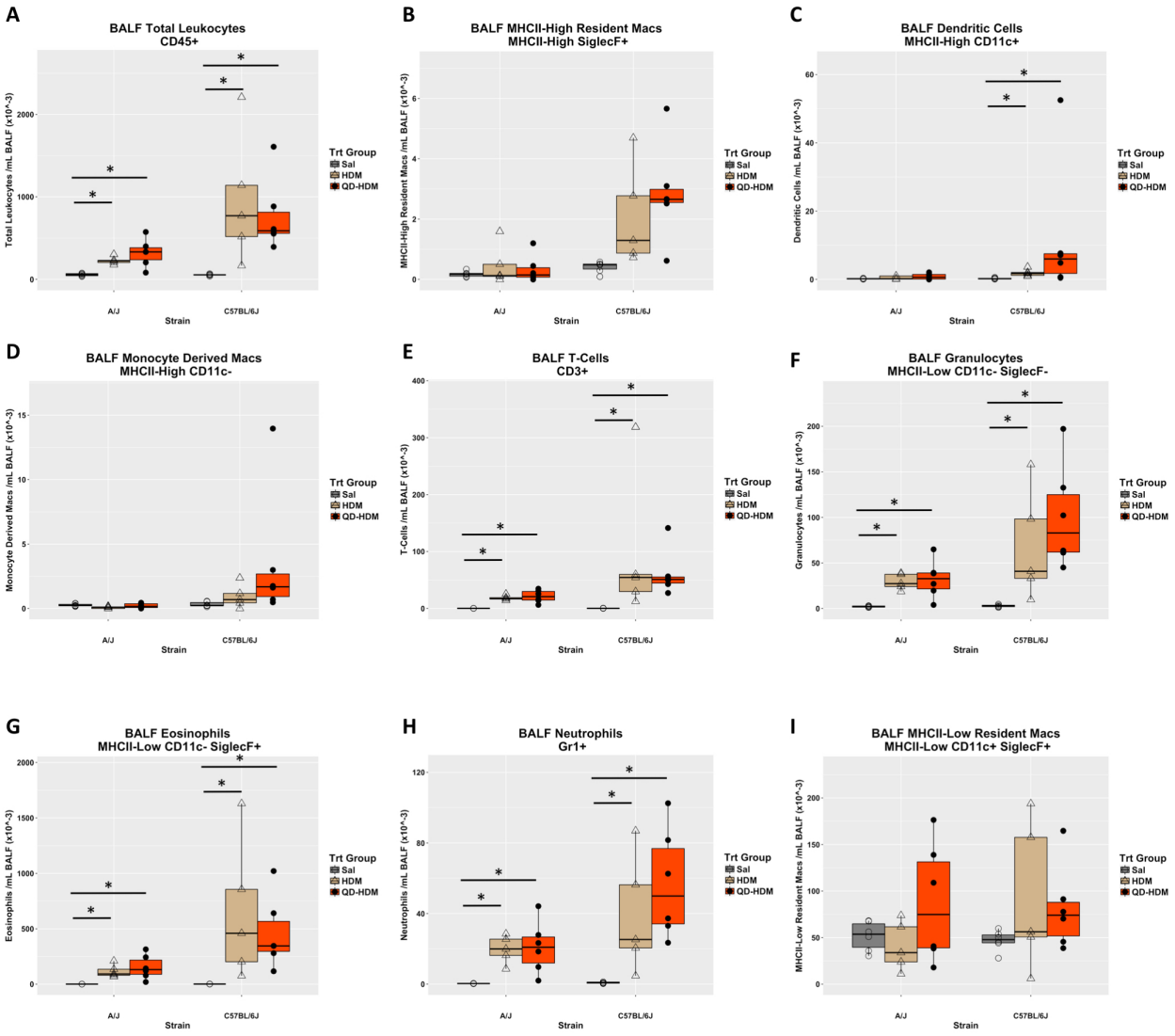

Figure 2. Concentrations of total CD45+ leukocytes (A), MHC-II high resident macrophages (B), dendritic cells (C), monocyte derived macrophages (D), T-cells (E), total MHC-II cells (F), granulocytes (G), eosinophils (H), neutrophils (I), and MHC-II low resident macrophages (K) for each mouse are shown overlaid on a box plot. *q<0.05 from Tukey's HSD test.

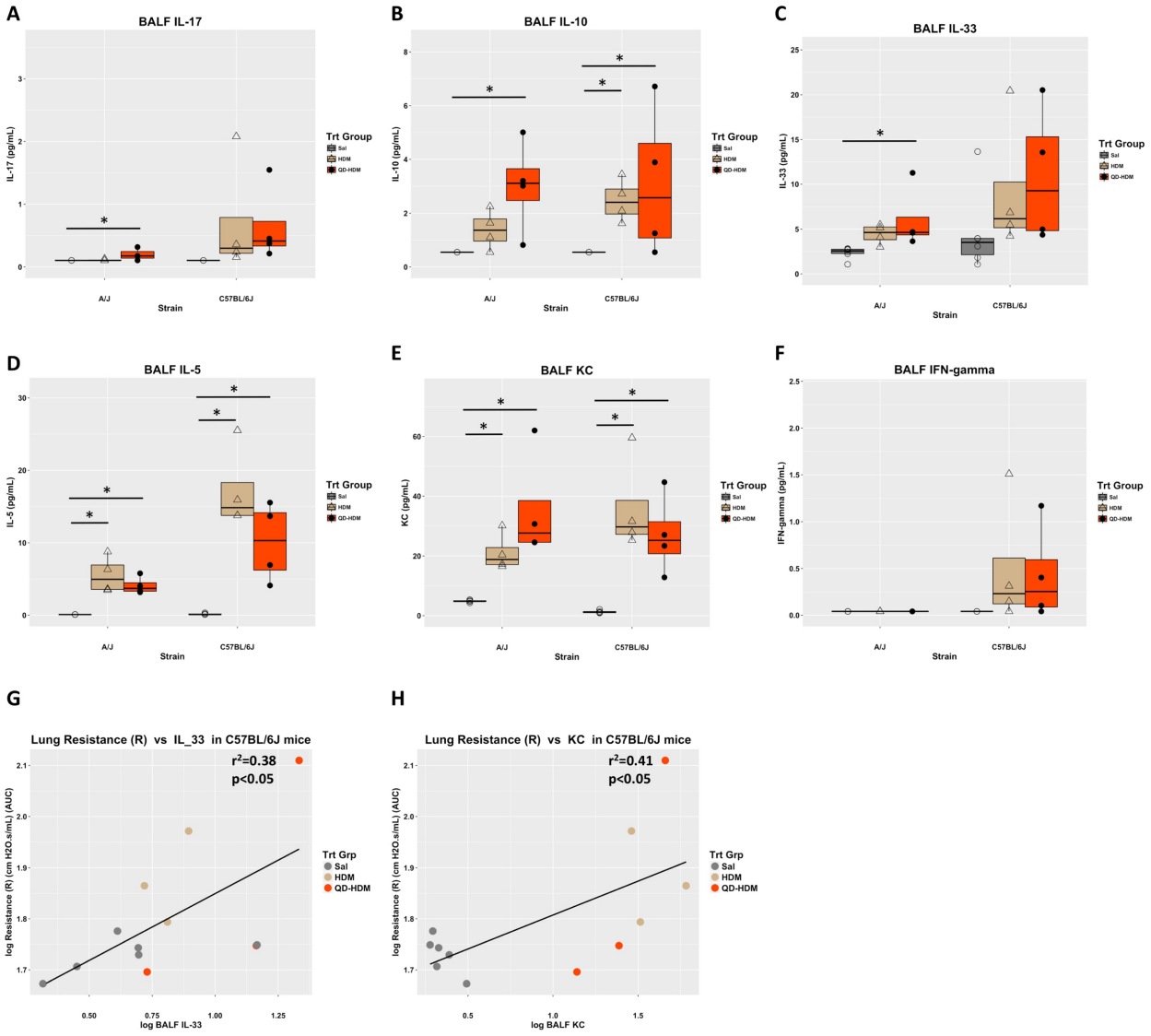

Figure 3. Concentrations of BALF IL-17 (A), Il-10 (B), IL-33 (C), IL-5 (D), KC (E) and IFN-γ (F) for each mouse are shown overlaid on a box plot (A-F). Correlations of R and IL-33 (G) and KC (H). The linear regression line is plotted along with the r^2 and p-value of the association. *q<0.05 from Tukey's HSD test.

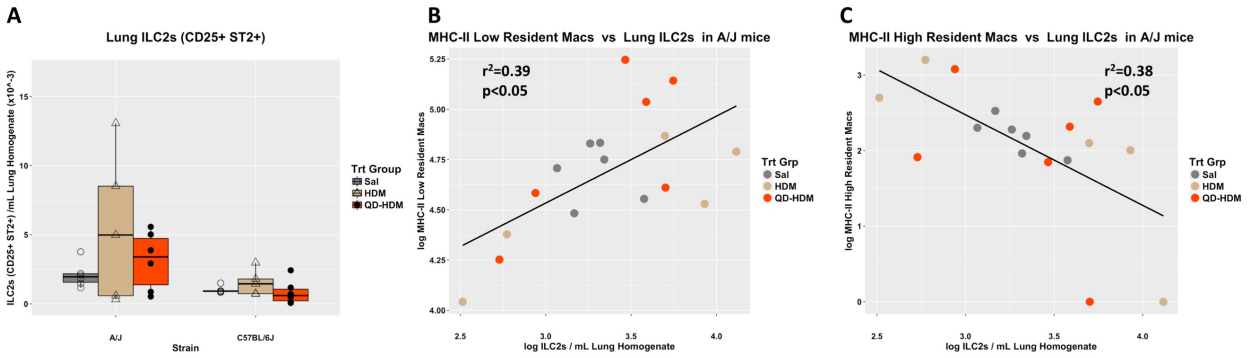

Figure 4. Levels of lung ILC2s for each mouse are shown overlaid on a box plot (A). Correlations of MHC-II^{low} resident macrophages (C), and MHC-II^{high} resident macrophages(C) and ILC2s. The linear regression line is plotted along with the r^2 and p-value of the association. *q<0.05 from Tukey's HSD test.

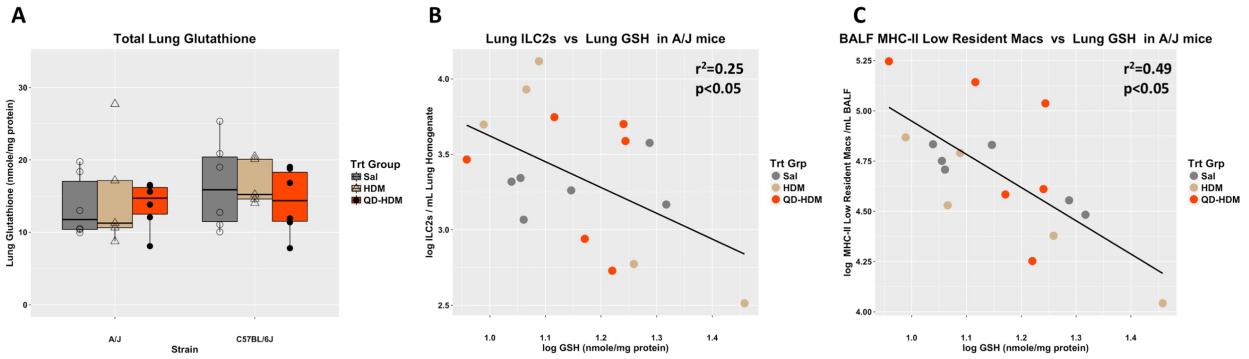

Figure 5. Levels of total lung glutathione for each mouse are shown overlaid on a box plot (A). Correlations between ILC2s (B), and MHC-II^{low} resident macrophages (B), and lung glutathione. The linear regression line is plotted along with the r^2 and p-value of the association. *q<0.05 from Tukey's HSD test.

Supplemental Information

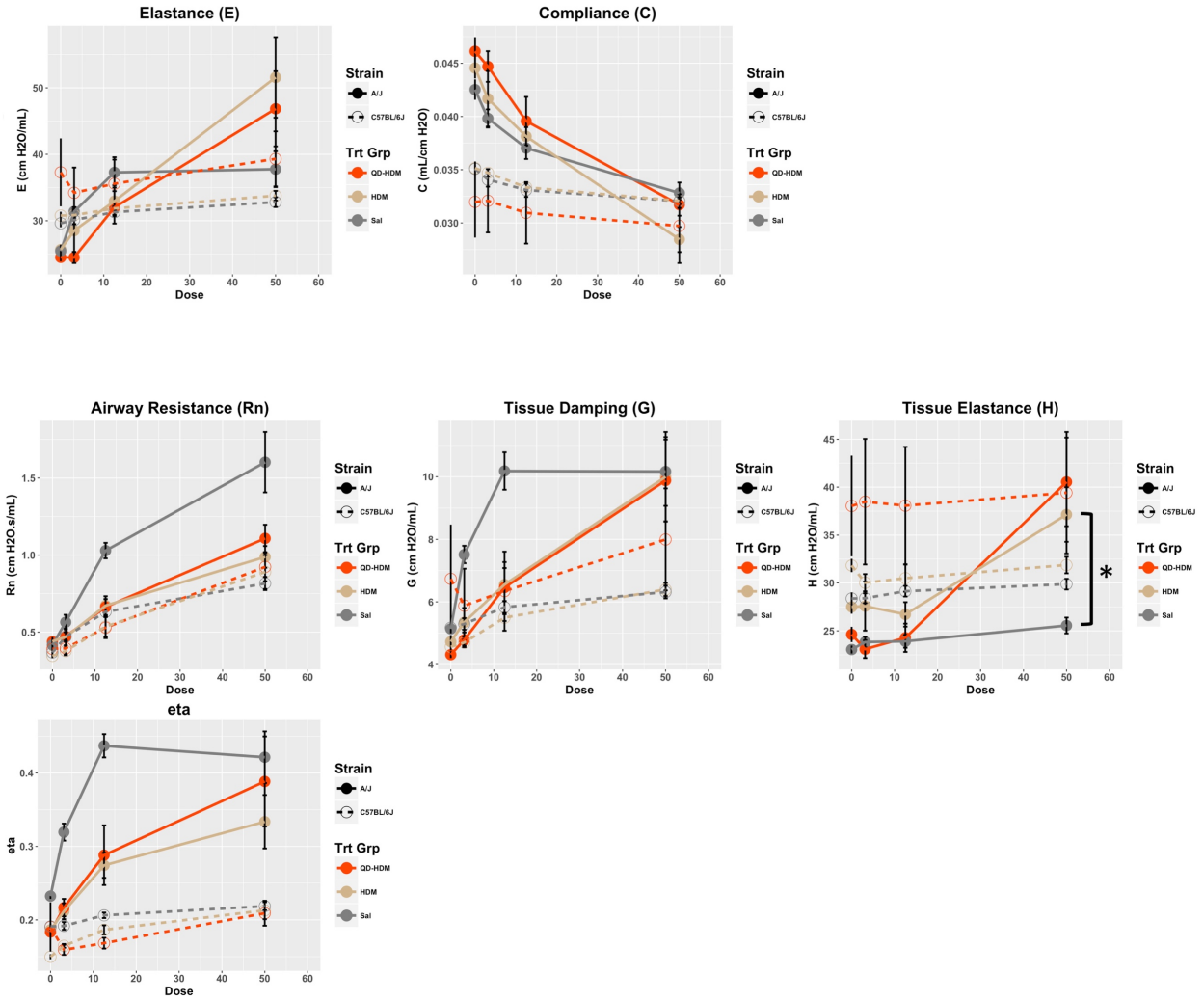

Figure S1. Additional measures of lung mechanics in saline, HDM-sensitized, and HDM+QD co-exposed C57BL/6J and A/J mice.

Chapter 7

Conclusions and Future Directions

David K. Scoville

The nanotechnology industry continues to grow as does the number of engineered nanomaterial-enabled products. Quantum dots (QDs) are ENMs often consisting of a cadmium and selenium core (CdSe) and a zinc sulfide shell (ZnS). Additional coatings are frequently added for stability and added function. QDs have useful fluorescent and semiconductor properties that have made them valuable in biomedical research and in the electronics industries. QDs have been shown to induce lung inflammation and cytotoxicity following pulmonary exposures in mice and rats. QD coating has been shown to modulate toxicity. Silver nanoparticles (AgNPs) are made from silver atoms but often contain other metals such as gold and can also be coated with additional materials for stability and function. AgNPs have been incorporated into numerous consumer products ranging from socks to toothbrushes and were identified by the NIEHS Centers for Nanotechnology Health Implications Research Consortium (NCNHIR) for inter-laboratory *in vitro* and *in vivo* toxicity testing. AgNPs have also been shown to induce lung inflammation and cytotoxicity in particle size, and coating dependent manner. AgNPs have been shown to negatively impact lung mechanics in rats. However, the role of genetic background in modulating toxicity has not been evaluated for QDs and in a limited capacity for AgNPs. The work in my dissertation focused primarily on evaluating the role of genetic background in modulating susceptibility for QD- and AgNP- induce lung inflammation and toxicity using multi-strain mouse models. The Collaborative Cross (CC) has focused on creating a genetically diverse recombinant inbred (RI) mouse panel for systems level genetics studies for over a decade. The basis of the CC are the 8 founder mouse strains that collectively capture more than 90% of known mouse genetic variability in *M. Musculus*. Chapter 2 discussed our work evaluating QD-induced acute lung inflammation across the 8 founder strains to robustly investigate the role

of genetic background. We found significant variation in QD-induced levels of BALF neutrophils and inflammatory cytokines. We identified that NOD/ShiLtJ and NZO/LtJ mice had significant increases in BALF neutrophils and that A/J mice had significant increases in cytokines KC, MIP-1α, MIP-1y, and G-CSF. In a sensitivity analysis where potential outliers were removed, A/J mice were found to also have increased levels of BALF neutrophils. We also found that KC and MIP-1α were the two most strongly correlated cytokines with BALF neutrophils. In conclusion, we determined that NOD/ShiLtJ and NZO/LtJ mice and A/J mice were susceptible strains; that C57BL/6 was the least sensitive strain; and that the observed significant inter-strain variability in susceptibility warranted future studies to identify specific QD-induced inflammation genetic susceptibility loci. In addition, potential future work could include testing C57BL/6 - C3H F_1 hypbrids (B6C3F1) mice, the test mouse strain for the National Toxicology Program, for their sensitivity to QD-induced lung inflammation. Determining where they rank in susceptibility among (or potentially outside) the CC founder strains would provide insight as to how protective potential risk estimates using data from B6C3F1 mice would be.

Building on results and recommendations from Chapter 2, Chapter 3 discussed our work further assessing the role of genetic background in QD-induced lung inflammation and toxicity across 12 CC RI mouse strains in collaboration with researchers at the University of North Carolina. As we had already established significant inter-strain variability across the CC founder strains in Chapter 2, the study discussed in Chapter 3 was designed to use GWA mapping to identify candidate genes and pathways in quantitative trait loci (QTLs) associated with QD-induced lung inflammation using replicate QD and saline treated mice from each strain. We found that % neutrophils in BALF, and levels of KC and total protein differed significantly between QD and saline treated mice overall and across the 12 CC RI mouse strains. We also found that levels of total protein in BALF exceeded the range of the CC founder strains. Using the EMMA R package, with individual mouse values for the three

phenotypes and QD treatment as a co-variate, we performed GWA mapping for levels of protein in BALF as our primary QD-induced lung inflammation phenotype using ~110K SNPs from the GigaMuga genotyping array. After Bonferroni correction we found 177 significant SNPs in broad QTL peaks on chromosomes 1,2,3, 4, 9, and 12, and individual SNPs on chromosome 6 and the X chromosome. Pathway analysis using Ingenuity Pathway Analysis (IPA) was performed with a list of over 300 genes from regions identified using the SNPs from chromosomes 1, 2, 3, 4, 9, and 12. IPA identified the visual cycle and nucleotide excision repair as the two most significantly enriched canonical pathways. The visual cycle genes from our list are involved with retinol/retinoic acid metabolism, while the NER pathway genes are involved with DNA damage surveillance and repair. Pathway analysis suggests that CC RI strains may be differentially susceptible to potentuial QD effects on retinol/retinoic acid metabolism and DNA damage. Even though this analysis would be greatly strengthened with transcriptomic data, which would allow for the determination of SNP effects on gene expression using expression QTL (eQTL) mapping, these results warrant future work characterizing potential QD effects on retinol/retinoic acid metabolism and DNA damage/repair. Assessing QD-induced lung inflammation in additional RI strains and eQTL mapping would likely provide the opportunity to narrow the list of candidate genes, which would be helpful for prioritizing future validation studies.

Differential AgNP-induced pulmonary inflammatory responses have been observed among inbred rat strains suggesting a role for genetic background in modulating AgNP-induced lung inflammation and toxicity. Chapter 4 discussed our work assessing AgNP induced lung inflammation across the CC founders and in additional inbred mouse strains in collaboration with researchers at NYU with the goal of GWA mapping to identify candidate susceptibility genes and pathways. We used % neutrophils in BALF as our phenotype for GWA mapping since we observed a large range of responses across 25 mouse strains in QD treated mice (0 in SWR/J to over 60% in BALB/c). We found 10 significant SNPs using a false discovery

rate (FDR) approach to adjust for multiple comparisons, an issue when testing 65K SNPs. Analysis of the SNP locations revealed that 2 of the 10 significant SNPs were located in *Nedd4l* on mouse chromosome 18 and that another 2 were located very close to *Nedd4l*. *Nedd4l* is ubiquitin ligase that can negatively regulate the levels of ENAC, a sodium channel located on the apical surface of epithelial cells in the lung and elsewhere. Mice that over-express *Enac* develop severe lung inflammation, as do mice lacking the *Nedd4l* gene. We also found significant SNPs in *Ano6* on mouse chromosome 15 and in *Rnf220* on mouse chromosome 4. *Ano6* is transmembrane protein with phospholipid scrambling activity and is thought to have ion-channel activity as well. Over-expression of *Ano6* in HEK293 cells has been shown to increase phosphatidylserine (PS) on the extracellular side of the cell membrane, which is a signal for apoptosis/efferocytosis. Reduced expression of *Ano6* could potentially result it reduced efferocytosis of lung inflammatory cells, possibly resulting in a lung that is more prone to inflammation. *Rnf220* is also a ubiquitin ligase thought to stabilize β-catenin in complex with another protein and therefore enhance canonical Wnt signaling, which has been shown to reduce LPS-induced inflammation. We found inverse associations in mRNA expression of all three of the aforementioned genes and % neutrophils in BALF across 4 mouse strains representing high, moderate, and low responders. Future work is needed, either through genetic or pharmacological manipulation, to further explore the role of these candidate genes in modulating susceptibility to AgNP-induced lung inflammation and toxicity.

ENMs including MWCNTs have been shown to have detrimental effects on mouse lung mechanics and concerns exist regarding the potential for occupational ENM exposure to impact worker lung function. Chapter 5 discussed our work investigating the impact of QDs on mouse lung mechanics and influence of genetic background in a preliminary manner using mouse strains we had previously identified as being more (A/J) and less (C57BL/6J) susceptible to acute QD-induced lung inflammation. We found that QDs increased lung

elastance (E) and tissue damping (G) in A/J mice compared to saline in a methacholine challenge suggesting that QD effects on lung mechanics are modulated by genetic background. Total lung resistance (R), which we interpreted as airway hyperresponsivenes (AHR) was increased by QD treatment compared to saline overall. We also found significant inverse associations between glutathione and R and G in QD treated mice. The observed overall effect on AHR and G and E in A/J mice warranted additional studies investigating the effects on QDs on lung mechanics in allergen sensitized mice, which was carried out and was discussed in Chapter 6. Additional future studies formally assessing the role of glutathione in mediating QD effects on lung mechanics are still needed.

Various ENMs have been shown to enhance mouse allergic sensitization to ovalbumin (OVA). MWCNTs have been shown to enhance mouse allergic sensitization to house dust mite (HDM) and to encourage lung fibrosis in HDM sensitized mice. Chapter 6 discusses our work investigating the impact of QDs on HDM allergic sensitization. We assessed the role of genetic background in a preliminary manner using C57BL/6J mice and A/J mice. We measured AHR, multiple BALF inflammatory leukocyte populations, BALF cytokines, and levels of type 2 innate lymphoid cells (ILC2s). We found that BALF eosinophils, and IL-5, both markers of Th2 inflammation used to characterize allergic airway disease were elevated by HDM in both mouse strains. We also found that co-exposure to QDs during HDM sensitization enhanced the production of cytokines IL-17, IL-33, and IL-10 compared to saline controls and that HDM sensitization alone did not elevate levels over controls. A/J mice, which are a Th2 type immune response mouse strain, had significantly higher levels of ILC2s than C57BL/6J mice. Glutathione levels and lung resident macrophages that are likely alternatively activated or M2 type macrophages that promote Th2 type responses, were significantly inversely associated with ILC2 levels in A/J mice. It has been proposed that ILC2s may play a supportive role with M2 macrophages. Overall, the results suggested that QDs may impact allergic sensitization by enhancing cytokine production and that

genetic background likely modulates QD effects on HDM sensitization and potential contributions of ILC2s to HDM allergic sensitization. Future work is warranted to further elucidate the influence of ILC2s and to formally evaluate the role of glutathione in HDM induced allergic airway disease.

Overall, the work presented in this dissertation provides insights into the role of genetic background as a modulator of susceptibility to QD- and AgNP-induced lung inflammation, and QD-induced effects on lung mechanics and allergic sensitization where prior information was non-existent or sparse. These studies performed in genetically diverse mice using oropharyngeal aspiration at occupationally relevant doses are important given the rapid rise in ENM manufacturing and human genetic heterogeneity. While surrogate methods such as oropharyngeal aspiration are different than inhalation, they are useful for screening purposes and in large studies such these where the cost, time and amount of ENMs necessary for inhalation would be prohibitive. Furthermore, recent ENM studies suggest that inhalation and aspiration result in similar outcomes when doses are properly compared.

Through GWA mapping with Collaborative Cross and other genetically diverse mouse strains, we have generated new hypotheses that may provide further mechanistic understanding of QD- and AgNP-induced lung inflammation. Our findings of substantial inter-strain variability in response to QD and AgNP pulmonary exposures presented in this dissertation have important regulatory implications for ENMs. Genetic background of test animals used to gather toxicity data for current risk models is important to consider such that uncertainty factors for regulatory standards ensure adequate protection for sensitive populations.